UNIVERSIDAD AUTÓNOMA DE BAJA CALIFORNIA

FACULTAD DE CIENCIAS QUÍMICAS E INGENIERÍA

MAESTRÍA Y DOCTORADO EN CIENCIAS E INGENIERÍA

Control de Potencia de Transmisión basado en temperatura y humedad relativa para Redes Inalámbricas de Sensores

T E S I S

que para obtener el grado de

DOCTOR EN INGENIERÍA

Presenta

César Ortega Corral

Director de tesis:

Dr. Luis Enrique Palafox Maestre

Co-Director de tesis:

Dr. José Antonio García Macías

TIJUANA, B. C. **Febrero de 2015**

Universidad Autónoma de Baja California

FACULTAD DE CIENCIAS QUÍMICAS E INGENIERÍA

COORDINACIÓN DE POSGRADO E INVESTIGACIÓN

FOLIO No. 138

Tijuana, B. C., a 27 de enero de 2015

C. Cesar Ortega Corral
Pasante de: Doctor en Ingeniería
Presente

El tema de trabajo y/o tesis para su examen profesional, en la Opción TESIS

Es propuesto, por los C. Dres. Luis Enrique Palafox Maestre y Dr. José Antonio García Macías

Quienes serán los responsables de la calidad del trabajo que usted presente, referido al tema: Control de Potencia de Transmisión basado en temperatura y humedad relativa para Redes Inalámbricas de sensores

el cual deberá usted desarrollar, de acuerdo con el siguiente orden:

I.- INTRODUCCIÓN
II.- REDES INALAMBRICAS DE SENSORES AMBIENTALES Y CONTROL DE POTENCIA DE TRANSMISION
III.- CONTROL DE POTENCIA DE TRANSMISION BASADO EN TEMPERATURA Y HUMEDAD RELATIVA
IV.- CONCLUSIONES

Dr. Luis Enrique Palafox Maestre
Director de Tesis

Dr. Juan Ramón Castro Rodriguez
Secretario

Dr. José Antonio García Macías
Co-Director de Tesis

Dr. Luis Enrique Palafox Maestre
Director

RESUMEN de la Tesis de César Ortega Corral, presentada como requisito parcial para la obtención del grado de DOCTOR EN INGENIERÍA. Tijuana, Baja California, México. Febrero, 2015.

Control de Potencia de Transmisión basado en temperatura y humedad relativa para Redes Inalámbricas de Sensores

Resumen aprobado por:

Dr. Luis Enrique Palafox Maestre
Director de tesis

Resumen

En este trabajo, se presenta un algoritmo novedoso de control de potencia de transmisión (TPC, del inglés *Transmission Power Control*), basado en cambios de la temperatura (T) y de la humedad relativa (RH, o *Relative Humidity*), cuyo modelo usa retroalimentación del indicador de intensidad de señal recibida (RSSI, *Recieved Signal Strength Indicator*). El espacio de aplicación incluye cualquier tipo de red inalámbrica de sensores (WSN, *Wireless Sensor Network*) que opere en exteriores. Se determinó la base de este concepto original después de implementar sistemas de sensores inalámbricos de largo alcance operando en un ambiente hostil, durante periodos extendidos. A partir de los datos recolectados y de las métricas de desempeño, se observó que los cambios de la T y RH siguen de cerca a los cambios de niveles registrados del RSSI de día y de noche, por lo que a este comportamiento se le llama gradiente TRH. El algoritmo propuesto emplea a dicho gradiente como argumento de una función logarítmica, junto con un factor llamado coeficiente α_0, para regular la ganancia de la potencia de transmisión. Y para acelerar el entendimiento del comportamiento del algoritmo, se desarrolló un ambiente de simulación que emplea valores reales de entrada para probar el modelo actualizado del algoritmo TRH TPC. A partir de varias corridas de la simulación, usando un amplio rango de entradas, se determinaron criterios de valores óptimos de los parámetros involucrados. Finalmente, se volvió a realizar la implementación real del TRH-TPC, esta vez con los criterios óptimos. Los resultados de esta última implementación real del algoritmo TRH TPC corroboraron el comportamiento esperado del algoritmo y los valores del RSSI obtenidos a través de la simulación, logrando un tasa de paquetes recibidos de más del 95%, sin retransmisiones.

ABSTRACT of the thesis, presented by César Ortega Corral in order to obtain the DOCTORATE of ENGINEERING DEGREE. Tijuana, Baja California, México. February, 2015.

Temperature and Relative Humidity based Transmission Power Control for Wireless Sensor Networks

Approved by:

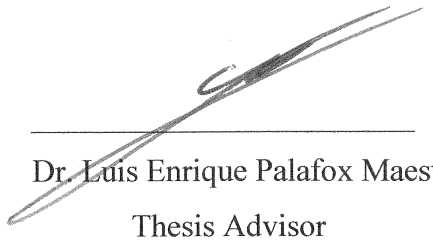

Dr. Luis Enrique Palafox Maestre

Thesis Advisor

Abstract

In this work, a novel temperature (T) and relative humidity (RH) based transmission power control scheme is presented; its model uses received signal strength indicator (RSSI) feedback. The intended application space comprises any long range outdoor wireless sensor network (WSN) communications. The basis for this original concept was determined after deploying long-range wireless sensor systems in harsh environmental conditions, for an extended period of time. From the gathered data and performance metrics, it was observed that T and RH closely follow changes of the day/night RSSI recorded levels, this is why this behavior is called the TRH gradient. The proposed algorithm uses this gradient as the argument of a logarithmic function, along with a parameter called α_0 coefficient, which regulates the overall transmission power gain. In order to accelerate the process of understanding the behavior of the TRH approach, a simulation environment was developed that uses the acquired information as inputs of an updated version of the TRH TPC algorithm. After many simulation runs, using a broad range of inputs, a set of optimal parameter values was determined where this TRH TPC scheme works best. And to confirm the usefulness of the developed criterion, the proposed algorithm was again deployed on real wireless sensor systems. The overall performance of the TRH TPC final deployment corroborated the simulations RSSI results obtaining more than 95% packet reception rate, without transmission retries.

Contents

List of Tables

List of Figures

Chapter I. Introduction

The study of wireless sensor networks (WSN) is a field that a few years ago was on the cutting edge of wireless communications research and development. Now, WSN concepts and applications are becoming common knowledge for graduate and undergraduate students [1,2]. There have been many proposals for WSN architectures and operations, such as cooperative routing protocols, alternative medium access methods and power saving schemes for extending their deployment [3,4]. Here, work was done developing an algorithm that controls the amount of transmission power with the aim of guarantying reliable data delivery and to limit power consumption. In this chapter, my motivations are explained, I also describe the problem definition, the proposed solution, and methodology, and finally, we outline the content of this document.

1.1 Motivation.

Transmission power control (TPC) has been around since the first wireless computer network developments [5]. Now, that wireless sensor networks (WSN) are at the forefront of ubiquitous deployments [6], power saving features are indispensable for long term deployments; and TPC is just one of several power management strategies [7]. In contrast, some consider that TPC is more a reliable data delivery technique, by minimizing data loss, and that power saving is a collateral effect rather than its main objective. The idea behind TPC is that transmission power can be dynamically adjusted according to a particular performance metric (i.e. received signal strength, link quality or packet received rate), with the objective of maintaining the observed performance as high as possible [8]. Another situation where TPC is useful is when the wireless channel is crowded with several interfering sources, dynamic power adjustment can help mitigate interference by increasing transmission power over such signals [9].

After experimentally observing the existing relationship between the TRH gradient and wireless signal power loss, it inspired the concept of using this TRH deterministic combined variable as a gain factor for TPC, which is a novel concept not considered in the current literature.

1.2 Problem description.

Environmental WSN deployments are usually characterized by being outdoor long range communications applications, where extreme climate changes and sun exposure pose difficult challenges for long term deployments [10-11]. Harsh weather conditions produce adverse effects on the wireless channel quality, such conditions represent the most appropriate situations for deploying TPC. One particular aspect of environmental WSN application spaces is marine sensor networks, here TPC is also a very convenient approach with the aim of reliable data delivery and optimal transmission power operation.

1.3 General and specific objectives.

The objective of this thesis is to develop and test an effective transmission power control algorithm, for environmental WSN, which depends on received signal strength feedback and the prevailing temperature and relative humidity (TRH) conditions.
The specific objectives are:

- Investigate the availability of suitable WSN technology, with enough configurable transmission power levels, to obtain an accurate TRH TPC algorithm characterization.
- Determine what kind of wireless communication performance metrics are useful for a TPC scheme based on temperature and relative humidity.
- Determine the parameters that affect the behavior of the proposed TRH TPC model.
- Evaluate the TRH TPC models performance, through experimentation in harsh conditions, and discover its optimal parameter ranges.

There are many hidden details pertaining to these project objectives. And it does not end with an initial TRH TPC model definition. The goals of this thesis are more ambitious than that; they aim at real testing with developed long range WSN technology for environmental monitoring. And these goals also aim to determine the optimal parameters for an effective TPC scheme based on proven TRH gradient observations and deployment results.

1.4 Methodology.

Initial activities revolved around a documental investigation of the state of the art of wireless sensor networks and their actual implementations, so as to determine the research problem. It then became evident that there are many areas of opportunity for different types of long-range outdoor applications (such as marine, environmental, and urban WSN). From the different WSN research aspects, it also became apparent that transmission power control has scarcely been investigated; although it promises an increase of data transfer reliability and of optimizing power use. This research effort led to narrowing down the possibilities to existing TPC algorithms and permitted to establish this thesis objectives according to formulated questions, derived from the current literature. After a thorough review, it was decided to construct WSN nodes as experimental devices tailored to a set of imposed requirements; such as using rapid development hardware and long-range radios that have a broad range of transmission power levels, for an effective TPC deployment. Experimentation began after these WSN systems were built and carefully evaluated, confirming the validity of their acquired temperature and relative humidity sensor data, and for determining the received signal performance of their wireless communications capabilities. The deployed WSN devices performance results and environmental condition measurements were observed, which led to the initial TRH gradient behavior assessments. From the cumulative performance and sensor data information, an original TRH TPC prototype model was proposed and tested under harsh conditions obtaining promising results. For further evaluation of an updated TRH TPC model, the wireless sensor system software was extended to acquire real simultaneous radio-frequency power assessments to determine the average channel noise-floor and potential interference sources. From the gathered data, with the intent of accelerating the experimental process, a knowledge-base was built as the input source for a realistic TRH TPC simulation platform. After many simulation experiments, which tested the full range of relevant parameter variations using real input data, an optimal set of TRH TPC parameter values were found. And finally, the conclusive experiment was a two-week real weather deployment; its results corroborated the TRH TPC simulation expected outcome, with the added benefit of experimentally determining the actual packet reception rate performance.

1.5 Document organization.

The organization of this document is as follows: In this chapter, I explained my motivation for doing this work and also presented the problem definition in general terms. I then proposed the solution as a general objective, and detailed some aspects through a set of specific goals. I ended this introductory Chapter by describing the methodology used for developing and testing the proposed TRH TPC scheme. Onwards, in Chapter II, I present the theoretical framework behind the state-of-the-art of WSN and concepts about wireless link metrics; and continue presenting related work done developing and testing an experimental long range marine habitat WSN. I end this second Chapter presenting the ideas behind TPC, including different proposed approaches and recent work done that considers temperature variations for power compensation. In Chapter III, my original proposal is presented, where I make observations of the correlation that exists between changes of temperature and relative humidity against received signal strength variations. I continue by establishing the initial TRH TPC model with a single TRH controller set-point. Later on, after implementing the single set-point TRH TPC prototype, I present its experimental results and determine its behaviour. From which, a modified dual set-point TPC is developed and then simulated using real RF noise and non-controlled received signal strength values. After several documented simulation runs and TRH TPC parameter adjustments, an optimum set of conditions is determined and proposed for implementation. And finally, in Chapter IV, I present an outdoor deployment and its results of the updated TRH-TPC scheme against a non-controlled wireless system. This last set of experiments corroborate the simulated TRH-TPC behaviour with hard results and the optimal parameter value criterion.

Chapter II. Wireless environmental sensor networks and transmission power control

Environmental wireless sensor network related issues are brought up and wireless alternatives are briefly discussed; followed by an overview of wireless sensor networks: architectures, protocols, technologies and performance metrics. A case study is also presented, of an experimental hierarchical WSN for marine habitat monitoring. Several days results of acquired temperature, relative humidity and received signal strength values are shown and discussed, paving the way for testing my TPC proposal.

2.1 Wireless sensor networks (WSN)

Notions of environmental sensor networks are not new, for years, electronic analog data logger systems had been deployed with the disadvantage that most often timely information was unavailable because the data logging was done on paper, and could not be accessed until the devices were manually retrieved from designated locations [12], usually far away. Digital electronic versions were later developed, but continued to require a direct wired connection to be able to download data from the systems memory. Modern environmental monitoring relies on recent sensor network technologies, consisting of spatially distributed autonomous devices that use various sensors to measure environmental conditions. Communication between sensing units, in most cases, is done wirelessly and they cooperate between them to transfer gathered environmental data to the end user in a timely manner. Many remote telemetry solutions have been applied with noticeable unreliable wireless channel conditions due to the surroundings.

When deploying wireless underwater monitoring systems (besides possible electrical shorts) communication problems have to do with energy absorption and dampening of electromagnetic (EM) signals, limiting wireless options [13, 14]. Alternative underwater solutions have been found using infrared signals for very short-range communications achieving distances of a few meters; this is because optical communications strongly depend on the seawater's transparency [15, 16]. In other words, opacity causes optical loss limiting communications in shallow seawater, where floating sediment is often the cause of turbidity in lagoons and river outlets. Another legacy wireless option is underwater sound messaging instead of EM signals [17-19], with possible collateral effects that may harm sea

mammals and other species threatening their survival by interfering with their abilities of using acoustic signals for hunting, communicating and undersea navigation [20,21]. Because of this, biologists and environmentalists are actively debating this issue, so in order to establish wireless communication in marine habitats the matter of choosing the propagation method it is not just of a matter of practicality but also a matter of ethics.

New wireless technologies have permitted the development of so called next–generation environmental science, where data resolution is ever increasing due to deployed sensor network growth, and application of heterogeneous approaches and technologies as shown in the example of Fig. 2.1 [22]. However, deploying dense sensors in harsh remote environments remains a challenge first of all because such a system has to be energy efficient to be able to do power consuming processes, such as sensing, computing and communicating over long distances. Battery operation is an issue that has to be addressed, and has to be a well thought fault tolerant design, some "out of the box" green energy solutions are already available, but cannot always be deployed in a dynamic environment. Also, common sense indicates that electronic sensing systems and communication links have to be robust enough to withstand harsh environments [23].

Although wireless sensor networks were originally envision for land operation at very short distances, WSN can be deployed at sea with increased power providing onsite distributed sensing at specific locations, and are complementary to existing satellite and airborne monitoring which tends to be very expensive [24].

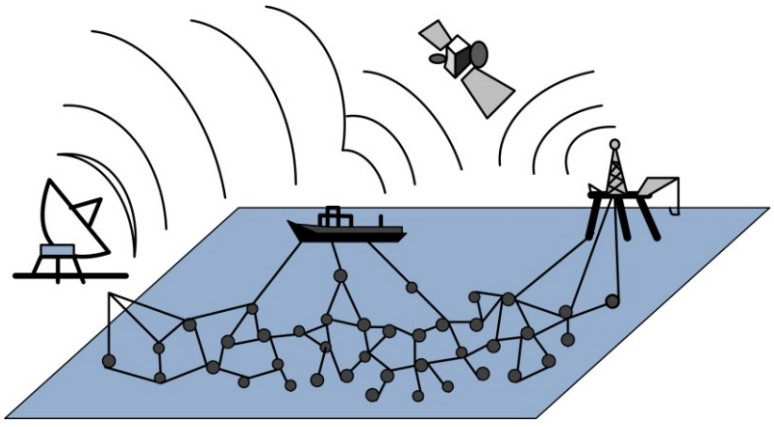

Fig. 2.1.1. Different technologies used in next-generation sensor network monitoring.

2.1.1 WSN application space.

Research projects and general ideas about WSN have been around since the late 1990's. A pioneering project in this field of study was called "SmartDust" [25 - 28], it envisioned that nanotechnology development would lead to the design, construction and deployment of very small, very low power optical wireless nodes (with sensors onboard) capable of forming self organizing networks for pervasive sensor data transmition. These devices would be as small as dust particles or motes, and thus the word "mote" was coined to symbolize a WSN node [29].

In general, a WSN is a collaborative collection of wireless nodes capable of sensing, processing, and communicating environmental data from one node to another, providing in some cases multi–hop data transmition [30 - 32]. These nodes are sometimes deployed to detect and track particular objects in a specific area. In a WSN the information of interest is sent through a gateway –or sink node– to the final user, as shown in Fig. 2.2.1.1.

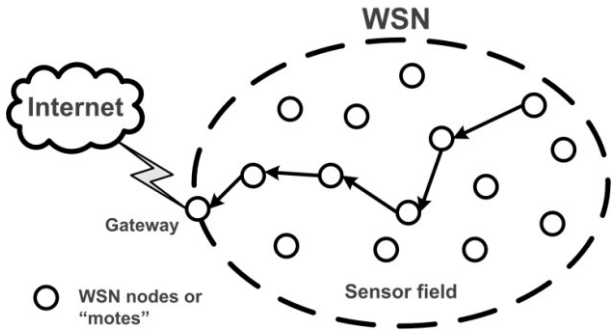

Fig. 2.1.1.1. Depending on the WSN architecture, data can take different paths when nodes become routers.

From the beginning of WSN development, work was started on building prototype motes trying to make them as small as possible [33, 34]. Mote prototypes were equipped with hardware composed of low power radios and sensors interfaced to a limited resource microprocessor, in Fig. 2.1.1.2 generic internal mote architecture is shown. The motes application software could be run on top of an operating system designed to manage input/output (I/O) operations with the motes' peripherals, such as: analog to digital (A/D) converter data requests, radio transceiver interactions and drive serial port communications, all this with the idea that motes would develop into ever smaller self-organizing data acquisition wireless computers.

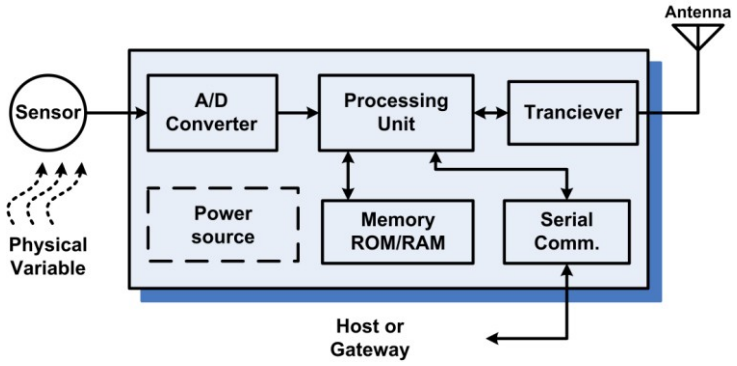

Fig. 2.1.1.2. Internal node architecture, a mote is considered a small wireless data acquisition computer.

Research in sensor networks has drawn much attention, extensive literature is now available focusing on different aspects of WSN theory, such as: wireless node and network architectures, routing protocols, data gathering techniques, power saving features and security [35-38]. Several recently published papers introduced pragmatic issues of so called "application-centric" approaches [39-41]. Most of recently published work can been divided in two research areas: (1) Algorithms and protocols, and (2) application-centric system design. Some argue that few try combining both areas leading to fatal flows when actual deployment comes around [42]. Most of the time, WSN nodes are low power devices with data acquisition capabilities for long term remote operation, this way conserving power supply energy is then a central issue in real world application designs. Because of this, many efforts have been done in proposing and developing data gathering, routing and power management protocols with energy awareness in mind [43-45].

On the WSN application side, there are many fields that can benefit from their deployment. In Fig. 2.1.1.3, some application areas are enclosed in circles with particular applications labeled at their side. In this work, for testing the proposed transmission power scheme, the intended application space is marine environment monitoring. Where, in most marine data transmition cases, the main problem is optimizing power consumption in order to deal with the great distances that usually separate WSN nodes in the field from their base station at the seashore. In this sense, conventional WSN fall short due to their initial conceptualization of forming personal area networks. This means that when considering WSN for marine deployments, where transmission power loss is a main issue, the right transceiver has to be evaluated and carefully selected in order to assemble an appropriate wireless sensor node.

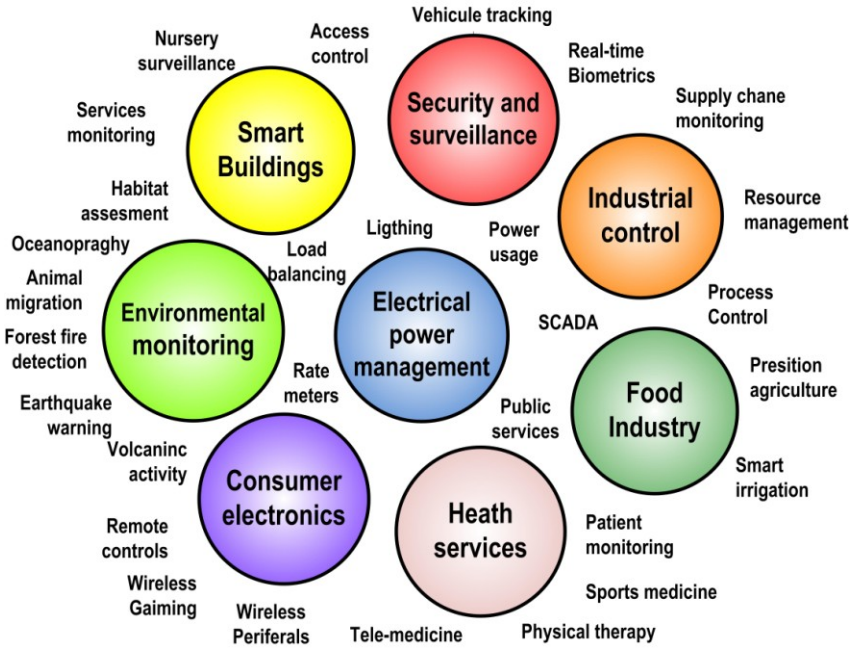

Fig. 2.1.1.3. Types of WSN application spaces.

2.1.2 WSN architectures and protocols.

In a general sense, WSN architectures are grouped in two classes: hierarchical and flat networks; this depends on the type of topology structure [46]. Also, another group of protocols has been proposed, the so called position based routing that takes advantage of recent Global Positioning System (GPS) technology [47]. In network theory, the oldest is the hierarchical or tiered architecture, which is based on tree or extended star topologies. Since the 1950's, legacy communication systems were based on tiered networks that had to deal with data congestion at the higher levels or backbones [48]. On the other hand, during the 80's flat networks based on mesh topologies started to gain prominence because they offer redundant data routes. In other words, flat architectures are multi–path networks with the advantage that if a particular route comes down –because it got disconnected, congested or is unavailable– other backup routes can take its place, looking to guarantee data delivery [49]. In WSN development, flat architectures were appealing from the start because of their cooperative and self-organizing features, which are very useful if node mobility is an issue. In Fig. 2.1.2.1, examples of both hierarchical and flat networks are shown.

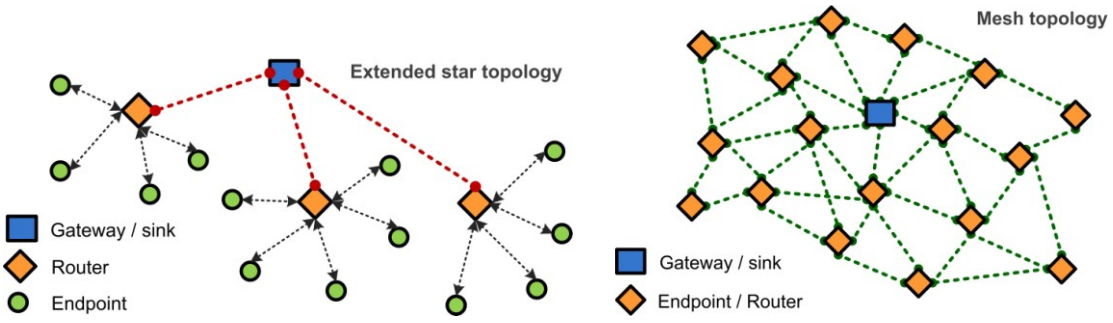

(a) (b)

Fig. 2.1.2.1.(a) WSN hierarchical network tree topology. **(b)** Flat WSN mesh topology.

Hierarchical WSNs usually use a two tier (or two level) extended star (or tree) topology. In the lower tier, sensor endpoints are organized into reduced area subnets (or clusters), and at the higher tier intermediate routing nodes (called cluster-heads) convey endpoint data to the gateway [50, 51]. In this case, two-hop routing is needed. In contrast, when the sensor nodes associate in a mesh topology (or flat network) every node can act as a router (or repeater) transferring data in a multi–hop manner to its destination. This type of WSN is popular because it can offer multiple data paths (or routes) in a dense network. If one route is unavailable other routes take its place. It is worth mentioning that many WSN use a combination topologies, and are called hybrid architectures [52] with partial mesh router topologies and at their boundaries the network endpoints associate with WSN routers in star topologies.

WSN Protocols

To ensure correct data gathering and transmission, many WSN protocols have been proposed to manage network operations. Static point to point radio links have been substituted with multi–hop networks and radio repeaters have been substituted with wireless routers, and now dense deployments are plausible and encouraged in many application scenarios. Dynamic routing in WSN schemes, for extended periods of remote operation, do not just determine routes but also need to have power awareness. A list of routing challenges and design issues that affect WSN reliability is presented next [53, 54].

- **Node deployment.** Sensor location deployment can be deterministic or random. In a deterministic deployment, sensor locations are chosen strategically beforehand usually forming a static WSN, and routes can be predetermined. While random

sensor deployments can be the result of non-planned placement of sensors or of WSN node mobility, in this case the network topology maybe dynamic and usually ad hoc routing is applied.

- **Energy consumption.** One of the main concerns in WSN remote deployment. Different power saving strategies have been proposed in route management, such as power balancing, clustering, sleep scheduling, route alternation, adaptive transmission power, etc.
- **Data Reporting Model.** The way data is going to be acquired and forwarded to the sink.
- **Node/Link Heterogeneity**. Where wireless devices have different resources and power capabilities, such as computing and transceiver power.
- **Fault Tolerance.** The hardware, accessories and encapsulation have to be suitable for the application environment and the electronics have to be tolerant to failure.
- **Scalability.** This depends on the projected network growth regarding the number of endpoints, routers and may need cluster network formations.
- **Network Dynamics.** If the network is static, mobile or a combination that might constantly change the networks topology.
- **Transmission Media.** Depends on the networks physical layer; in other words, depends on the particular wireless medium propagation characteristics.
- **Connectivity**. In many cases, expected line of sight scenarios connectivity shouldn't be a problem if the distance requirement is met. But in other applications line of sight might be lost at times. For example, in marine deployments when wave activity is considerable radio links might be block.
- **Coverage**. Depending on the sensor location coverage may be an issue if it's not positioned correctly, or if the sensor is too far from the variable of interest.
- **Data Aggregation.** Sensor nodes may generate significant redundant data; similar information from different nodes can be aggregated to reduce transmissions. Aggregation is often suggested as an energy saving technique and for routing optimization.
- **Quality of Service (QoS)**. This depends on the end user requirement of timely variable measurements and data retrieval. In cases where data streaming is a must,

any samples that don't get sent on time impact on the overall information gathered from the sensor field.

In general, WSN routing protocol proposals have been envisioned from different perspectives, they can be grouped based on network structure or on the protocol's operation, as shown in Fig. 2.1.2.2 [55]. The first view addresses particular application issues where the WSN's architecture or topology is at the heart of the matter; while the second classification groups protocols by their operational characteristics. These two general classifications aren't mutually exclusive, meaning that any of the WSN protocols can be associated to both classification groups. In this case, the main interest in classifying protocols is in the network structure's perspective, because any real deployment of a WSN starts with obtaining application specific requirements from which common sense will yield the appropriate topology during the problem solution formulation.

Another important aspect of WSN routing protocols is if the network is homogeneous or heterogeneous in nature [56]. When all WSN nodes have the same resources and play the same role then it's called a homogeneous network. On the other hand, if the network nodes have different resources and different roles to play then it's called a heterogeneous WSN. The following protocol descriptions will focus on network structure based protocols and will address the issue of heterogeneity.

2.1.3 Types of embedded wireless modules.

In the late 1990's, researchers and engineers working for the University of California at Berkeley became pioneers of modern WSN device integration. Those efforts led to the first general WSN device architecture known as the Berkeley mote and developed the basis for

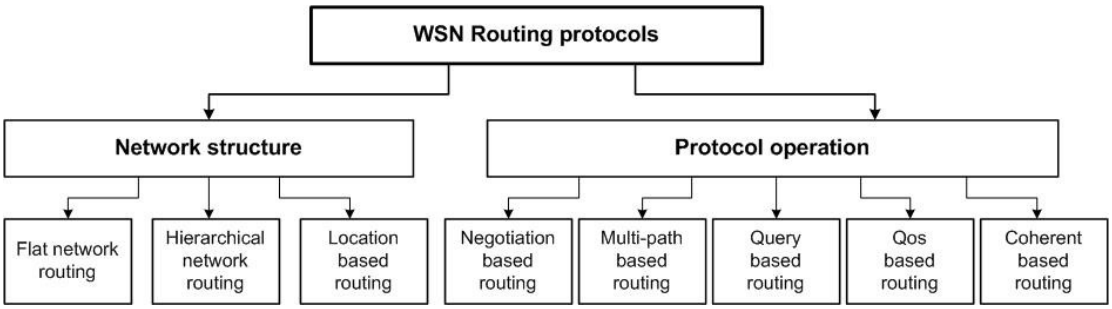

Fig. 2.1.2.2. WSN routing protocol family classification.

what now we call middleware [57, 58]. Although other universities, research centers and private companies were starting to develop WSN technologies; many efforts were similar to the Berkeley architecture. Others opted towards developing standalone configurable transceivers, which sometimes are interfaced to other external microcontrollers for more powerful master-slave application development, building custom "mote type" devices in the process.

Modern *transceivers* are configurable wireless digital modules, internally they are made up of serially connected radio systems (transmitters and receivers, TX/RX) to host microprocessors (or microcontrollers) that serve as interfaces between the wireless data exchange and the end user [59]. In order to hold their startup configuration, these transceivers usually use non-volatile memories, where permanent values are stored in ROM (Read Only Memories), or in read/write memory spaces such as EEPROMs (Electrical Erasable Programmable Read Only Memories), or in NV-RAM (NV Random Access Memory) chipsets, or even in FLASH data storage devices [60]. This NV memory approach enables on-the-fly radio configuration and data exchange with the outside world. These transceivers are part of a larger embedded digital system that can be reconfigured and operated by uploading routing and application software to their internal host program memory. Another approach uses serially issued commands to write configuration parameters directly to the transceivers registers to modify their behavior. The use of AT style protocol commands (ATtention protocol, which is a legacy alphanumeric character modem configuration protocol, developed by Hayes Inc.) is sometimes used for efficient transceiver configuration with little effort involved. Originally, AT commands were designed for human interaction by an operator conveying serial communication alphanumeric attributes and parameters to a device for its correct operation [61, 62].

On the other hand, open frequency ranges for these readably available transceivers are in the internationally accepted Industrial-Scientific-Medical (ISM) license free bands, in Mexico, these are located at: 915MHz, 2.4GHz and 5.8GHz center frequencies [63]. Most up to date WSN transceivers operate at 910MHz or 2.4GHz bands, complying with the IEEE802.15.4 standard. The first frequency band, 902 to 928 MHz, has the advantage that communication at these lower frequencies leads to longer distances with less power compared to 2.4GHz communications due to longer operational wavelength. The main

advantage in working within the 2.4GHz frequency band is that it has wider bandwidths compared to 910MHz range. Two such commercial transceivers are the 2.4GHz XBee Pro [64] (by Digi Inc.) and the 900MHz AC4490LR-1000 [65] (by Laird Tech). Their main characteristics are presented in table 2.1.3.1.

Table 2.1.3.1 Transceiver characteristics comparison between the XBee Pro Series 1 and the AC4490LR-1000.

	Transceivers	
Feature	**XBee Pro S1**	**AC4490LR-1000**
Manufacturer	Digi Incorporated	Laird Technologies
Channel contention	Direct sequence spread spectrum (DSSS)	Frequency hopping Spread spectrum (FHSS)
Carrier frequency	2.4GHz	915MHz
Operating voltage	3.3 V	3.3 – 5 V
Max. Transmitter power	63dBm	1000dBm
Receiver sensitivity	–100dBm	–110dBm
Distance	1.5Km	20Km
Sleep current	0.6 µA	6mA
Throughput	250Kbps	76.8Kbps
WSN standard	IEEE802.15.4	Proprietary MAC
Transmission power levels	5 levels [10,12,14,16,18] mW	81 Non-linear levels [5, ... , 1000] mW
10-bit ADC inputs	6	1
Digital I/O pins	8	2
Encryption	AES 128-bit	DES 56-bit
Configuration	Proprietary AT commands API Frames	Proprietary AT commands API Frames

The XBee Pro is a transmition power boosted version of the 2.4GHz XBee Series 1 transceiver, which complies with the IEEE802.15.4 standard for forming and maintaining 1Km range WSN. It has six configurable Tx power levels: 10, 12, 14, 16, 18 dBm. Its throughput is of 250Kbps. Meanwhile, the AC4490LR-1000 is a high power transceiver (5mW to 1Watt) with extended range capabilities of up to 20Km in line-of-sight (LOS). Its throughput is only 76.8Kbps, but it has an enhanced -110dBm reception sensibility, making it suitable for long-range sensor data communications.

The XBee Pro can operate in a standalone fashion, with automatic sample and transfer capabilities, while the AC4490 does not have much intelligence in that sense. The AC4490 needs a host system in order to do automatic sampling and data transmition. Another difference is that the XBee has linear transmission power levels, while the AC4490 has non-linear Tx power levels. This meaning that any of the 81 levels are not linearly proportional to the actual power values, this non-linearity is shown in Fig. 2.1.3.1.1, where the transmission power levels fit a curve against the discrete (0 to 80) AC4490 power levels is shown [66].

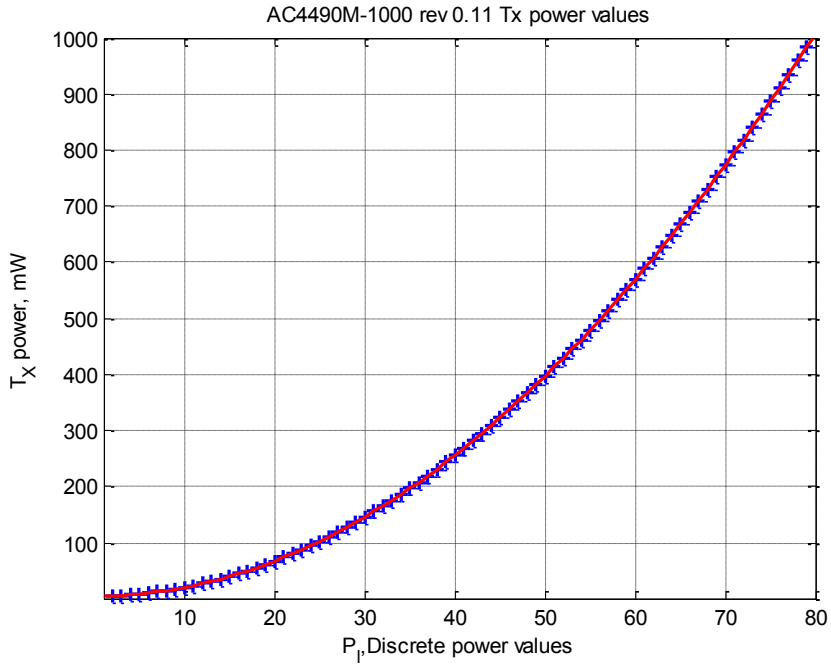

Fig. 2.1.3.1.1. AC4490-1000 transceiver non-linear discrete transmission power values.

On the other hand, when the AC4490 is receiving, it also has a non-linear Rx power reading, this is discussed in section 2.1.4.1.

Host microprocessors and their role in WSN

Any up-to-date communication device has a microprocessor, microcontroller, digital signal processor or digital embedded system at its core. In the field of WSN, the microprocessor (programmed or firmware configured) is the main interface device that enables information to flow into and out of a network. An early host-target or master-slave

scheme in WSN is the Berkeley mote, today there are many other types of wireless sensor devices. A commercial example of a WSN device that uses XBees is known as the Wasp mote [67], shown in figures 2.1.3.1 and 2.1.3.2. It is an integration of an XBee module interfaced to an Atmel microcontroller based on the ArduinoMega open hardware system [68] and other peripherals.

Fig. 2.1.3.1. Wasp mote based on XBee and Atmel processors.

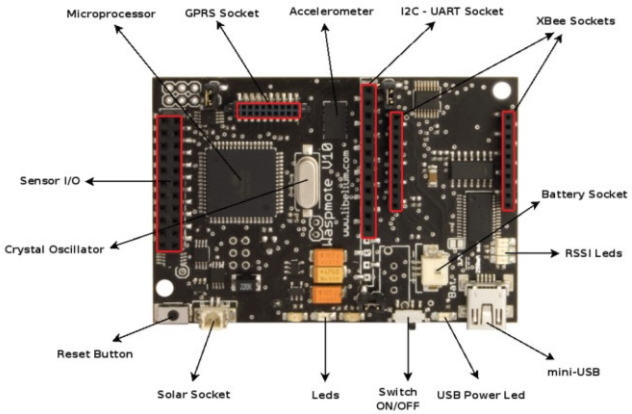

Fig. 2.1.3.2. Wasp mote board layout showing interface and expansion sockets.

Open Arduino platforms have become very popular because they offer high-level embedded C++ programming capabilities, and extensive input/output (I/O) libraries for connecting and managing peripherals.

2.1.4 Wireless link quality metrics.

Different metrics can be used to determine the quality of wireless links. The most common metric at the wireless physical layer is the received signal strength indicator (RSSI) [69,70], which is represented as a digital value at the medium access control (MAC) layer. Another metric is the packet reception rate (statistically obtained at the routing and application layers). These concepts and their usefulness are presented next, as well as related deployment issues.

2.1.4.1 Received signal strength indicator (RSSI).

All modern WSN transceivers have a way of reporting to their host system the power level at which RF signals is being received. The most commonly used RF link quality estimator is called the *received signal strength indicator*, RSSI, measured in mW or dBm, in either analog or digital form. It is a value that is updated by the wireless receiver each time it recognizes and decodes a valid wireless message received at its antenna. This RSSI is usually employed in systems that use radio channel co-existence schemes, such as frequency hopping and listen-before-talk (LBT) paradigms. A simple and popular type of LBT is known as *carrier sense multiple access* (CSMA), where the transmitting device senses signals on a particular channel from a set of channels and it postpones any transmission if the channel is being used by another signal source. Afterwards, with certain timing, CSMA tries again on another channel in a pre-determined manner.

For example, authors in [71] state that "The IEEE 802.11 standard defines a mechanism by which RF energy is to be measured by the circuitry on a wireless NIC. This numeric value is an integer with an allowable range of 0-255 (a 1-byte value) called the Receive Signal Strength Indicator (RSSI)".

"RSSI may be used to determine RF link quality and is very useful in dense traffic scenarios where interference is of major concern. RSSI is typically employed in channelized systems utilizing co-existence schemes such as adaptive frequency hopping and listen-before-talk (LBT). A carrier sense multiple access (CSMA) device implements one type of LBT. If a channel is sensed busy, transmission is postponed. If several channels are available the transmitter can first check if the channel is idle. If not, the transmitter will try a different channel." [72]

"While RSSI can be used as a tool to give an indication of link quality, it does not always give definitive results. In addition to normal variation in received signal levels, the signal level can also be affected by in-band interference sources. When this occurs, a strong signal level can be reported, but data can be corrupted. Communication systems should be designed with some link margin". [73]

The way the RSSI is interpreted and used depends on the type of transceiver. For instance, the well known 2.4GHz XBee Pro transceiver has an internal register, called DB, which holds the RSSI value of the last successfully received packet in dB, which actually represents the direct RSSI value in dBm. This value is reported in every XBee Receive Data API packet, or it can also be queried with an XBee API command. Another example is the previously mentioned long range Laird AC4490 [74], which also has an internal register called the "validated" RSSI, or VRSSI, which according to the AC4490 users manual is an 8-bit coded word that must be converted to dBm with the following expression.

$$\mathrm{RSSI}_{\mathrm{AC4490}}(\mathrm{dBm}) = -46.9 * \frac{\mathrm{VRSSI}}{255} - 53.9\ \mathrm{dBm} \qquad (2.1.4.1.1)$$

Equation (2.1.4.1.1) shows that the maximum RSSI that the AC4490 can read is -53.9 dBm. This means that the radio is designed to be used in a far-field application. Likewise, the last valid RSSI value is also reported within each header of its Enhanced Received API packets or within API send data complete packets, all this is explained in section 2.3.3. It is worth noting that the reported AC4490 RSSI does not follow a linear behavior. The information that the manufacturer gives out on this matter is very limited. The only hard data available from the manufacturer about possible RSSI values are shown in Table 2.1.4.1.1, which after curve fitting yields the charted function that is shown in Fig. 2.1.4.1.1. On both RSSI chart and table a shadowed area indicates the RSSI values that are not reliable, and definitely non-linear. Meanwhile, validated RSSI values are the ones bellow the maximum readable RSSI at -54dBm (equal 0x16 = 20_{10} code word). Nevertheless, its apparent in Fig. 2.1.4.1.1 and Fig. 2.1.4.1.2 that the RSSI function is linear in certain operating sections, such as the ones between -60dBm and -70dBm, from -70dBm to -74dBm, and between -80dBm and -94dBm. Although this transceiver's RSSI is non-linear, it can be approximated in a linear piecewise fashion.

Table 2.1.4.1.1. AC4490 discrete RSSI values given by its manufacturer

Signal Strength (dBm)	RSSI value (HEX)	Signal Strength (dBm)	RSSI value (HEX)
4	0x0E	-62	0x2B
-2 to 1	0x0D	-66	0x40
-12 to -6	0x0C	-69	0x55
-36 to -22	0x0B	-72	0x62
-42 to -39	0x0C	-76	0x71
-46	0x0D	-79	0x78
-49	0x0E	-82	0x84
-52	0x11	-86	0x9A
-56	0x17	-89	0xAD
-59	0x1C	-92	0xBD

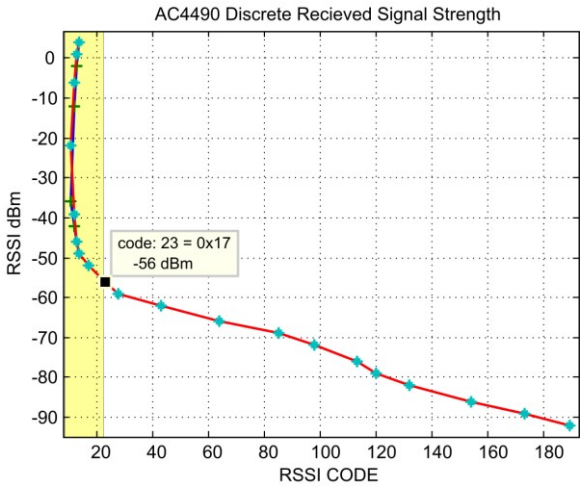

Fig. 2.1.4.1.1. AC4490 non-linear RSSI.

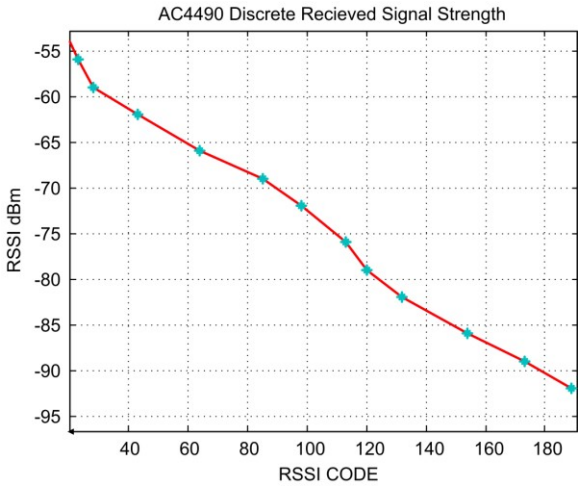

Fig. 2.1.4.1.2. AC4490 operational non-linear RSSI.

2.1.4.2 Packet reception rate (PRR) assessments

The packet reception rate (PRR) sometimes called packet success rate (PSR) is a straight forward statistical value expressed as a percentage that is obtained over time by averaging the amount of received packets, N_{RP}, against the total number of sent packets, N_{SP}, times 100%, as stated by (2.1.4.2.1).

$$PRR = \frac{N_{RP}}{N_{SP}} \text{ x } 100\% \qquad (2.1.4.2.1)$$

Because packets are groups of bits organized as bytes, the PRR is closely related with the well known physical layer performance metric called bit error rate (BER), but if just one erroneous bit comes within a packet, then the hole packet is deemed bad and discarded [75]. This PRR is indispensable to determine a communications link data transfer efficiency at higher layers, such as at the networking layer or at the application level. Meaning that PRR is a measure of the end-to-end data transfer reliability of any communications system. The amount of packets to be averaged depends on the particular system and its specified data throughput. When data transfers are far apart in time, one per second or less (such as environmental monitoring), the total number of received packets to average can be as low as 100 packets so as to obtain a short term PRR value. On the other hand, when data transfer is high (such as in Wi-Fi multi-media networks) the total number of packets to average may be from 10^3 to 10^6.

2.1.4.3 Base station performance metrics feedback.

Any TPC algorithm, running on a remote sensor node, needs data transfer performance feedback from the destination (or sink) node for it to determine the communications channel reliability [76,77]. This feedback depends on what network layer the TPC is working on. If the transmission power controller operates between the physical (PHY) layer and the medium access control (MAC) layer, it usually has either RSSI feedback and/or knowledge of the resulting BER. Otherwise, if it is a routing or application layer (or cross-layer) TPC scheme, then the best choices are either a RSSI signal or a PRR feedback approach. Some choose a combination of both RSSI and PRR, which represents a double feedback TPC system.

2.2 Case study: A hierarchical marine WSN and related work.

In marine monitoring applications, long distance between nodes and the harsh environment are the main challenges encountered during the problem definition [78]. In this case, modern mesh topologies may not be the best choices because usually a marine application WSN is not very dense, and their nodes are far apart. A better-suited topology is a star topology or even a hierarchical extended star approach. The WSN architectural choice depends on the size of the monitoring area and how dense the network is needed to be.

2.2.1 Application space: oyster farming at Baja California coasts.

The actual long-term deployment of a marine WSN using the proposed transmission power control scheme is intended to operate at a shallow bay called Bahía Falsa, at the western coast of the peninsula of Baja California, Mexico. In Fig. 2.2.1.1 a composite satellite image of this deployment site is shown.

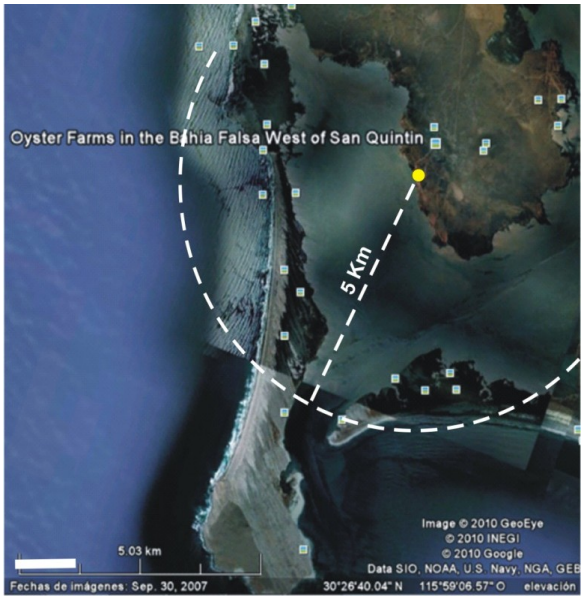

Fig. 2.2.1.1. WSN deployment site at Bahía Falsa, Mexico.

Because fresh seawater comes in with the tide, the local oyster industry is thriving at Bahía Falsa. In other words, the resulting water circulation brings plankton that serves as nutrients for the filtering species, which are 'farmed' with aquaculture techniques within sites leased to the oyster cooperatives by the Mexican government [79]. The oyster farm operators have an interest in deploying "real-time" inexpensive monitoring systems for updated information on the bays habitat conditions. Timely water quality information will

allow them to anticipate unhealthy conditions for the oyster species, which is determined by knowing habitat variables such as temperature, salinity, pH and dissolved oxygen concentration (DOC) levels [34,35]. Another important issue is distance, as shown in Fig. 2.2.1.1, the water inlet is 5Km away from an aquaculture facility known as Ostrícola Nautilus, located at Bahía Falsas inner peninsula. In general, a WSN that spans square kilometers can be considered a wide area (WA) network [80].

2.2.2 Hierarchical WSN architecture and its wireless nodes.

Considering several practical issues, such as: deployment cost per node, power requirements, maintenance, gateway distance, scalability and domain specific conditions; the proposed solution for the application scenario described above is the deployment of a dual frequency two tier hierarchical wide area WSN, composed of two levels or tiers. The upper (or higher) tier communicates using 900MHz open frequencies and the lower tier uses 2.4GHz frequency bands. As shown in Fig. 2.2.2.1, lower tier minimal hardware end-point (EP) nodes make up short range sensor clusters that send their data to more powerful cluster-heads (CLH) nodes, which serve as intermediaries between their associated lower level nodes and the overall Internet enabled upper tier Base Station (BS) system. Dual frequency communications by CLH nodes is accomplished by attaching two radios to the host controller: a 900MHz digital long range transceiver and a medium range 2.4GHz digital radio for EP communications.

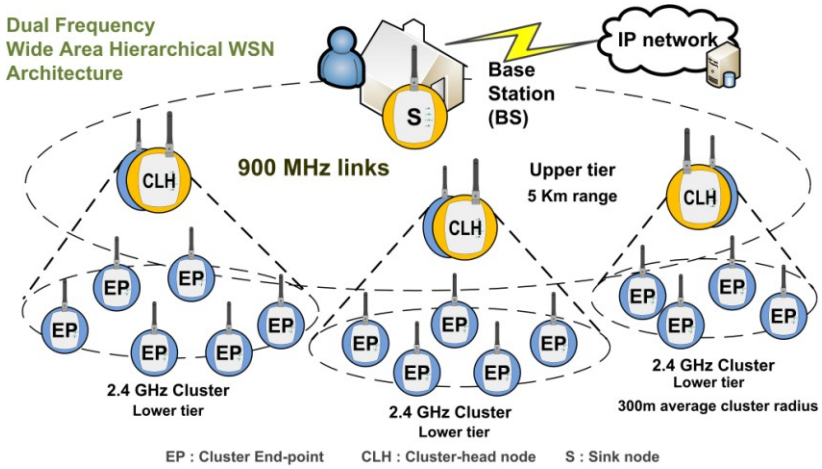

Fig. 2.2.2.1. Hierarchical WSN topology for long range marine habitat monitoring.

In this case, dual frequency nodes do not take turns to be CLH, under this scheme they are fixed CLH systems with local sensor sampling capabilities. This means that in this solution, CLH are permanent, canceling ideas that some have suggested of dynamic or adaptive CLH selection during start-up, aimed at balancing cluster node energy consumption [81,82]. The assumption here is that CLH systems have enough resources for their projected operational lifetime. One important advantage with this hierarchical approach is that, during a real deployment, most of the networks power consumption and short-term maintenance will be focused on a few CLH systems, instead of the need of constant maintenance of the entire network. For prolonged remote operation, in this deployment CLH and EP nodes are fitted with solar panels, for daytime battery re-charging. Likewise, for extending the life of EP nodes, the chosen lower tier technology permits Cyclic Sleep Scheduling, CSS, which saves up to 80% of battery consumption compared with normal EP operation where there is no CSC [83]. In Fig. 2.2.2.2, general use cases are shown that describe interaction between different tier agents.

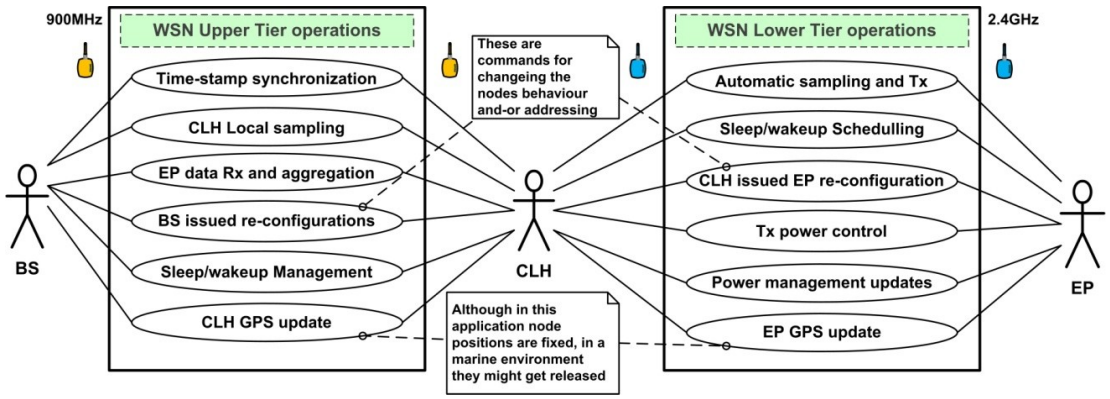

Fig. 2.2.2.2. Hierarchical WSN agent uses cases.

2.2.3 Long range communications, technology selection and device integration.

In order to build the hierarchical WSN, as shown in Fig. 2.2.3.1, three device integration designs were done: (1) the standalone XBee EP transceiver board, for lower tier sensor sampling, (2) the CLH systems, for lower tier sensor sampling, data gathering and upper tier long range communications, and (3) the base station, which acknowledges all received higher tier messages that translates and conveys to a DBS through its Internet gateway. The particular devices for testing a transmission power control algorithm, relevant to this thesis,

are the CLH and the BS systems, which make up the upper tier long-range communication links.

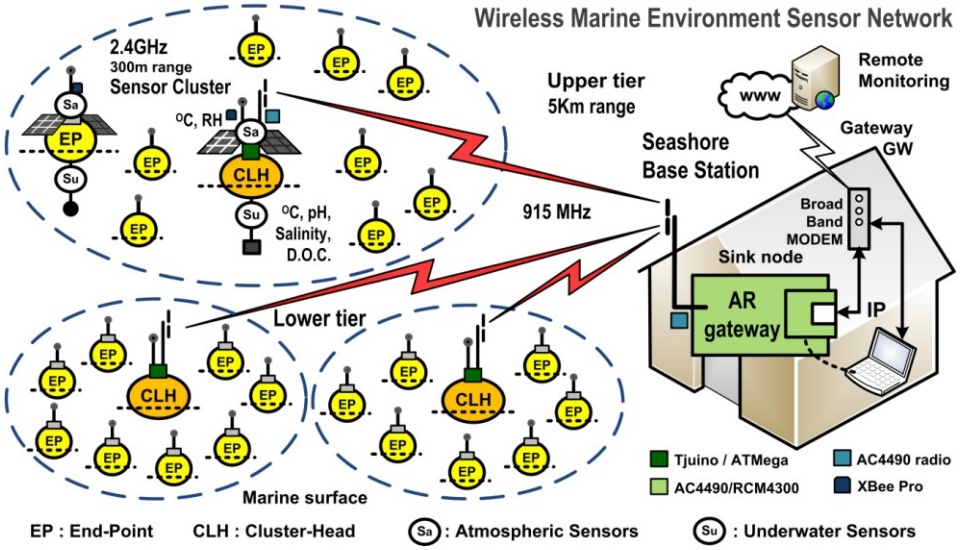

Fig. 2.2.3.1. Dual tier marine WSN and base station.

After an updated technology review, it was decided to integrate experimental CLH systems using programmable ArduinoMega2560 platforms for rapid application development [84,85]. And to enable CLH dual frequency communications, the previously described XBee Pro 2.4GHz and the 900MHz AC4490LR transceivers were connected to the corresponding ArduinoMega Serial 1 and Serial 2 interfaces. The resulting two-radio prototype CLH board is shown in Fig. 2.2.3.2.

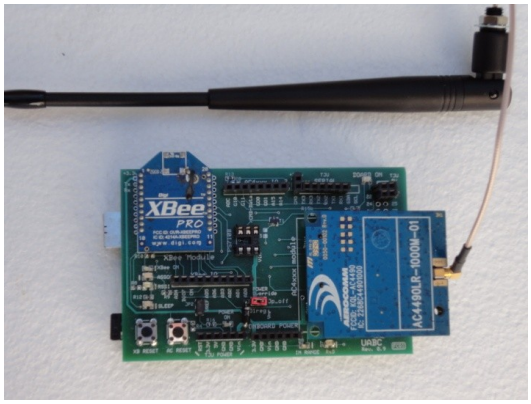

Fig. 2.2.3.2. Cluster-head communications shield on top of an ArduinoMega.

The main reasons for choosing the AC4490LR-1000 transceiver are: (1) it has long range communication capabilities (up to 30Km), and (2) it can be configured with any of

81 transmission (Tx) power levels, from 5mW all the way to 1000mW (with a 2dB antenna). This will help greatly in testing the discrete transmission power control (TPC) algorithms response and performance with adequate "granularity", against adverse and variable wireless channel conditions.

Similarly to EP systems, in this deployment the CLH nodes have their own sensor connections onboard, for acquiring local sensor data that is subsequently sent to the BS within upper tier application messages. Particularly, the CLH controller has at its disposal several 10-bit A/D input lines, four of them are initially used to acquire air and seawater temperature, air relative humidity and remaining battery voltage. Other variables that are considered are seawater pH and salinity levels. In most habitat monitoring systems, the sampling period usually is equal to several seconds or minutes. This means that most of these applications are not data intensive, and long intervals of inactivity can be used to put the node to "sleep" in periodic cycles aimed to conserve battery charge.

In figures 2.2.3.3.(a) and 2.2.3.3.(b), the EP and the CLH stack architectures are respectively presented. In can be observed that the CLH node has two different stacks representing both lower and upper tiers.

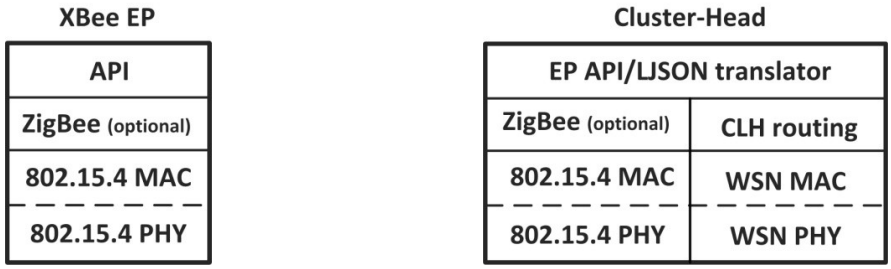

(a) (b)

Fig. 2.2.3.3. Hierarchical WSN device protocol stacks: (a) End-point and (b) Cluster-Head.

The microprocessor on board the CLH is the intermediary between both tiers, and can be considered working at the application layer level as well. This is because the CLH extracts lower tier data from incoming XBee API messages, then constructs upper tier aggregated messages destined to be relayed to the BS system. The upper tier application messages are fashioned according to a modified web application messaging protocol called "Light" JavaScript Object Notation, or LJSON [86]. After the BS system receives the higher tier CLH messages, its host microprocessor translates them to conventional JSON, opens an

Internet socket and sends them to a PHP application working as a custom JSON decoder for data validation and final DBS storage. In figures 2.2.3.4.(a) and 2.2.3.4.(b), the BS and the hierarchical WSN web service stack architectures are presented.

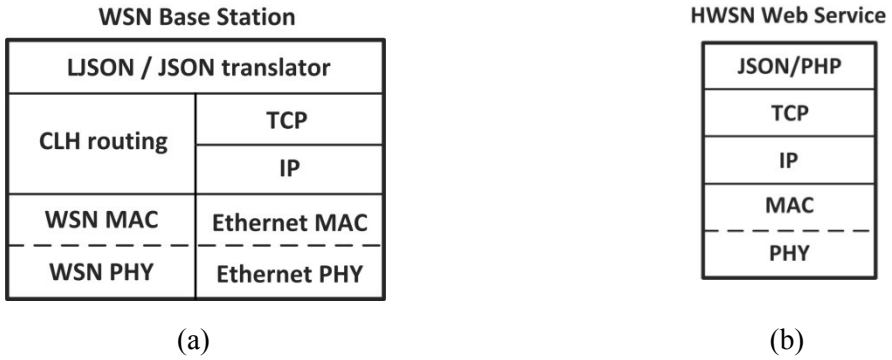

(a) (b)

Fig. 2.2.3.4. Hierarchical WSN protocol stacks: (a) Base Station/Gateway and (b) JSON enabled web service for WSN data storage.

The upper tier AC4490 transceiver operates in a master-slave configuration, or what the manufacturer calls a server-client scheme with the aim of synchronizing multiple clients' turn to send data through the wireless channel [87]. The server radio is in charge of sending a synchronizing channel beacon. The drawback is that with this scheme the server transceiver has to consume much more power than a client transceiver, which is why is usually placed as the sink transceiver at the BS where it is more certain that there will be enough available energy.

The Laird AC4490 can communicate in two states: as a transparent line or can be configured for API communication, which is meant for receiving and transmitting data in a more reliable way. This API is based on a framing structure that the host writes or reads from a pre-configured serially attached AC4490. Four kinds of API packet exchanges can be enabled: *Receive*, *Transmit*, *Send Data Complete* and *Enhanced Receive.* When a host is in this type of communication modes with the AC4490, specific packet structures are expected; the general API formats are shown in figures 2.2.3.5, 2.2.4.6, 2.2.3.7 and 2.2.3.8.

0x83	Payload data length	Source MAC	Payload data

Fig. 2.2.3.5. Laird API Receive packet

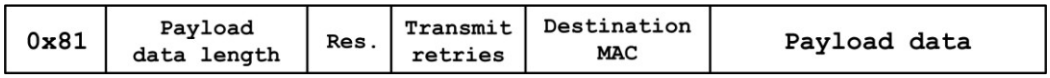

Fig. 2.2.3.6. Laird Transmit API packet model.

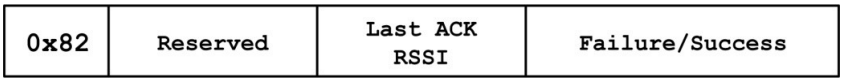

Fig. 2.2.3.7. Laird API Send Data Complete packet.

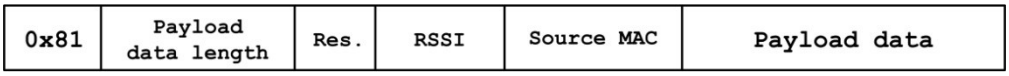

Fig. 2.2.3.8. Laird Enhanced API Receive packet.

In this deployment, the AC4490 radios are configured to operate in Transmit API mode and in Enhance API Receive mode. The Transmit API mode is useful because the BS can specify the destination CLH address on-the-fly saving the trouble of modifying configuration data stored within the transceivers EEPROM. Taking into account that an EEPROM has a limited amount of memory recording cycles, by performing as few as possible of these recording cycles, it avoids shortening the EEPROM lifespan. Likewise, the Enhanced API receive feature is convenient because it holds cross-layer information such as the RSSI value and the MAC address identifying the source node for performance measurement and routing purposes.

Although both CLH and BS have an AC4490 radio, we selected the Rabbit Controller Module RCM4300 to be the BS core processor module, because it has an Ethernet interface onboard that fully supports Internet connections [88]. The RCM4300 comes with a complete TCP/IP stack software library, through which the network interface is efficiently configured. Its software can run several semi-independent operations seamlessly using its so called main code Co-States and Co-Functions, in a unique state-machine paradigm for multi-task operations. In this project, the developed RCM software can work both as a client and as a server. As a client, the BS opens an active TCP connection only when it is required, such as during time synchronization or when LJSON messages arrive and have to be turned into standard JSON, then are sent to the custom WSN database web server. The resulting hardware in the form of an enclosed BS with antenna is shown in Fig. 2.2.3.9, along with the crossover connection to the DBS computer.

Fig. 2.2.3.9. Base station and crossover connection to the portable DBS server.

Two types of general information are conveyed from the CLH to the BS and stored at the DBS: (1) *sensor data* values, which are stored for the user's benefit; and (2) *performance metric* values, which log the RF communications channel quality and the message-received rate. The latter are useful for both TPC and/or power efficient routing purposes.

WSN application message integrity:

As previously mentioned, at the upper WSN tier, sensor data communication between the CLH systems and the overall BS is done using a modified Internet application layer messaging scheme called LJSON (or "light" JSON) [89]. This notation is limited to 8-bit characters and some redundant symbols are excluded from the conventional JSON syntax with the aim of composing highly structured character messages with shorter lengths.

Further CLH messaging refinements for experimentation, debugging and device testing purposes, led to include communication performance and reliability metrics. In this implementation, sensor data and performance metrics are grouped separately as arrays within the LJSON message structure. An example of such a message is shown in Fig. 2.2.3.10, where C:2 indicates that the message was generated by CLH number 2, En:0 means that no EP data is included in the message, An:5 symbolizes that the message holds five analog sensor values in the Av:[ ] vector array. These values are represented as integers to simplify their notation. Likewise, in the LJSON example the m:[ ] array includes the current performance metrics such as: the number of ACK messages, the total messages sent, the RSSI mean average, the calculated RSSI standard deviation, the instantaneous RSSI value when receiving the BS ACK message, and the sample message

ends with the CLH AC4490 transceivers transmission power level, used to send the message towards the BS.

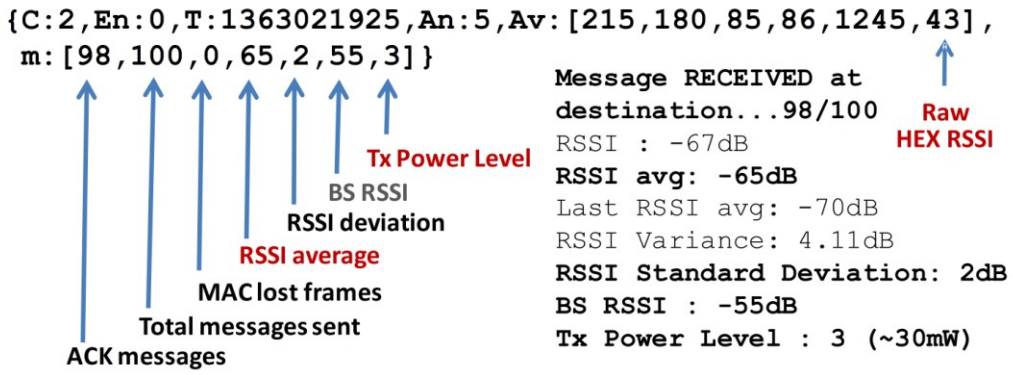

Fig. 2.2.3.10. CLH message structure example using LJSON.

In this thesis, for transmission power control purposes, the pertinent variables are: air temperature (^{o}C), Av(1), current RH, Av(3) and Av(4), the RSSI mean average and the transceivers transmission power level currently being used, m(7). This LJSON message is translated to standard JSON by the BS software, then, it is sent through a TCP socket connection to a custom JSON service, which extracts all pertinent information and performs its database storage.

2.2.4 Real environment prototype testing.

Seashore weather condition testing was carried out at the beach of Ensenada, Baja California, México. Fig. 2.2.4.1 shows the relative distance and elevation of the deployed EP and CLH nodes, as well as the far off placement of the BS on top of a hill overlooking the ocean [90].

Test Scenario #1:

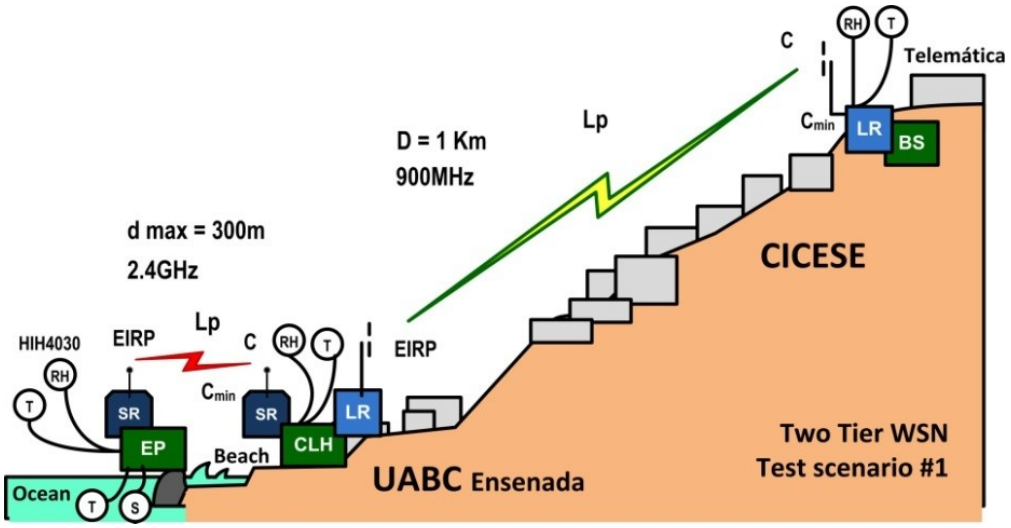

Fig. 2.2.4.1. WSN test scenario where the BS is located on top of a hill.

The experimental setup was left running for a week at the Ensenada test site. Periodically, the CLH software acquired its own sensor data, constructed a time-stamped message, aggregated the most recently received EP data, and sent it to the BS. This occurred every ten seconds. In fig. 2.2.4.2 the resulting cluster-heads air temperature measurements are presented, where day/night oscillations can be clearly identified. Also, fig. 2.2.4.3 shows relative humidity (RH) values measured by both RH sensors onboard the CLH system. During most of the nights and some mornings, the measured RH reached 100% and stayed high during some daylight hours, as expected at the sea shore. This weeklong test served to prove the selected hierarchical WSN approach, as well as the LJSON messaging operation implemented between the CLH system and BS.

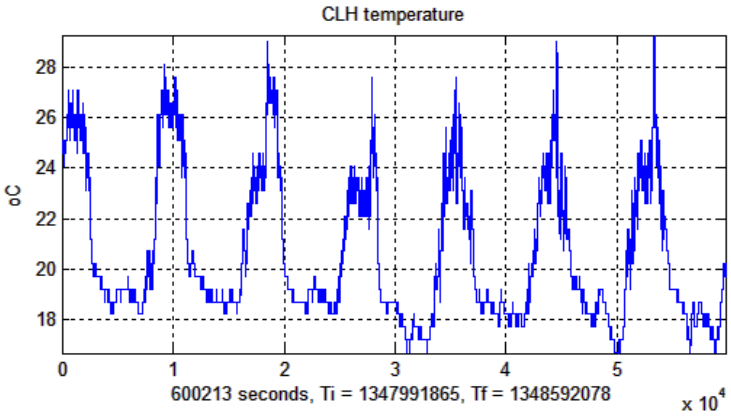

Fig. 2.2.4.2. CLH air temperature measurements.

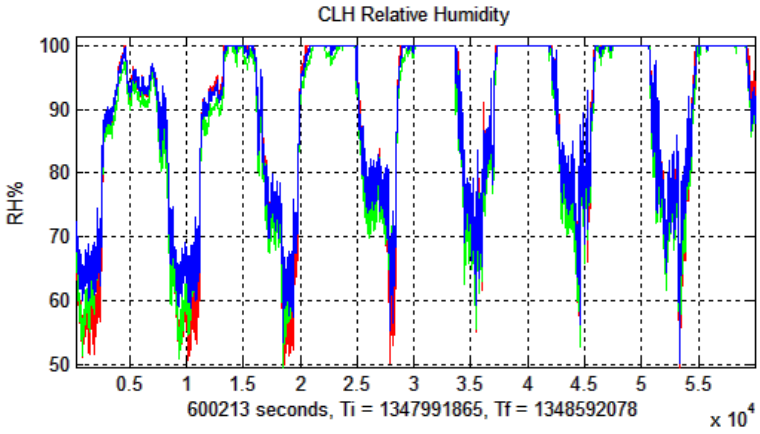

Fig. 2.2.4.3. CLH air relative humidity readings.

Test scenario #2:

Other experiments were carried out near the beach, at a second selected location at Playas de Tijuana, Mexico. Software refinement for this new round of experiments included the base station RSSI assessments, extracted from every incoming CLH API packet. This RSSI information was then fed back to the CLH systems through ACK packets, sent by the BS as the expected response for every received CLH message. As an example, six days of recorded RSSI values are shown in fig. 2.2.4.4, where a very weak received signal can be identified. Besides logging RSSI values, the CLH node also keeps track of the BS acknowledgements as a measure of the operating information delivery performance, with every ACK packet the CLH updates its packet received rate (PRR)

register. An example of eighteen hours of recorded a PRR values is shown in Fig. 2.2.4.5, where most of the lost packets occurred during the day at the beginning of the experiment.

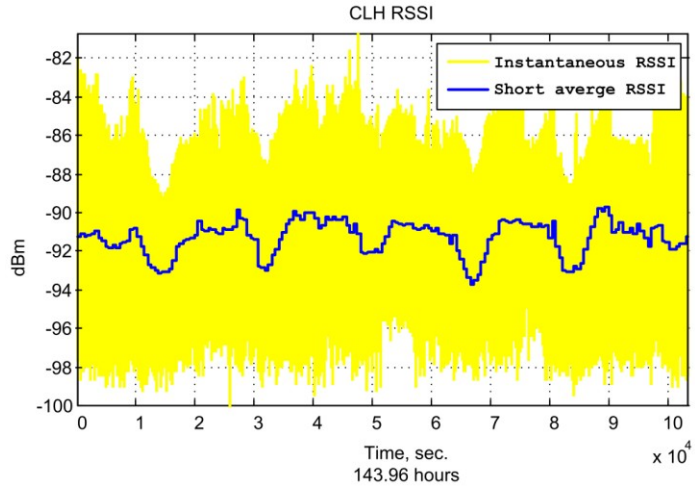

Fig. 2.2.4.4. Instantaneous RSSI and its average in dBm.

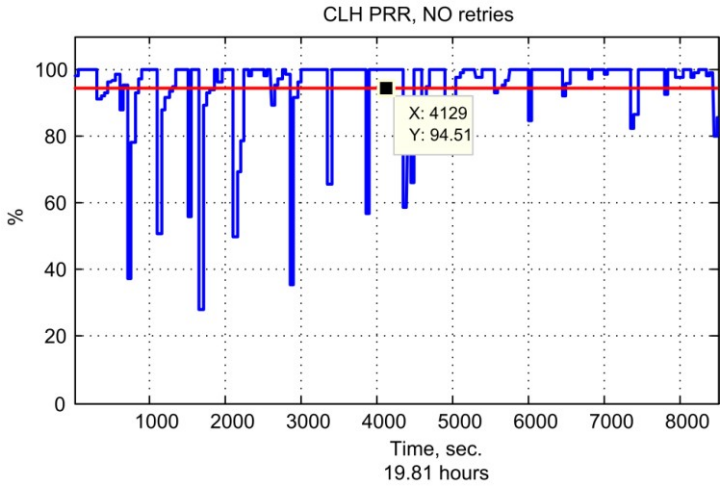

Figure 2.2.4.5. PRR result after 18 hours of operation, with a 94% average.

2.3. TPC approaches in WSN.

TPC adjusts a wireless transmitters power output according to a link quality that depends on the channels changing conditions. Usually the RSSI level is the metric used by a TPC algorithm, or it may take into account the quality of information using averages such as the BER or the PRR [91,92]. Two views of TPC have developed: one aims to save energy without altering the topology, and the other approach aims to change the network topology, which may or may not have energy conservation in mind. This second TPC approach is

used to restrict the range of a particular node and to limit the number of neighbor nodes it can route data for. This is a kind of topology control useful when a network is very dense, with a large number of neighbors in a multi-routing scenario.

2.3.1. Conventional TPC algorithms

Because of differing implementation goals, there is no agreement on what layer of the WSN should TPC algorithms operate. In initial wireless network deployments, such as in 802.11 protocols and cellular phone networks, their TPC algorithms work at the medium access control (MAC) layer [93]. Others that aim for direct topology control through TPC have moved these algorithms to the networking layer. Likewise, modern data-centric approaches now deal with TPC at the application layer as well. A list of known TPC proposals is presented next:

- **Iterative B-MAC (B-MAC-PCI)** [94]. Exchanges ACK messages at the node level and the sender determines minimum Tx power level.
- **Attenuation B-MAC (B-MAC-PCA)** [95]. Using ACK mechanisms, the receiver determines minimum power and informs the sender.
- **Power Control with Black Listing (PCBL)** [96]. Authors propose a topology control protocol that works at the networking layer. It uses PRR instead of RSSI feedback. Their justification is that RSSI is unreliable as a metric for TPC because the radio link is significantly influenced by distance, multi-path fading, interference, and time. And also state that PRR is a better indicator to determine the link quality and the amount of transmission power needed to maintain the desired PRR. However, a large number of packets have to be transmitted in order to build the PRR metric at different transmission power levels, besides time to converge it also may reduce the lifetime of the network due to overhead.
- **Power Control MAC (PCM)** [97]. It is based on 802.11 ad hoc protocols, uses a request-to-send/clear-to-send (RTS/CTS) handshaking protocol for channel contention. Designed for data transfer efficiency. The sender starts at maximum transmission power, then gradually lowers Tx power until an optimum RSSI level is reached that meets a specified PRR threshold. When the PRR worsens, the algorithm starts over.

- **Power Controlled Multiple Access (PCMA)** [98]. It was designed for ad hoc wireless networks, improves throughput of the 802.11 standard. It was thought out for data transfer efficiency and not for extending battery lifetime.
- **Variable Range TPC (VR-TPC)** [99]. The authors use variable transmission power to build a minimum spanning-tree for dense networks. They show the benefits of TPC for topology control and that at higher Tx power more interference is induced affecting the overall data transfer efficiency. Also, this algorithm works between the MAC and routing layers in a cross-layer approach.
- **Adaptive TPC (ATPC)** [100]. It employs a feedback based adaptive algorithm to dynamically maintain a desired link quality. It depends on an initialization phase, where every node broadcasts a beacon with differing transmission power levels, their neighbors measure the corresponding link quality and send back these values within a notification packet. With this information, after several neighbor notifications, the beaconing node determines the optimum transmission power level using a slow converging least square approximation. This means that this algorithm suffers from initialization overhead that requires wasting energy.
- **On-Demand TPC (ODTPC)** [101]. This on-demand scheme determines the link quality between a pair of nodes after the sender and the receiver exchange data-ACK packets. The author states that ODTPC is fast because it works in two phases, which calls the large-scale and the small-scale phases. It starts at a large-scale, transmitting at maximum power the receiver measures the RSSI and feeds it back to the sender, which determines the excess power and lowers its Tx power level in one large step, to an approximation that is expected to yield an optimum RSSI. Afterwards, when the sender has another packet for the same receiver, the algorithm enters the small-scale phase, where the sender transmits it and any subsequent packets at the optimum calculated power. The receiver measures the corresponding RSSI and feeds it back to the sender. If the RSSI falls below a pre-established lower threshold value, the sender increases the power level in fixed steps. Otherwise, if the RSSI is over an upper threshold, the sender reduces the Tx power level.
- **Dynamic TPC (DTPC)** [102]. It uses PRR feedback, although it is a topology control algorithm, besides attempting to improve the networks throughput it

strongly emphasizes its power consumption restraints in a multi-hop WSN. It works in two steps, a router node probes neighbor messages and then adjusts the transmission power until it only hears the selected neighbors.

- **Practical TPC (P-TPC)** [103]. In this scheme, the receiver determines the PRR and feeds it back to the sender. A proportional-integral controller with anti-windup (PI-AW) is deployed, which is a canonical linear controller widely studied in control systems theory. It calculates the transmission power based on the difference between the current PRR and a specified PRR set point or thresholds, applying a classical proportional-integral gain factor.

Most of these protocols have only been simulated, few that have been implemented in real platforms were tested in a limited fashion within the laboratory, under controlled conditions, far from harsh outdoor weather conditions. Much experimentation needs to be done with these proposals to determine their actual performance in the presence of real interference and noise.

2.3.2. Recent advances in TPC using temperature readings.

Very little work has been published regarding the effects of temperature and weather conditions on RSSI levels. Authors in [104] recorded outdoor temperature variations measured by sensor nodes and compared them to the RSSI values measured at the destination, this comparison showed a correlation between temperature rise and fall against RSSI decreases and increases, respectively. And although these experiments measured relative humidity (RH%), the authors did not pick up the idea that RH% is involved in signal loss as well. Meanwhile, the authors of [105] have empirically established an indirect correlation between temperature and relative humidity with the resulting RSSI, this while studying radio propagation in a potato field, but their discussion ends in merely implying such a dependence exists without elaborating more on how to use it as a criteria for Tx power compensation. And in [106], the authors made experiments in a greenhouse and they claim to have found a linear relationship between temperature changes and RSSI variation, within a temperature range between 25^{o}C and 65^{o}C.

- **Temperature-aware TPC.** Based on previous findings, authors of [107] propose a temperature gain coefficient TPC algorithm that requires receiver RSSI feedback

and uses in its approach instantaneous temperature measurements for linear Tx power compensation. Their tests were carried out within an empty building, where temperature ranged from 29^{o}C and 35^{o}C. They justified their experimental site selection by saying that it avoids external radio interference, focusing only on the effects of temperature variations on the overall RSSI levels. Nevertheless, this site selection is very limited because it is under a roof, so it is protected against solar radiation, which is the primary natural RF interference and heat source in real outdoor deployments, such as environmental monitoring.

Finally, authors of [108] are the only ones who, until now, have made extensive experimentation to determine if weather influences RSSI variations. Their experiments were done using IEEE802.15.4 protocol 2.4GHz compliant transceivers. Based on their six months worth of results, they concluded that a strong negative correlation exists between temperature changes and RSSI variation. They also measured humidity, precipitation and sunlight intensity. After their analysis, they concluded that humidity also affects the RSSI levels, but with a weaker influence compared to temperature. Regarding rain, they detected a contradictory result stating that no significant RSSI dampening effect was observed, although authors of [109] state that rain does play a significant role in received signal loss.

In summary, in this chapter I presented a background of theoretical WSN issues and application-centric approaches for remote environmental sensing and data transfer. Afterwards, I focused on a case study involving a long range marine environmental sensor network, where the challenge was operating under harsh conditions and having reliable data delivery through a noisy wireless channel. From this experimental setup, initial temperature and relative humidity data was obtained, and simultaneous RSSI values were also gathered, for future comparison to determine how the received signals are affected by the surroundings. This chapter ends with a list of recent TPC schemes, it reflects the scarcity of these types of algorithms for WSN which use environmental information for transmission power compensation. In the next Chapter, I present my original proposal, it includes the TRH TPC model definition and initial deployment, followed by the updated model simulation and its results, which reflect an optimal set of parameter values; and end the Chapter by showing the final deployment and its results, confirming the optimal TRH TPC behavior.

Chapter III. TPC based on temperature (T) and relative humidity (RH)

In this Chapter, I propose a temperature and relative humidity transmission power control algorithm. I start describing the experimental wireless system setup. Afterwards, I explain the proposed temperature and relative humidity TPC scheme, showing that there is an evident relationship between low valued RSSI loss and changes in T and RH. The latter, leads to the characterization of a relative normalized TRH gradient that follows changes in RSSI levels. With this framework, I then propose a TRH gradient function that depends on a constant coefficient. It uses real environment measured data and RF channel day-night RSSI performance metrics to do transmission power compensation. This function is meant to determine an appropriate gain factor, according to weather conditions, for controlling the transmission power level used by a radio transmitter of an environmental WSN node. I describe a complete TPC prototype algorithm with RSSI feedback and present test results with different coefficient values that leads to determining an optimal range where the TRH TPC works best.

3.1 Physical layer parameters and performance considerations.

In long range WSN design, we have to consider certain physical layer details. A power loss analysis, due to dispersion and the surroundings, is needed to approximate an optimal radiated power link budget. This analysis takes into account known parameters, such as distance and frequency, which can include an adequate excess power margin to avoid unreliable links. Or (on the contrary) it may be useful to avoid wasting power supply energy in the process. One such parameter is the minimum amount of transmission power needed to establish reliable wireless communications between nodes [110]. And besides considering transmission power and antenna gain issues, a sufficient understanding of the types of losses due to distance and fading sources is presented in a simplified line-of-sight wireless channel model.

3.1.1 Wireless channel gain-loss model.

A wireless communications channel gain-loss analytical model can be viewed as a "black box" [111], as illustrated in Fig. 3.1.1.1, where its input is the current transmitted

power level $P_L(z)$, and its direct output is the received signal strength indicator RSSI(z). Moreover, the packet received rate PRR(z) is normally considered as a second indirect output for data communication performance evaluation purposes. In the case of a model applied to TPC, the input signal is a discrete power level that establishes the actual transmitted power value in mW, which is used to transfer data from the information source to a designated destination. The different parameters included in the model, which are needed to do a wireless link power budget analysis, are presented in Table 3.1.1.1.

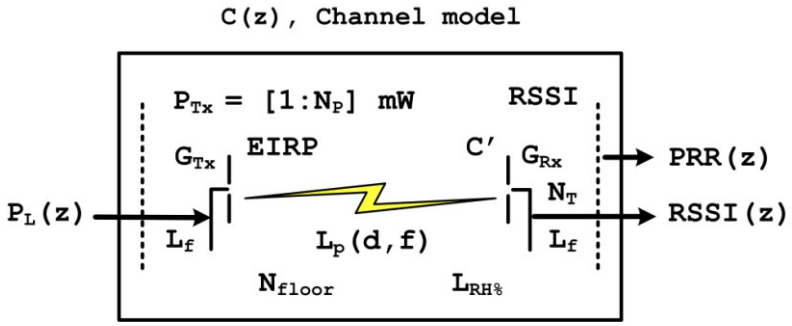

Fig. 3.1.1.1. Wireless channel "black-box" model.

It is important to note that path loss, L_P, is the most significant communications parameter because it describes the loss due to the distance between source and destination, which also depends on the operational wave length (or frequency).

Table 3.1.1.1 Parameters needed for a LOS link budget analysis.

Parameter/variable	Type G:Gain / L:Loss / P:Power	Description
$P_L(z)$	--	Tx Power level for P_{Tx}
P_{Tx}	P	Transmission power, mW (dB_m)
G_{Tx}	G	Tx antenna gain, (dB_i)
G_{Rx}	G	Rx antenna gain, (dB_i)
L_f	L	Wave guide Feed loss (dB)
N_T	L	Thermal noise (dB)
$L_{RH\%}$	L	Loss due to humidity (dB)
L_p	L	Path loss (dB)
N_{floor}	L	Noise floor (dB_m)
EIRP	P	Effective Irradiated power, (dB_m)
C'	P	Received signal power, (dB_m)
RSSI(z)	P	Received signal strength (dB_m)
C_{min}	Power Threshold	Receiver minimum power, threshold or Sensitivity (dB_m)
D	--	Distance between Tx and Rx (m).
PRR(z)	--	Packet received rate, %

Effective isotropic radiated power (EIRP) is considered to be the transmission power value times the Tx antenna absolute gain [112].

3.1.2 Point to point transmition power budget

To estimate a power link budget, the process starts off with determining the overall system gain (G_s in dB), which is represented with the following general expression.

$$G_s = P_{Tx} - C_{min} \ \text{dB} \tag{3.1.2.1}$$

And it has to satisfy the following condition to guarantee signal reception.

$$P_{Tx} - C_{min} \geq \sum \text{losses} - \sum \text{gains} \ \ \text{dB} \tag{3.1.2.2}$$

Taking into account losses and gains listed in table 3.1.1, the previous expression takes the following form:

$$P_{Tx} - C_{min} \geq N_{floor} + L_p + 2L_f - G_{Tx} - G_{Rx} \ \text{dB} \tag{3. 1.2.3}$$

In this expression feed loss on both sides (Tx and Rx) are considered equal for simplicity, but in a real situation they might differ. Although this is a trivial simplification it yields an approximation that is useful for actual system deployment, because it permits setting minimum transmission power without losing signal reception. Also worth mentioning is that the three key parameters in expression (3.1.2.3) are: Path Loss (L_p), noise floor (N_{floor}) and Receiver Sensitivity (C_{min}) [113]. The only known parameter is the receiver sensitivity, which is part of the manufacturer's specification. On the other hand, the actual noise floor value can be measured experimentally at the deployment sight using a radio frequency spectrum analyzer to determine the average day and night RF noise level, within the operational frequency bands. Usually, noise levels are around -90dBm during the day and less than -100dBm at night. Meanwhile, path loss L_p in dB may be determined using Eq. (3.1.2.4).

$$L_p(\text{dB}) = 92.4 \ + 20\text{Log}(f_{\text{GHz}}) + 20\text{Log}(d_{\text{Km}}) \ \text{dB} \tag{3.1.2.4}$$

Finally, for practical and deployment purposes, a minimum Tx power value, $P_{Tx\ min}$, can be approximated at the lower boundary of Eq. (3.1.2.3), which leads to Eq. (3.1.2.5).

$$P_{Tx\,min}(\text{dB}) = C_{min} + N_{floor} + L_p + 2L_f - G_{Tx} - G_{Rx} \ \text{dB} \tag{3.1.2.5}$$

Knowledge of the minimum transmition power value due to distance, is very important to be able to configure in an optimal way the power needed by wireless sensor nodes deployed in the field.

3.1.3. Distance emulation using antenna line attenuators.

Distance and loss estimates with the previously described wireless link power equations can be done starting with the ideal received or captured power (C) in dB, using eq. (3.1.3.1), which expresses the difference between the transmitted power plus antenna gain against the incurred path loss (L_P), due to distance and operating frequency range, which can be determined according to the well known Friis approximation using (3.1.3.1) and (3.1.3.2), where ERP is the transmitters overall *effective radiated power* [114,115]

$$\mathrm{ERP(dB)} = \mathrm{P_{Tx}(dB)} + \mathrm{G_{Tx}(dB)} - \mathrm{L_f(dB)} \qquad (3.1.3.1)$$

$$\mathrm{C(dB)} = \mathrm{ERP(dB)} - \mathrm{L_p(dB)} \qquad (3.1.3.2)$$

With these and previous power budget equations, results of short to medium distance calculations of L_P, C and RSSI are shown in Table 3.1.3.1. For simplicity, the ERP was fixed at 15dBm (according to the real transmitted power, just over P_{Tx}=30mW), which includes the antennas gain and line-feed loss. And in order to complete the data needed, the actual noise floor (N) was measured with a portable radio-frequency (RF) spectrum analyzer and determined to be -90 dBm on average.

Table 3.1.3.1. Received signal power at different distances, 915 MHz.

d ***Km***	**ERP,** ***dBm***	**L_P** ***dB***	**C** ***dBm***	**Fm = Cmin-N** ***dBm***	**RSSI (C + Fm)** ***dBm***
0.005	15	46	**-31**	**- (100-90) = -10**	**-41**
0.095		71	**-56**		**-64**
1		92	**-77**		**-87**
1.3		94	**-79**		**-89**
2		98	**-83**		**-93**

When the CLH node and BS -under the described conditions- are 5m apart one another, the calculated path loss equals 46dB, as presented in table 3.1.3.1 and illustrated in fig. 3.1.3.1.(a). For the purpose of emulating large distances between the BS and any CLH in the field, a 25dB RF attenuator can be attached to the base stations antenna and its line

feed. The result is as if the BS were to be moved 75 meters away from the experimental CLH node, as shown in fig. 3.1.3.1.(b). Furthermore, if at each CLH similar attenuators were to be fitted at their respective antenna it would be as if their individual distances were extended even more. The result would be similar as if the CLH were to be move 1Km away from the BS, which is illustrated in fig. 3.1.3.1.(c). This setup will prove useful for emulating large distances when experimenting within the laboratory.

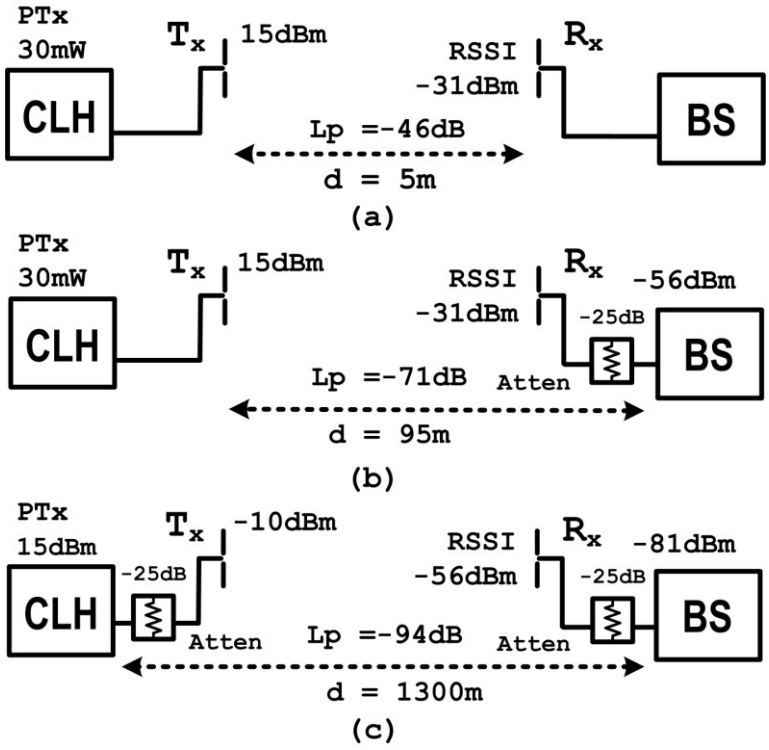

Fig. 3.1.3.1. (a) Actual distance separating the CLH from the BS without attenuators. (b) Distance emulation using an antenna line feed RF attenuator at the BS. (c) Distance emulation using attenuators at both BS and CLH.

3.2 T and RH conditions and their relationship with the RSSI behavior.

As mentioned in section 2.3.3, further CLH software refinements led to include communications performance metrics in the transmitted messages, such as RSSI and PRR averages. After logging six days worth of T, RH and RSSI data, and observing the results, as the ones shown in Fig. 3.2.1 and published in [116], it can be inferred that changes of temperature and air humidity produce differing amounts of loss reflected on the averaged RSSI magnitude at the destination. By simply factoring air temperature, T, times relative

humidity, RH, a curve is obtained, as the one shown in fig. 3.2.2, which in its scaled form fits the short mean averaged RSSI.

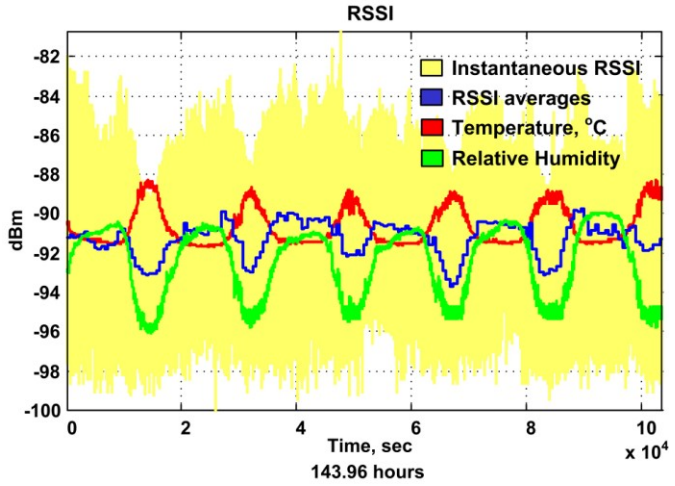

Figure 3.2.1. RSSI and its short averages in dBm, along with scaled versions of measured T and RH.

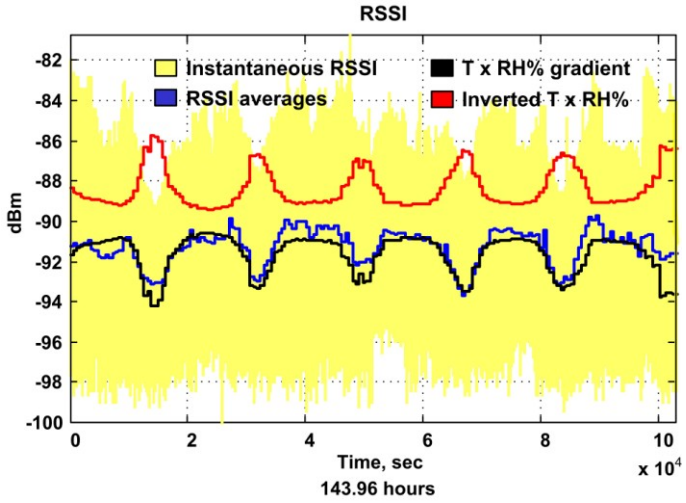

Fig. 3.2.2. The scaled TRH gradient fits the RSSI average curve.

The amount of gradient change is relative to upper and lower limits considered for both T and RH variables. For RH the natural limits are obviously 0% to 100%. But air temperature is a different matter, it depends on the part of the world where the radios will operate. In this case, we have opted to limit temperatures to the ones at the coasts of Baja California, Mexico, where this marine monitoring system will operate. Because of the

previous reasons and for practical purposes, the operating temperature limits taken into account are the following:

$$1\ ^{o}\mathrm{C}\ \leq \mathrm{T} \leq 50\ ^{o}\mathrm{C}$$

With temperature and RH limits established, the proposed gradient normalization is expressed by (3.2.1).

$$\nabla(\mathrm{t}) = \frac{\mathrm{T(t)\ RH(t)}}{\mathrm{T_{max}RH_{max}}}\ ; \quad 0 < \nabla \leq 1 \tag{3.2.1}$$

Eq. (3.2.1) represents the T and RH normalized product, which means that within the for mentioned bounds, the normalized T and RH product can only take real values between 0.02 and 1. Meanwhile, the inverse effect to TRH gradient changes here is considered as a gain factor, symbolized Δ(t), which is expressed with eq. (3.2.2):

$$\Delta(\mathrm{t}) = 1 - \nabla(\mathrm{t})\ ; \quad 0 < \Delta \leq 1 \tag{3.2.2}$$

Here the opposite effect of Δ(t) is proposed as a gain factor, which increases when TRH conditions worsen, and decreases when the gradient is in favour of a strong received signal.

3.3 TRH inverse gradient for TPC compensation.

A scaling issue becomes apparent when both temperature and RH are at their maximum, the direct factor would reach the maximum limit saturating the transmitter. To avoid this, I propose using a "compressed" gain factor, represented by (3.3.1), which states:

$$\Delta_{\mathrm{N}} = [1 - \mathrm{e}^{-\alpha_0 \Delta}] \tag{3.3.1}$$

Where α_0 is a dampening coefficient, which can take different values that affect the resulting compensation factors magnitude, Δ_N. In Fig. 3.3.1, a set of curves for different α_0 values are shown against the direct TRH gain factor.

For large normalized T x RH% values, using a particular set of low valued α_0 coefficients, leads to small Δ_N increments, which is intended to reduce chances of transmitter power saturation. And for small normalized T x RH% values, larger Δ_N increments are desirable to avoid insignificant increments that will not set into action the controller and the Tx power might not reach the minimum set point. Therefore, a set of optimal α_0 values has to be determined if this gain coefficient is to be used as an effective means of Tx power compensation.

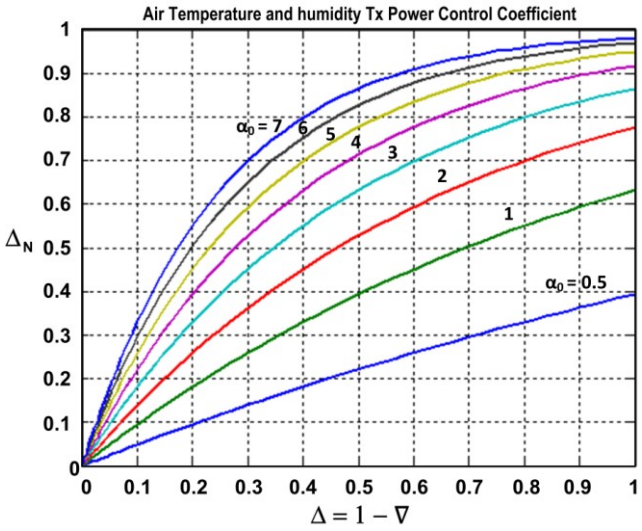

Fig. 3.3.1. Dampening of the normalized TRH power gain factor occurs bellow $\alpha_0 < 1.5$.

3.4. TRH gradient compensation prototype model using RSSI feedback.

The goal of this TPC scheme is to maintain the RSSI values within required limits, controlling the transmitted power according to averaged RSSI levels in a closed loop manner. Here, the initial proposal is to use short-term temperature and humidity conditions to dictate the amount of transmission power compensation needed.

In Fig. 3.4.1, the simplest TPC system with RSSI feedback is shown, its inputs are: T, RH and r_{Thr}, which is the minimum desired RSSI value or threshold. The system is represented with blocks, where C(z) symbolizes the wireless channel previously illustrated in Fig. 3.1.1.1, G(z) is the proposed controller, r(z) is the latest RSSI value measured at the receiver, which is fed back with a delay to the transmitter. The difference between r_{Thr} and the delayed r(z) gives an RSSI error, symbolized by $e_{RSSI}(z)$ and expressed by eq. (3.4.1), which is needed by the controller to compensate the transmition power level, $P_L(z)$.

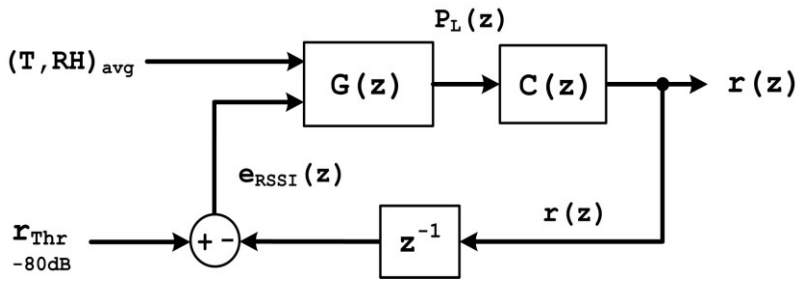

Fig. 3.4.1. Simple TRH TPC model with RSSI feedback.

$$e_{RSSI}(k) = r_{Thr} - r_{avg}(k) \tag{3.4.1}$$

In this scheme, the TRH compensator is used to establish the power level increment, ΔP_L, as indicated by (3.4.2).

$$\Delta P_L(k+1) = \Delta_N e_{RSSI}(k) = \Delta_N\left[r_{Thr} - r_{avg}(k)\right] \tag{3.4.2}$$

After solving (3.4.2), the power level update is done with (3.4.3), which adds the power level increment to the previous power level value.

$$P_L(k+1) = P_L(k) + \Delta_N e_{RSSI}(k) = P_L(k) + \Delta P_L(k+1) \tag{3.4.3}$$

To ensure power limits, after every RSSI assessment, bounds must be imposed on the controllers power level output, $\mathbf{P_L(k)}$. Noting that if a BIBO (Bounded Input / Bounded Output) system is ensured, then a stability condition is met for the controllers response, in this case easily imposed by software.

The simple topology of Fig. 3.4.1 is useful for explaining the basic feedback principal, but yet not totally practical. The problem is that, unless the error is exactly zero, such a controller will continually increase or decrease the $\mathbf{P_L(z)}$ level near and around the threshold, $\mathbf{r_{Thr}}$, without settling on a stable value. The solution is to include a second power limit given by a maximum RSSI, which produces a hysteresis zone that stabilizes the controller operation, with the added benefit of avoiding excessive transmission power. In Fig. 3.4.2, the basic block system with hysteresis is shown. Now there are two thresholds $\mathbf{r_{min}}$ and $\mathbf{r_{max}}$, and two feedback errors $\mathbf{e_{Rmin}(z)}$ and $\mathbf{-e_{Rmax}(z)}$ expressed by eq. (3.4.4) and eq. (3.4.5). For algorithmic purposes that later will be apparent, the maximum RSSI error is considered negative because the goal is to keep the RSSI level of surpassing $\mathbf{r_{max}}$.

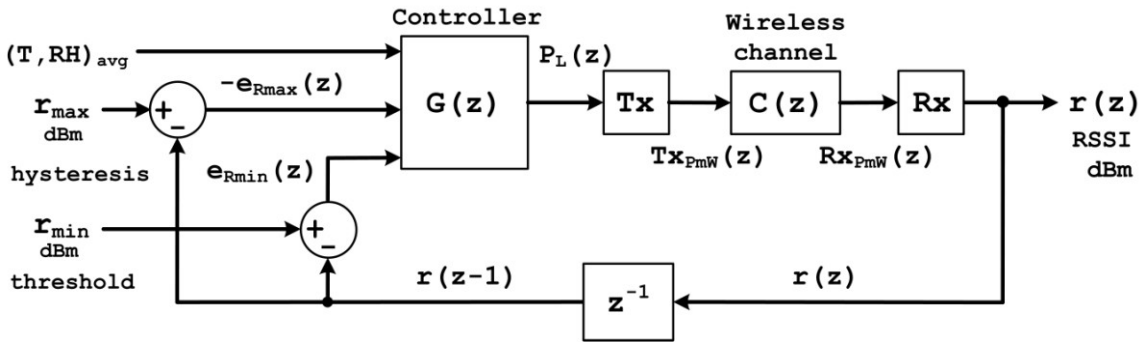

Fig. 3.4.2. TRH control system with RSSI hysteresis, limited by r_{min} and r_{max}.

$$e_{Rmin}(k) = r_{min} - r_{avg}(k-1) \tag{3.4.4}$$

$$-e_{Rmax}(k) = r_{max} - r_{avg}(k-1) \tag{3.4.5}$$

Within the G(z) controller, a decision has to be made on which error to take into account for Tx power compensation, the following pseudo code describes possible actions to take:

`If (`**`r(k-1) < r`**$_{min}$`)` `then` // RSSI is below minimum threshold

$$P_L(k+1) = P_L(k) + \Delta_N e_{Rmin}(k) \tag{3.4.6}$$

`Else If(`**`r(k-1) > r`**$_{max}$`)` then // RSSI exceeds maximum threshold

$$P_L(k+1) = P_L(k) - \Delta_N e_{Rmax}(k) \tag{3.4.7}$$

`Else` // Within RSSI limits, use previous Tx power level

$$P_L(k+1) = P_L(k)$$

`End`

Returning to the system in Fig. 3.3.2, the Tx block represents the transmitter, in this paradigm its input is a discrete power level $P_L(z)$ that configures the transmitters actual Tx power in mW. Similarly, the Rx block represents the receiver that senses power in mW and outputs an RSSI dBm value accordingly, which is fed back to the transmitting node. At this stage, it is worth emphasizing that the radio used in this thesis is the AC4490-1000M, its actual Tx power values in mW (5 to 1000mW) are not linear against the discrete power configuration levels (0 to 81) issued by the host controller, as was shown in previous fig. 2.1.3.1.1 in Chapter II. Another issue is on the side of the AC4490 receiver, Rx, its RSSI is not linear as well. Additionally, the minimum valid RSSI value that the AC4490 can issue

is −53 dBm because its intended for long range use. All this was also discussed previously in section 2.1.4.1. In general, the proposed control system is not linear because the radios are not linear in their power output levels and in their RSSI readings.

3.5 Initial laboratory TRH-TPC emulation and testing.

Experimentation was done to determine the proposed TRH compensators behavior with different alpha values, α_0={4, 3, 2, 1, 0.9, 0.8, 0.7, 0.6, 0.5, 0.3, 0.2, 0.1}. The testing conditions were such that there was no sunlight interference, with a 50% to 60% RH and a 25°C temperature average. For fairness, at both reference and control transceivers, their transmission retry feature was disabled for worst-case scenario. In this case, the AC4490 transceiver comes factory configured with ten retries when sending addressed packets, and with three retransmissions in broadcast mode.

For this experimental deployment, the controller's minimum RSSI was fixed at -80dBm, and the maximum RSSI at -70dBm. After using the RF power budget analysis, reviewed in Chapter III, a Tx power value was calculated. Then, after attaching antenna line attenuators to both CLH-1 and CLH-2 systems located at 5m distance from the BS, the appropriate Tx power value was set for the node radios. The expected RSSI average was estimated at −89 dBm, but the actual measured RSSI average was -95dBm, as shown in Fig. 3.5.1.(a). The resulting PRR of the un-controlled CLH-1 was measured to be 82% with no retransmissions, as shown in Fig. 3.5.1.(b).

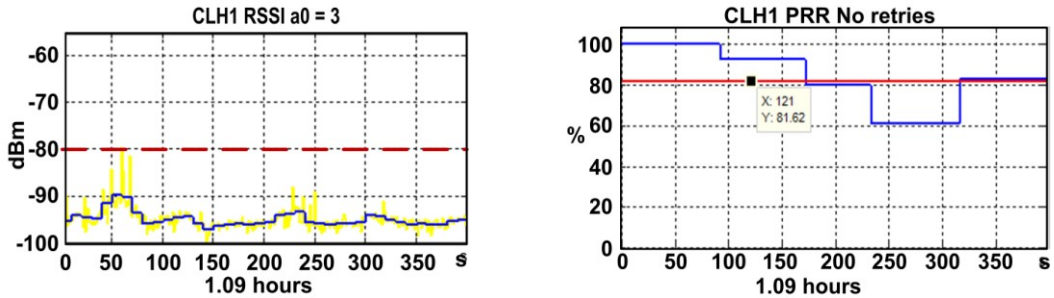

(a) (b)

Fig. 3.5.1. CLH-1 reference node with no TPC and no Tx retries: (a) RSSI plot, -95dBm average, and (b) PRR behaviour, 82% average.

Meanwhile, RSSI results of the TRH controlled CLH-2 with α_0=4, shown in Fig. 3.5.2.(a), started at -95dBm; and after the TRH controller converged, the RSSI average increased to -73dBm. Although TRH controlled CLH-2 PRR graph is not shown here, the

overall CLH-2 PRR was measured to be 98%, which obviously means that it outperformed CLH-1 by 16%. Most of CLH-2 lost packets occurred at the beginning of the exercise, before the TRH compensator converged. In Fig. 3.5.2.(b), the TRH controlled radio started transmitting with a power level equal to 3 (nearly 30mW), and after the first ten transmissions, with RSSI feedback and TRH compensation, the transmission power value reached level 16. This represents a Tx power increase, from 30mW to almost 150mW, so with a large α_0=4 coefficient the power compensation increments are large as well. This may not be convenient because of possible wide RSSI variations, which makes the controller unstable. It then implies a trade-off between power consumption and dependable data delivery. Furthermore, with α_0=4 there is considerable Tx power usage which might be wasted if the PRR does not improve.

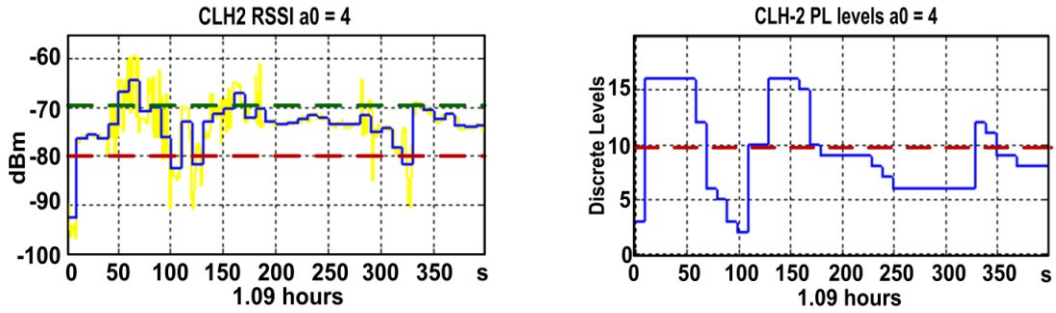

(a) (b)

Fig. 3.5.2. CLH-2 TRH controlled, no Tx retries, with α_0=4: (a) RSSI plot, -73dBm average, and (b) Tx power level behaviour.

Similar results to α_0=4 were obtained using α_0=3. In contrast, with α_0=2 results (plotted in Fig. 3.5.3.(a) and 3.5.3.(b)) show that with a smaller coefficient, the RSSI enhancement is smaller and power level variability is smaller as well, improving the overall power consumption, which implies that less power is wasted with a small enough α_0. Likewise in this experiment, CLH-1 (with no TPC) measured a 79% PRR performance, while CLH-2 with α_0=2 obtained a perfect 100% PRR.

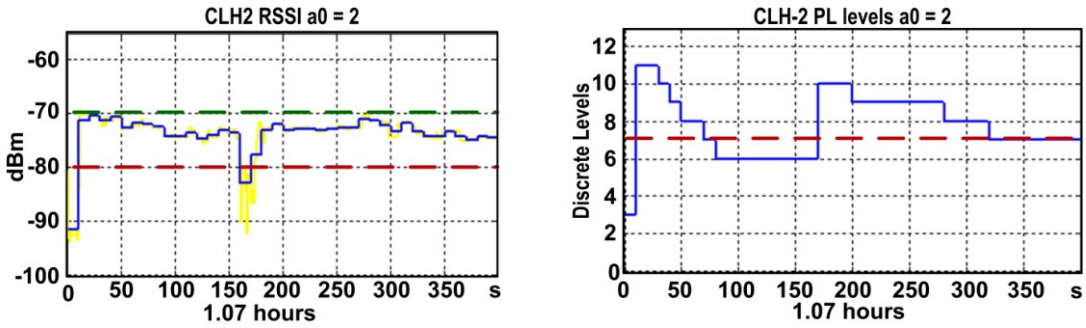

(a) (b)

Fig. 3.5.3. CLH-2 TRH controlled, no Tx retries, with α0=2: (a) RSSI plot, with a -72dBm average, and (b) Tx power level behaviour.

On the other hand, in Fig. 3.5.4.(a), with an even smaller α_0=0.5 value the average RSSI converged within the desired limits, but some values dipped below -90dBm. And in Fig. 3.5.4.(b), with α_0=0.5 the PRR averaged 92%. This means that by using a smaller α_0 coefficient, the transmission power variation are also smaller with the disadvantage that the PRR starts to decay if compensation is not done fast enough. This is evident in Fig. 3.5.4(a), where the power level rise was more gradual with α_0=0.5 compared to power level increments using larger α_0 coefficients, such as in figures 3.5.2.(b) using α_0=4 and 3.5.3.(b) using α_0=2. And the overall average power level reached P_L = 6, while with α_0=2 the average reached P_L = 7, was with α_0=4 the average reached an even higher P_L = 10.

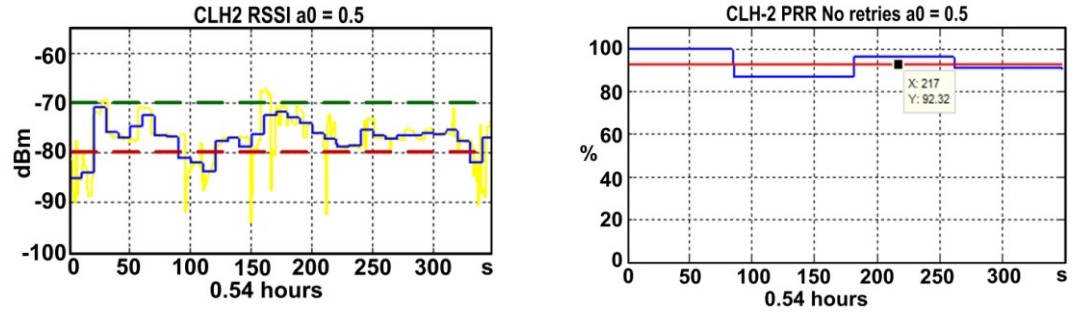

(a) (b)

Fig. 3.5.4. CLH-2 TRH controlled, no Tx retries, with α_0=0.5: (a) RSSI plot, -77dBm average, and (b) PRR behaviour, 92% average.

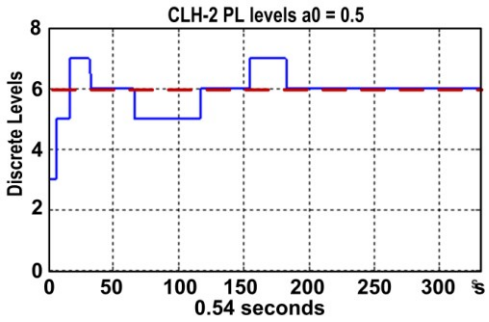

Fig. 3.5.5. CLH-2 power levels with TRH TPC, α_0=0.5.

Further experiments showed that below α_0=0.5, the TRH compensator stops working as such, and it just does unity power level adjustments. And as previously discussed, with a small α_0 coefficient the controller's response is too slow to compensate against deep and sudden fading. After doing an overall analysis, we found that this TRH TPC scheme works fine within the α_0 coefficient range expressed by (3.5.1):

$$0.5 \leq \alpha_0 \leq 6 \tag{3.5.1}$$

Although these experiments were done during short periods of time in laboratory conditions, preliminary results served to determine the adequate coefficient range expressed by (3.5.1).

3.6 Harsh environment TRH-TPC testing.

Several day outdoor TRH algorithm testing was done with two α_0 coefficients. Noting that the main differences compared to previous laboratory tests was the presence of much higher RSSI variance and a higher noise floor, day-night temperature and RH had a much wider variance as well. This time, three cluster-heads were deployed simultaneously, CLH-1 with no TPC, CLH-2 operating with α_0=1 and CLH-3 with α_0=0.5.

Fig. 3.6.1.(a) illustrates RSSI values of CLH-1 transmitting at a fixed power level, and in fig. 3.6.1.(b) shows the CLH-1 PRR plot, which averaged 75%. Meanwhile, in fig. 3.6.2.(a) the resulting CLH-2 RSSI is plotted and in fig. 3.6.2.(b) overall PRR reached a 93% average, which means that CLH-2 outperformed CLH-1 by 18%. Similarly, in Fig. 3.6.5.(a) and 3.6.5.(b) CLH-3 RSSI and PRR plots are illustrated, which show that CLH-3 also outperforms the fixed power CLH-1, this time by 17%.

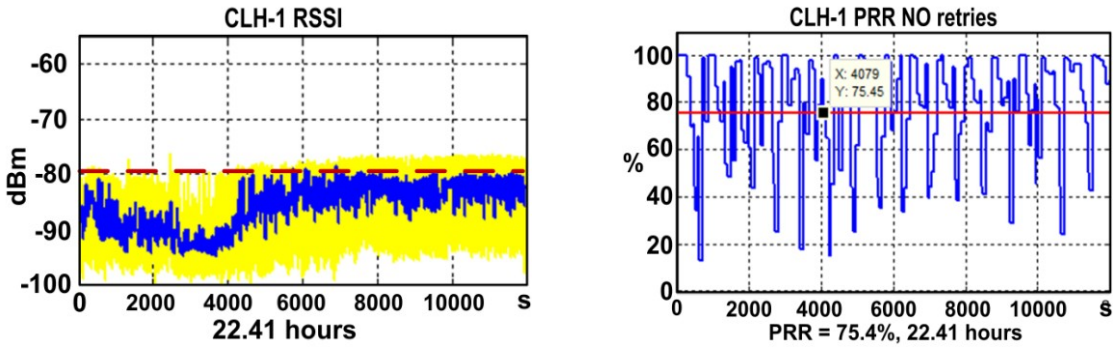

(a) (b)

Fig. 3.6.1. CLH-1 with no TPC: (a) -85dBm RSSI average and (b) PRR with a 75% average.

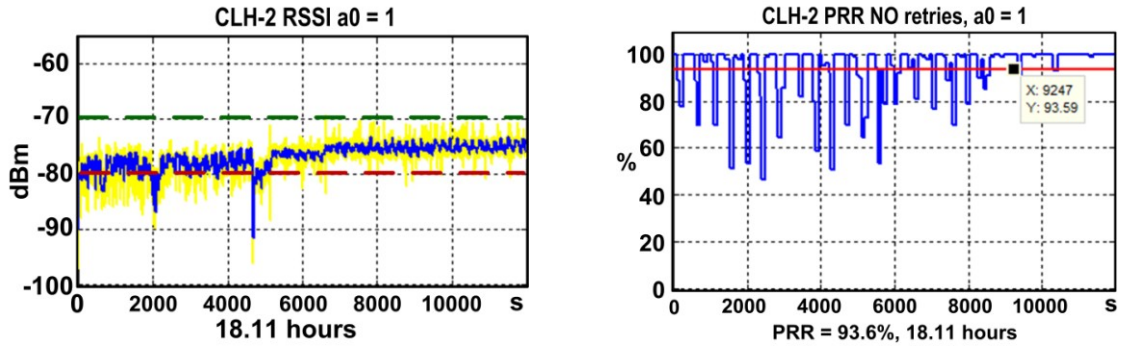

(a) (b)

Fig. 3.6.2. CLH-2 with TRH TPC, α_0=1: (a) RSSI values and (b) PRR with a 93% average.

On the other hand, in Fig. 3.6.3.(a) and 3.6.3.(b), the overall recorded RH and T behaviors are shown, respectively. While in Fig. 3.6.4.(a) the inverse TRH gradient is plotted, and when compared to CLH-2 power levels, shown in Fig. 3.6.4.(b), there appears to be a match at several points in time. Similar results for the CLH-3 with α_0=0.5 are shown in figures 3.6.6.(a), 3.6.6.(b), 3.6.7.(a) and 3.6.7.(b).

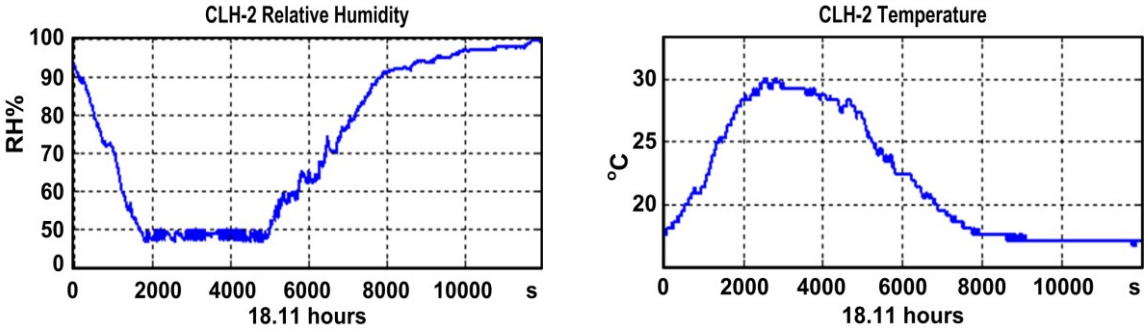

(a) (b)

Fig. 3.6.3. CLH-2: (a) relative humidity and (b) air temperature.

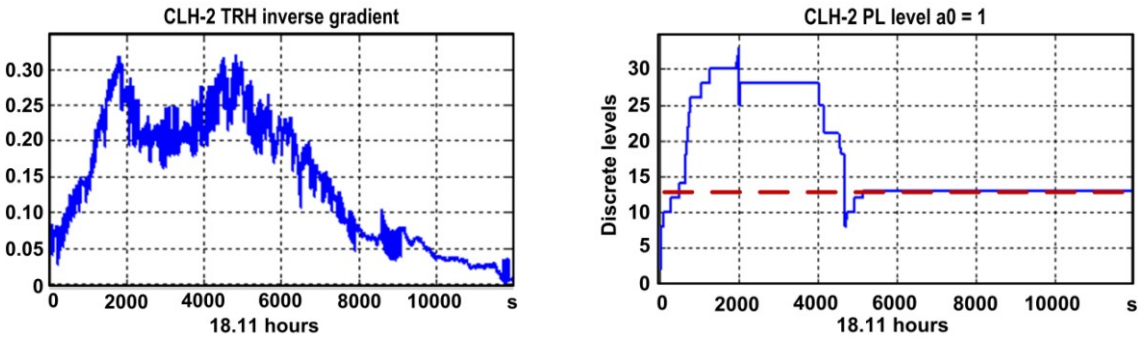

(a) (b)

Fig. 3.6.4. CLH-2 (a) TRH upside down gradient and (b) Tx power levels.

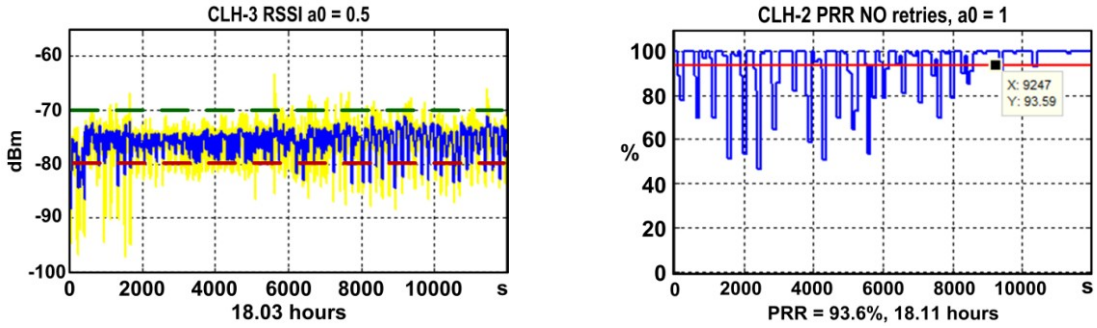

(a) (b)

Fig. 3.6.5. CLH-3 with TRH TPC, α_0=0.5: (a) RSSI values and (b) 92% PRR average.

Table 3.6.1. Performance comparison and TPC results.

CLH	**RSSI avg** Day / Night dBm	**PRR** %	**PL**	**P_{Tx}** mW Non-linear Day / Night	**P_{Tx}** (dBm)
1 (no TPC)	-95 / -85	75	3	31	14.9
2 (α_0 = 1)	-78 / -74	93	35 max 13 min	357 / 133	25.5 / 21.2
3 (α_0 = 0.5)	-78 / -75	92	25 max 14 min	255 / 143	24 / 21.5

Although all obtained results could not be included in this document, of the many laboratory experiments, as well as of several real environment tests done with the wide range of selected α_0 coefficients, all of them showed an improvement of at least 10% and up to 20% in PRR performance. In table 3.6.1, comparative results are shown of the CLH

harsh environment test bed. It summarizes day and night RSSI averages, Tx power level averages and the approximate Tx power average used, in mW and dBm. Between both CLH-2 and CLH-3 (with TPC), the resulting power average day consumption reached 306mW (approx.), which means that a larger fade margin needs to be applied to determine the minimum P_{Tx} considering the worst conditions. This would yield excessive power consumption during night operation if no TPC is deployed. We consider these test bed results as preliminary, which now have served to verify the conceptual aspect of the proposal.

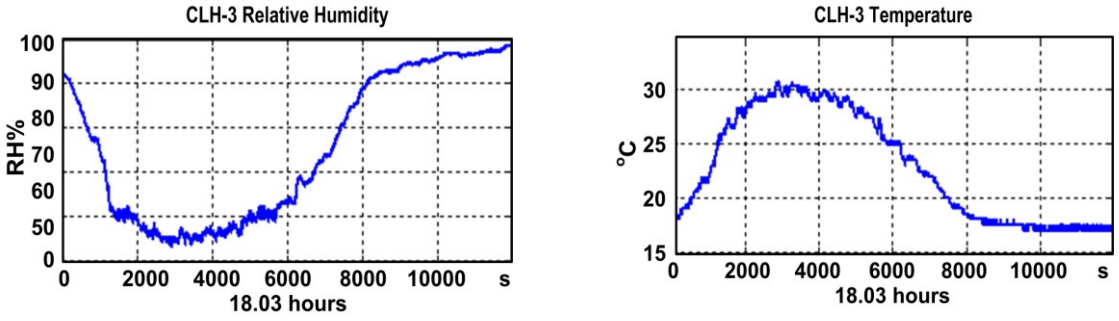

(a) (b)

Fig. 3.6.6. CLH-3: (a) relative humidity and (b) air temperature.

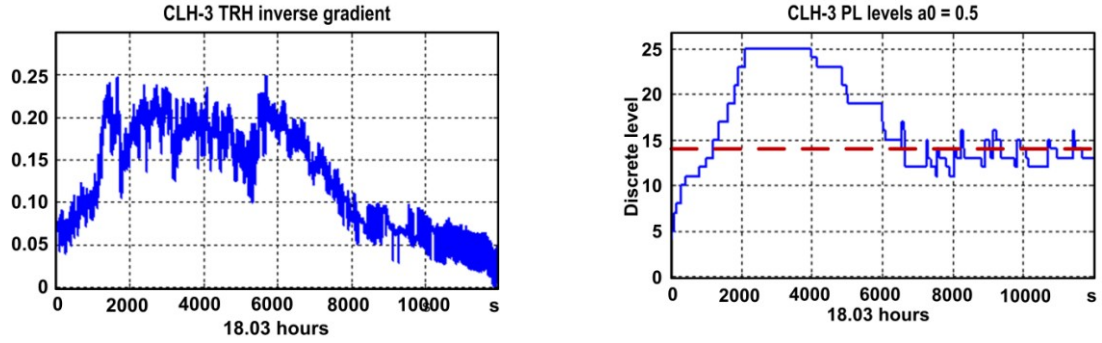

(a) (b)

Fig. 3.6.7. CLH-3 (a) TRH upside down gradient and (b) Tx power levels.

Simulation code that emulates the proposed TRH TPC using real RF noise samples and several test results are presented in the next section that permits determining the power consumption impact that the selected α_0 coefficient value has.

3.7 The updated TRH TPC model and emulation using real RF noise samples.

I made modifications to the original TRH-TPC scheme, it use to compare short average RSSI feedback against a single target set point, considered as the minimum RSSI threshold, r_{min}. Fig. 3.7.1 shows our TRH TPC updated version that now includes a maximum RSSI threshold, r_{max}.

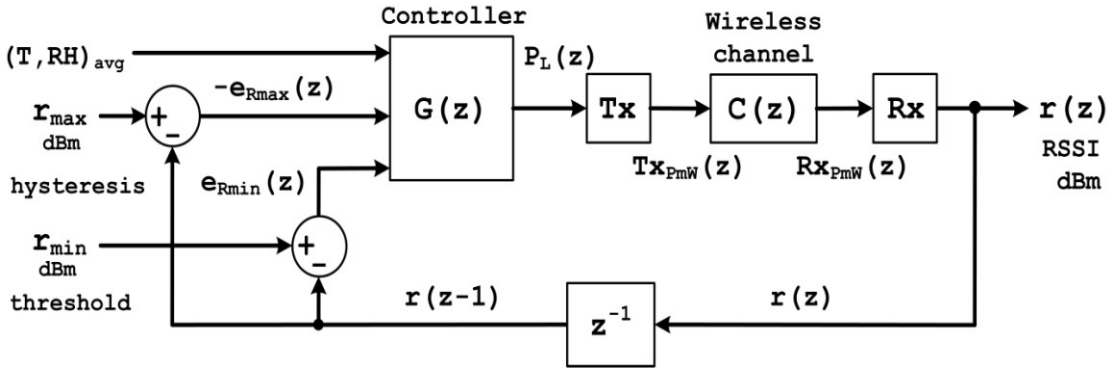

Fig. 3.7.1. TRH TPC system with RSSI hysteresis, bound by r_{min} and r_{max}.

In Fig. 3.7.1, I illustrate the transmission power controller, G(z); Tx is the transmitter, C(z) is the wireless channel, Rx is the receiver, and r(z) is a short average RSSI value, measured at the receiver and fed back to the controller. Furthermore, $P_L(z)$ is the discrete power level established by G(z) that sets the transmitters actual power, $Tx_{PmW}(z)$. Meanwhile, $Rx_{PmW}(z)$ is the instantaneous RSSI measured by the receiver that is later sent to the CLH with a delay, **r(z-1)**, which is compared to two thresholds, $\mathbf{r_{min}}$ and $\mathbf{r_{max}}$, yielding two feedback errors $\mathbf{e_{Rmin}(z)}$ and $\mathbf{-e_{Rmax}(z)}$ expressed by equations (3.7.1) and (3.7.2).

$$e_{Rmin}(k) = r_{min} - r_{avg}(k-1) \tag{3.7.1}$$

$$-e_{Rmax}(k) = r_{max} - r_{avg}(k-1) \tag{3.7.2}$$

In classical control system applications, the range between maximum and minimum thresholds is called a hysteresis zone [18]. In this scheme, the hysteresis approach is used to avoid continual Tx power compensation around the minimum RSSI set point. Within the G(z) controller, the decision is made on which error to take into account for Tx power compensation. Algorithm 3.7.1 shows the corresponding pseudocode that describes actions

that should be taken by the controller, where $P_L(k)$ is the discrete power level output by G(z), and the $P_L(k+1)$ is the updated power level that the transmitter will use during the next data transmission.

There are two possible power adjustments because there are two error comparisons. Eq. (3.7.3) is the updated power value if the delayed r(k) is below the minimum threshold, and eq. (3.7.4) is the next power value if the delayed r(k) value is over the maximum threshold. Algorithm 3.7.1 shows the entire TPC process.

$$P_L(k+1) = P_L(k) + \Delta_N(k)e_{Rmin}(k) \quad (6)$$

$$P_L(k+1) = P_L(k) - \Delta_N(k)e_{Rmax}(k) \quad (7)$$

Algorithm 3.7.1. Updated TRH TPC algorithm with r_{min} and r_{max} thresholds.

```
Constants: RHbias, TRHscale, Navg, a0
Input:     Tavg(k), RHavg(k), rmin, rmax, r(k), ravg(k), PL(k)
Output:    PL(k+1), PTxmW(k+1)
Initializations:  k = 0, jj = 0
1:  loop:     TRH(k) = (Tavg(k).*(RHavg(k)+RHbias))/TRHscale
2:  Gain:     TRH_delta(k) = 1-exp(-a0.*TRH(k))
3:  Average RSSI: ravg(k) = mean(r(k), NAVG)
4:  Compensation: jj++ == Navg ?
5:                    ravg(k) < rmin ?
6:                        PL(k+1)=PL(k)+abs(TRH_delta(k).*(rmin-ravg(k)))
7:                    ravg(k) > rmax ?
8:                        PL(k+1)=PL(k)-abs(TRH_delta(k).*(ravg(k)-rmax))
9:                    else : PL(k+1)=PL(k)
10:                   jj = 0
11:           k++   // next loop
```

For the purposes of acquiring and logging RF noise present within the 901MHz through 924MHz frequency bands, the prototype CLH sensor data acquisition program was extended to include RF noise sampling. Where the host ArduinoMega software queries the serially connected AC4490 several times every sampling period, for the instantaneous reading of whatever signal is present at its antenna. The measured RF signal power is then digitized, averaged and sent to the BS, along with other pertinent sensor variables (RSSI, T,

RH and a PRR estimation for future reference). The server program was also modified to store the received data in files with a comma separated values (CSV) format. Fig. 3.7.2 illustrates the CLH side, it depicts the set of variables that are handled, such as: timestamp, acquired sensor data, operational states and performance metrics. Where **$P_L(n)$** is the current discrete Tx power level code, **P_{Tx}** is the actual power in mW, and **Sd(n)** is a vector, which comprises sensor samples acquired every Ts seconds (where **Ta** is air temperature and **Tw** is water temperature -both in ^oC-, **RH1** and **RH2** are relative humidity percentage values). Likewise, **Sd(n) -** shown next **-** includes the current battery voltage, **Vb**, and the CLH message ends with the last raw 10-bit RSSI value, **$rssi_{raw}$** fed back to the CLH by the BS.

Sd(n) = [Ta:°C,Tw:°C,RH1:%,RH2:%,Vb:V,$rssi_{raw}$:10-bits]

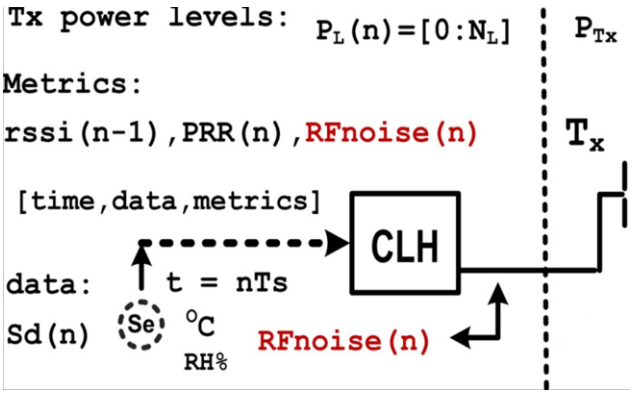

Fig. 3.7.2. CLH sensor and RF noise sampling.

On the other hand, the performance metrics vector, **M(n)**, comprises the following variables:

M(n) = [N_rp:Int, N_sent:Int, PRR_avg:%, rssi_avg:dBm, rssi_sdv, P_L:Int, 100a0:Int,*RF_{noise}:Int] *:Optional

N_rp is the number of received packets, **N_sent** is the number of sent packets, **PRR_avg** is the average packet received rate, **a0** is the current TRH gain coefficient (it is multiplied by 100 so it can be relayed as an integer value within the CLH message), and **RF_{noise}** is the last measured signal in dBm present at the CLH radio antenna. In fig. 3.7.3, an illustration shows a CLH to BS communication representation, it comprises the

following tow general actions: (1) the CLH sends its data and metric aggregated message to the BS, and (2) the BS responds with an ACK reply.

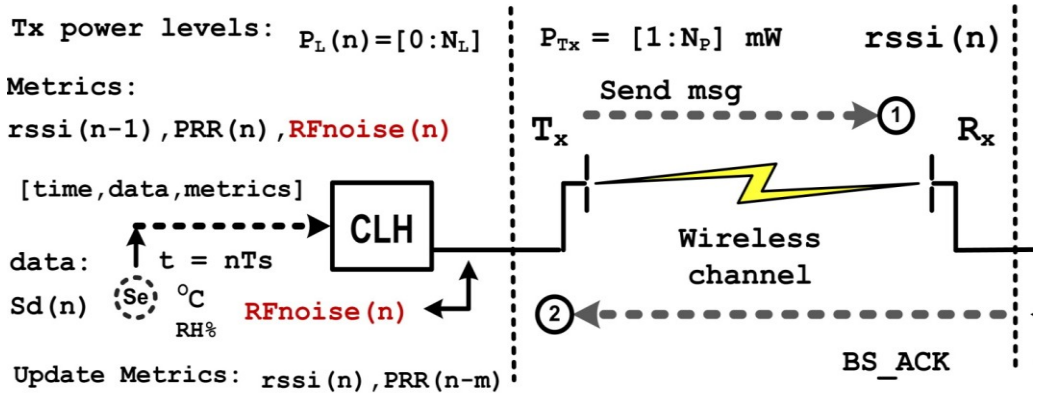

Fig. 3.7.3. CLH sent message and BS ACK response.

In Fig. 3.7.4, the BS side of the upper tier data transfer process is presented, it shows both send and reply events. After the BS receives the CLH message, it extracts the RSSI raw value from the incoming AC4490 API frame (explained in Chapter II), it naturally extracts the payloads CLH LJSON message, coverts it to a conventional JSON and sends it off to the remote JSON server application for DBS storage.

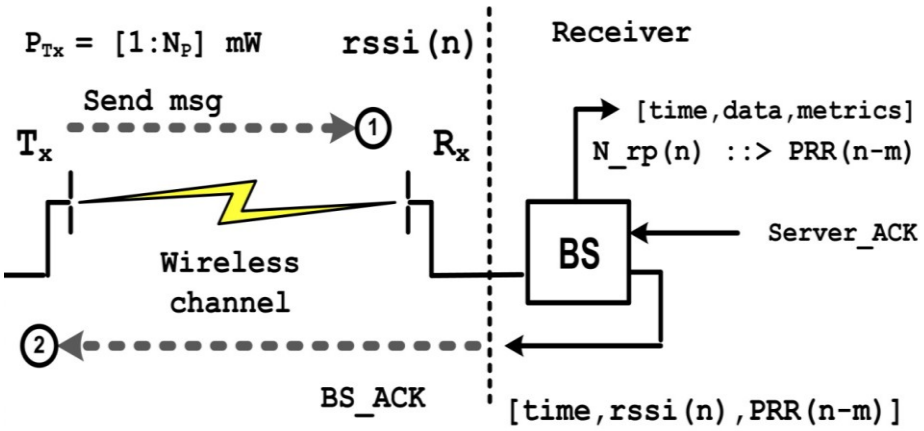

Fig. 3.7.4. (1) The BS measures the RSSI level after the CLH Send message, and (2) includes it along with PRR information in the BS_ACK response.

Examples of CLH measured temperature and RH data are shown in Fig. 3.7.5.(a) and 3.7.5.(b).

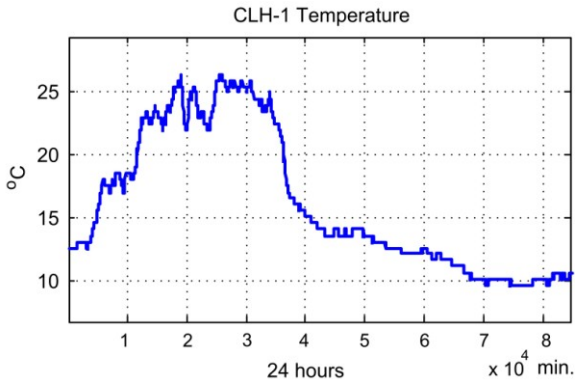

(a)

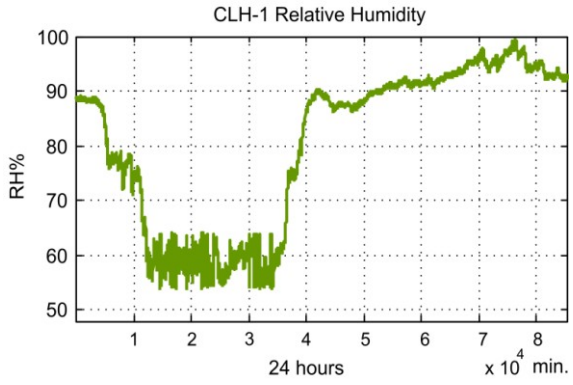

(b)

Furthermore, Fig. 3.7.6 illustrates both TRH gradient and its inverse. In Fig. 3.7.7 the measured RF signals are illustrated, and show that for the most part their gain is similar to the TRH gradients behavior, and the inverse TRH may be used as a gain factor for Tx power loss compensation.

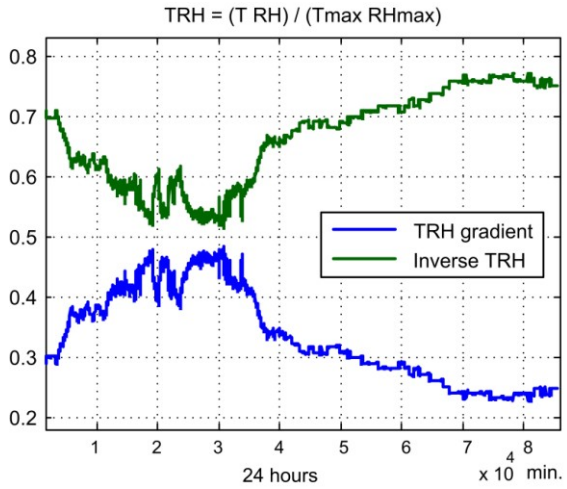

Fig. 3.7.6. TRH gradient is the shape in the lower half of the plot, and the inverse gradient is at the top.

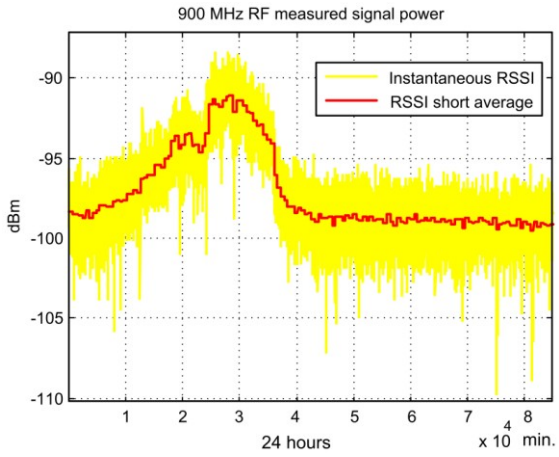

Fig. 3.7.7. Arbitrary RSSI signals captured by CLH-1, they represent RF noise and/or possible interfering signals.

These real values are vital to approximate the TRH TPC simulation results to a real deployments behavior. With this aim, at the start of the simulation, the developed code loads the measured values, and with pre-configured initial conditions (such as path loss due to distance, Tx power level, antenna gain, minimum RSSI and maximum RSSI thresholds) the simulation code uses the required Tx power budget expressions for calculating two received signals: (1) an uncontrolled RSSI behavior (for reference) and (2) a TRH transmission power controlled RSSI. Furthermore, it is a known fact that the AC4490 transceiver has a non-linear Tx power level behavior and a non-linear RSSI as well. Therefore, with the aim of approximating even more the Tx power simulation to real deployment, the actual non-linear full range discrete Tx power levels in mW (shown in previous Fig. 2.1.3.1.1) were saved as an array to a CSV file, along with their corresponding dBm conversion. This simulation loads these power values in its work space, and in an indirect manner, the discrete Tx power level serves as the index for extracting the actual mW power used by the AC4490, while transmitting data with a particular P_L value.

A simulation environment was developed that uses the RF power budget equations described earlier, it also considers the AC4490 radio non-linear Tx power levels. And to simulate a more realistic response, the code loads from CSV files real T, RH and RF noise data. Algorithm 3.7.2 shows the simulation constant declarations and parameter initialization, along with real data vectors loaded from files. In this simulated environment, the TRH gradient and TPC gain factor calculation can be done *a priori* because the code has at its disposal knowledge of T and RH behaviors.

Algorithm 3.7.2. TRH TPC algorithm initialization section.

```
S_Rx = -100; % dBm AC4490 Rx sensitivity
Lp = -92; % dB 1.2Km path loss
AntGain = 2; % dBi
rmin = -80; rmax = -75; % dBm , min and max RSSI thresholds
CLH_vals=load([my_data_path  'RF915MHz_ACTUAL_noise.csv']);
CLH_T = CLH_vals(:,1);         % Acquire Temperature array
CLH_RH = CLH_vals(:,2);        % Acquire RH array
Nt = CLH_vals(:,3);            % dBm RF noise sample array
L = length(Nt);                % Number of samples
TRH = (CLH_T.*(CLH_RH+100))/scale;   % 100% biased TRH Gradient
TRH_delta = 1-exp(-alpha.*TRH); % TPC gain factor
PtxdB = 10.*log10(pLEVEL); % dBw, pLEVEL is predefined
```

In Algorithm 3.7.3, the simulation does RSSI power calculations without TPC for future comparison purposes, with and without TPC. Followed by RSSI short average estimations that will be used later during the actual compensation at the end of every averaging period. Moreover, in Algorithm 3.7.3, non-linear AC4490 Tx power values in dB are loaded from a CSV file and converted to the dBm scale by subtracting 30dB. And the power level vector $P_L(k)$, (set to the same RSSI vector dimension), is initialized with the pre-configured user selected mW power level converted to dBm.

Algorithm 3.7.3. RSSI calculation without TPC, RSSI short averaging and loading of non-linear AC4490 Tx power values.

```
Rssi = PtxdB - (S_Rx+Nt) + Lp + AntGain; % ref RSSI, without TPC
Navg = 10; % compensation window size
Nblock = 10; % RSSI Averaging every Nblock samples

% Short average every RSSI Nblock samples at a time
Rssi_avg = short_mean(Rssi,Nblock);

Tx_Pw=load('AC4490_Tx_Pl.csv')-30; % dBm
Pl = abs(ones(size(Rssi)).*10.*log10(TxPwmW); % dBm
```

Algorithm 3.7.4 shows our TRH TPC simulations main loop. It determines RSSI short average estimations every N_{avg} samples, followed by its comparison with the minimum and maximum RSSI thresholds. If the RSSI average is below the r_{min} threshold then the compensation is positive, increasing power. Else, if the RSSI average is over the maximum

r_{max} threshold, then the power compensation is negative, decreasing the radios power level. Else the Tx power is unchanged because the RSSI level is within the hysteresis zone.

Fig. 3.7.8.(a) shows the simulation environment input dialog, where the user chooses the key TRH TPC parameters, and Fig. 3.7.8.(b) shows plots of a two day simulation example that uses previously acquired RF noise, T and RH data loaded from CSV files. The resulting RSSI levels without TPC, in dBm, is calculated adding the negative path loss and subtracting noise power from the constant transmission power.

After power compensation, the controlled RSSI (shown in green and averaged in red at the left hand lower corner of Fig. 3.7.8) tends to stay within the minimum RSSI and maximum RSSI thresholds. In order to determine the algorithm performance, the minimum RSSI error is determined by counting the RSSI values that fall beneath the minimum RSSI threshold and dividing the result by the vectors total RSSI. Other useful plots in Fig. 3.7.8 are the TRH biased gradient (upper right), the AC4490 discrete power levels (at the middle) and the radiated transmission power levels in mW (at the lower right corner).

Algorithm 3.7.4. TRH TPC main loop.

```
for i=Navg:L-1,  % Main simulation loop
   % RSSI emulation using gain - loss equation affected by TRH TPC
    Rssi_adj(i) = Tx_Pw(floor(abs(Pl(i))))-(S_Rx+Nt(i))+ Lp + AntGain; %dBm

    if(jj==Navg)  % Do RSSI average after every Navg samples
        % Do a RSSI short average
        rssi_mean2(i)=mean(Rssi_adj((i-(Navg-1)):i));

        % Minimum Tx power threshold comparison
        if(rssi_mean2(i) < rmin),
          % PL update : INCREASE Tx power
          Pl(i+1)=Pl(i)+abs(TRH_delta(i).*(rmin-rssi_mean2(i)));
        else
          % Maximum Tx power threshold comparison
          if(rssi_mean2(i) > rmax),
            % PL update : DECREASE Tx power
            Pl(i+1)=Pl(i)-abs(TRH_delta(i).*(rssi_mean2(i)-rmax));
           if (Pl(i)<0), Pl(i+1) = 0; end % ensures Pl not negative
           else
              Pl(i+1)=Pl(i); // power level unchanged
          end
        end
        jj=1; % re-initialize compensation window counter
    else
        jj = jj + 1; % increment compensation counter
        rssi_mean2(i)=rssi_mean2(i-1);
      % keeps a constant average until it is time to update it
    end
end
```

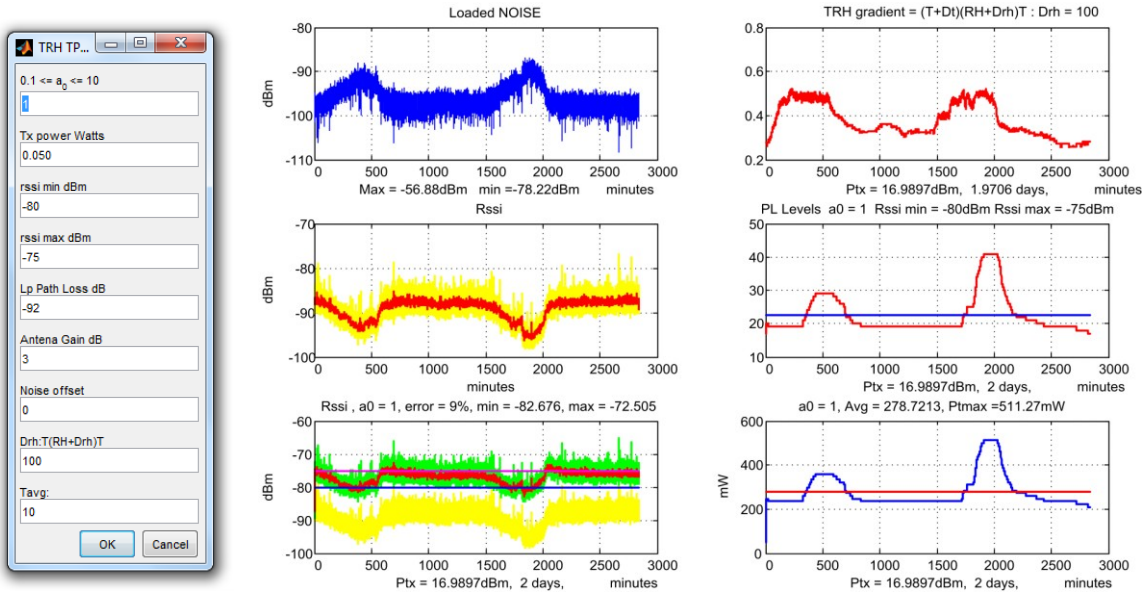

(a) (b)

Fig. 3.7.8. Simulation environment example. (a) TRH TPC input dialog. (b) Set of plots that show real input noise, TRH gradient and results of two days worth of samples.

3.8 TRH gradient behavior during low RH.

The system was left running exposed to real conditions for several days. Fig. 3.8.1 shows that during this time, humidity measurements fell towards extreme dry conditions. And Fig. 3.8.2 illustrates that the air temperature was 10°C higher during the day when RH dropped below 20% (Fig. 3.8.1).

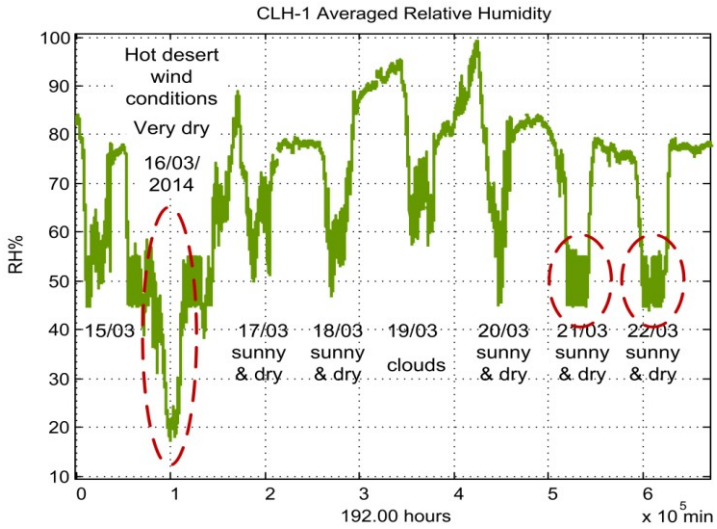

Fig. 3.8.1. RH readings on a six-day experiment, with conditions below 50% RH.

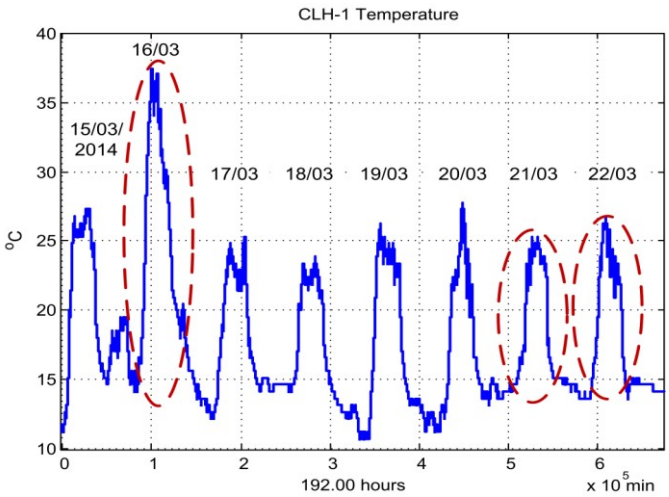

Fig. 3.8.2. Temperature readings of a eight-day experiment.

Fig. 3.8.3 shows the resulting TRH gradient and Fig. 3.8.4 illustrates the RF background noise. After comparing both figures with Fig. 3.8.1, it is apparent that when RH is below 50% the TRH curve does not follow the RF background noise trend. Noting that the TRH gradient, eq. (3.2.1), can be useful as a TPC gain factor only if it follows the RF noise variations. The TRH distortion is remedied by adding an RH bias value to the TRH equation. After experimentation we found that the gradients useful behavior is guaranteed by adding 100% RH bias, the updated formula is expressed by (3.8.1).

$$\nabla(t) = \frac{T(t)(RH(t)+100)}{T_{max}RH_{max}} \tag{3.8.1}$$

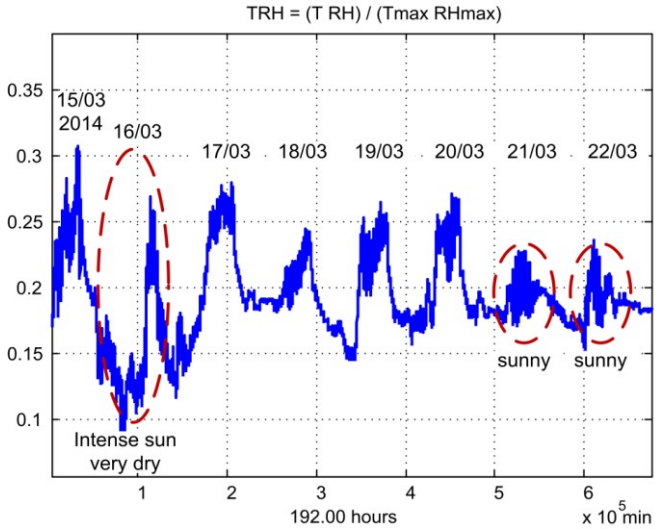

Fig. 3.8.3. Plot of TRH during the eight-day experiment.

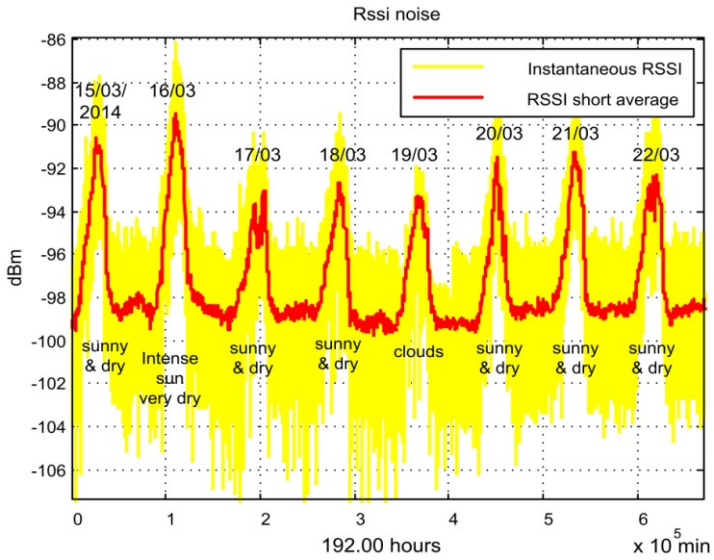

Fig. 3.8.4. RF noise and interference measurements on a eight-day experiment.

Fig. 3.8.5 illustrates the biased TRH. Its values increase and decrease in a similar manner as the noise behavior (Fig. 3.8.4). Now this TRH gradient is more useful in the TPC gain factor equation expressed by (3.3.1).

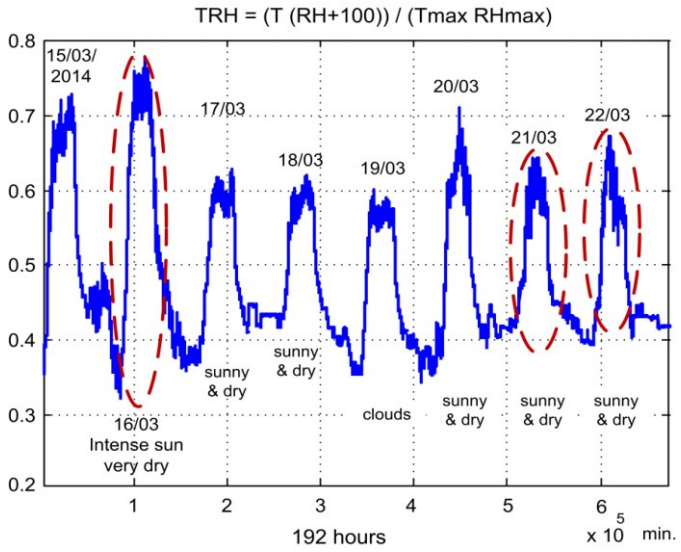

Fig. 3.8.5. Biased TRH, which follows RF noise changes on a eight-day experiment.

3.9 TRH parameter optimization and results.

The TRH TPC algorithm operates using key parameters such as the alpha TRH gain coefficient, α_0, the controllers hysteresis zone, which ranges from r_{min} to r_{max}, and the selected time to do RSSI averaging, T_{avg}. Here we did several experiments using our simulation environment changing these parameters to determine which values offered the best TPC results.

3.9.1 Alpha coefficient selection.

The α_0 argument affects the power gain step size; for example, Fig. 3.9.1.1.(a) illustrates a close up view of the resulting RSSI of a TRH TPC simulation experiment with a low α_0=0.5 and Fig. 3.9.1.1.(b) shows it with a high α_0=8. Comparison of both plots confirms that power compensation is slower with a low valued α_0 than with a high alpha. With α_0=8, the TPC response overshoots the maximum RSSI threshold by almost 5dB. Another useful comparison is between the RSSI plots shown in 3.9.1.2.(a) and 3.9.1.2.(b), which are a zoomed out versions of Fig. 3.9.1.1.(a) and Fig. 3.9.1.1.(b) respectively, it shows that compensation is faster with a high alpha because the RSSI level tends to go near the minimum RSSI threshold instead of staying mostly at the top near the maximum RSSI limit.

Originally, we proposed it as a compressed gain factor to avoid unstable RSSI compensation. Also, it was previously found that below 0.5, this alpha coefficient yields unitary power steps that cause a very slow convergence. At the upper limit, it was suggested that alpha should be equal or less than 2 to avoid larger Tx power step sizes. Here we reevaluated the upper power limit because the RSSI variable changes faster in harsh sunlight interference than first observed.

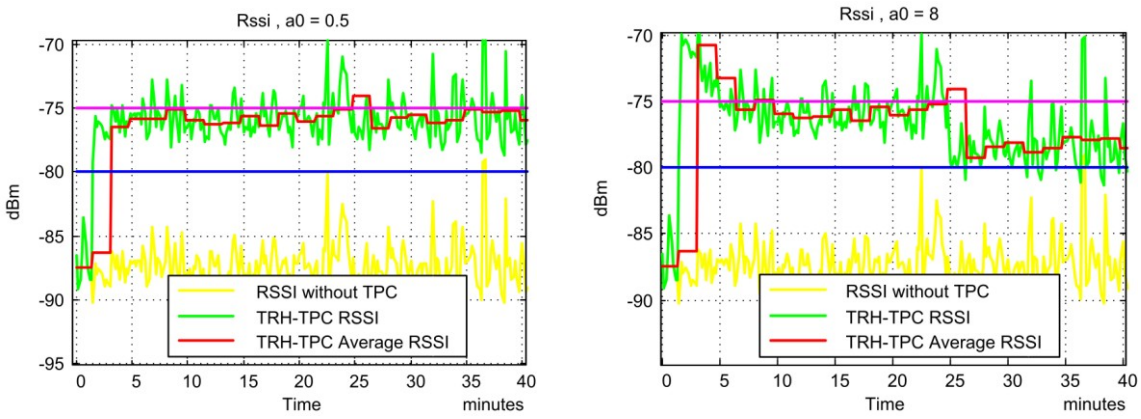

(a) (b)

Fig. 3.9.1.1. TRH TPC simulation RSSI plots, (a) using $\alpha_0 = 0.5$ and (b) using $\alpha_0 = 8$.

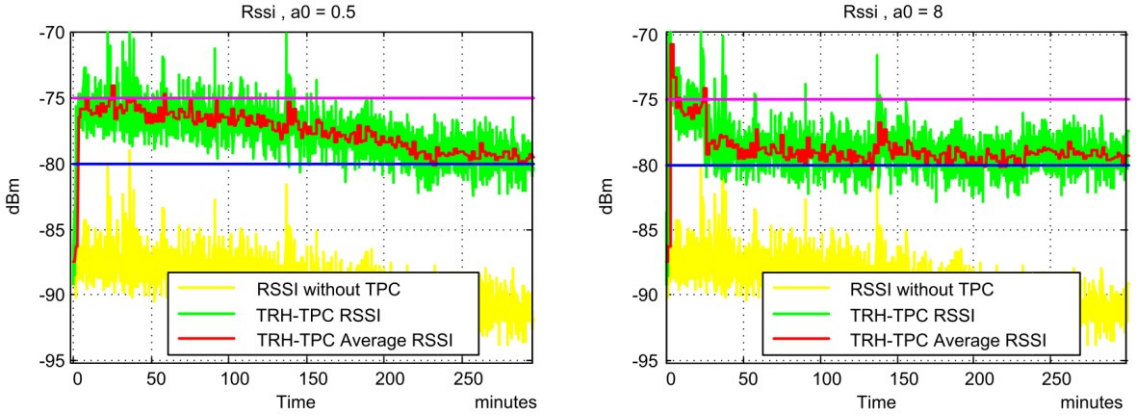

(a) (b)

Fig. 3.9.1.2. TRH TPC zoomed out simulation RSSI plots, (a) using $\alpha_0 = 0.5$ and (b) using $\alpha_0 = 8$.

Figures 3.9.1.3.(a) and 3.9.1.3.(b) show plots of the resulting transmission power with α_0=0.5 and α_0=8, respectively. Fig. 3.9.1.3.(b) shows that with $\alpha_0 = 8$ the initial compensation increases Tx power to more than 800mW. In contrast, in Fig. 3.9.1.3.(a) with α_0=0.5 the transmission power increase is less than 300mW.

The question remains on what α_0 value can be considered an optimum limit. We decided to do several experiments with different α_0 values, and through trial and error, good results were obtained with α_0 less or equal to 6.

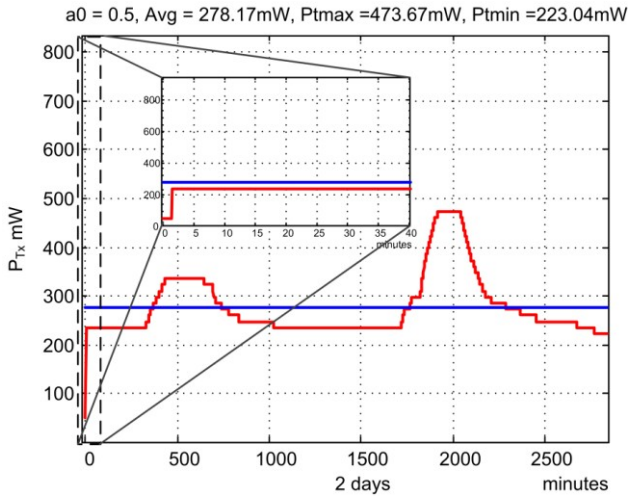

(b)

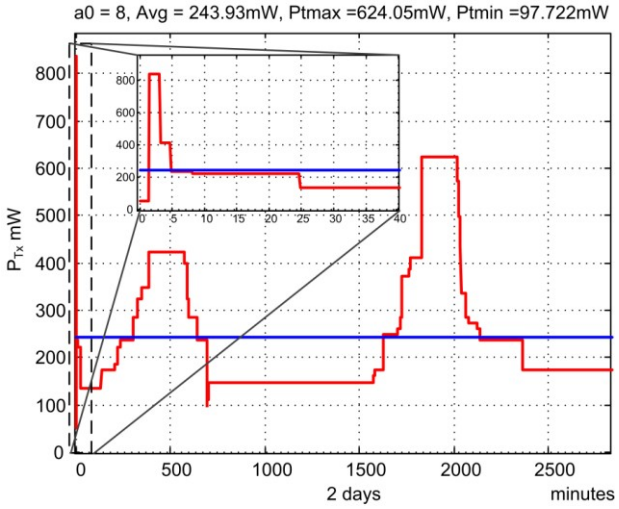

(a)

Fig. 3.9.1.3. Transmission power plots in mW, (a) using α0 = 0.5 and (b) using α0 = 8.

Fig. 3.9.1.4 shows the resulting RSSI values with α_0=4 during the first iterations and Fig. 3.9.1.5 represents the corresponding mW transmission power levels.

The TRH controllers aim is to regulate transmission power, so the RSSI levels rise or fall within the pre-established hysteresis zone. During this process, the received power may overshoot the r_{max} threshold, which represents an error that we call the maximum RSSI threshold error, ε_{max}. Or on the contrary, the RSSI levels may go below the r_{min} causing a minimum RSSI threshold error, ε_{min}. The latter is the least desirable error state for TPC because packet loss increases due to poor signal reception.

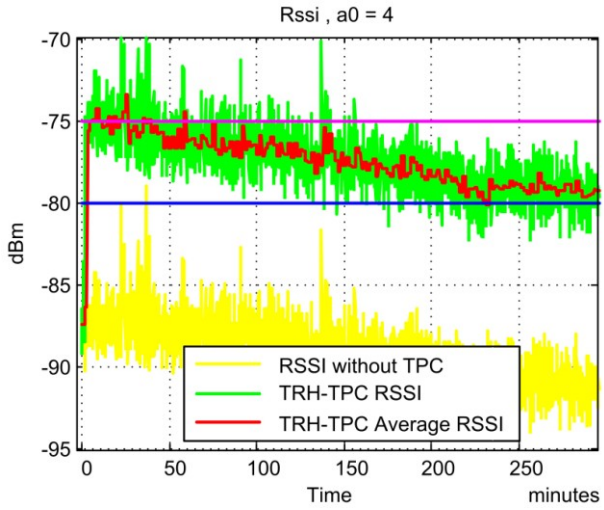

Fig. 3.9.1.4. Initial 300 minutes of the simulated RSSI using $\alpha_0 = 4$.

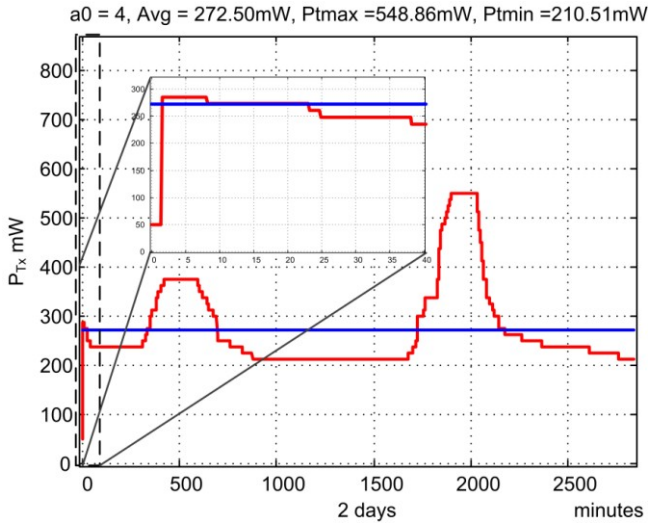

Fig. 3.9.1.5. Transmission power plot in mW using $\alpha_0 = 4$.

To determine the TRH algorithms performance with different α_0 values, we included a variable that counts the RSSI short averages that go below the minimum RSSI threshold to obtain an estimate of the ε_{min} metric. Likewise, to determine ε_{max} a maximum RSSI error counter was included in the model and incremented when the RSSI short averages go over r_{max}. Many TRH experiments were done changing the alpha parameter and logging the amount of RSSI threshold errors. In Table 3.9.1.1 the estimated ε_{min} and ε_{max} values of an eight-day experiment are shown, along with the Tx power metrics corresponding to different alpha values.

Table 3.9.1.1. RSSI minimum error and Tx power metrics of an eight-day simulation with different α_0.

α_0	ε_{min} %	ε_{max} %	P_{Txavg} (mW)	P_{Txmin} (mW)	P_{Txmax} (mW)
0.5	13.1	14.3	294	210	612
1	11.3	10.6	292	198	674
2	**9.9**	**8.2**	**291**	**198**	**724**
4	**8.5**	**7.0**	**289**	**185**	**800**
6	**8.3**	**6.7**	**288**	**185**	**840**
8	8.2	6.6	294	185	870
10	8.1	6.6	300	185	900
12	8.1	6.6	310	185	915
14	8.1	6.6	310	185	920

In Table 3.9.1.2 twelve-day simulation results are presented, where estimated ε_{min} and ε_{max} values are shown, with corresponding transmission power characteristics.

Table 3.9.1.2. RSSI minimum error and Tx power metrics of a twelve-day simulation with different α_0.

α_0	ε_{min} %	ε_{max} %	P_{Txavg} (mW)	P_{Txmin} (mW)	P_{Txmax} (mW)
0.5	12.4	13.7	297	210	611
1	10.7	10.2	295	198	650
2	**9.3**	**7.9**	**293**	**198**	**700**
4	**8.1**	**6.6**	**291**	**185**	**770**
6	**7.8**	**6.4**	**291**	**185**	**810**
8	7.8	6.4	296	185	845
10	7.7	6.3	310	185	874
12	7.7	6.3	315	185	880
14	7.6	6.3	315	185	890

In Table 3.9.1.1 and Table 3.9.1.2, after α_0=4 the minimum errors did not change much. After several simulations using samples from different days, the Tx power behavior and RSSI values reflected similar results. Noting that they imply that the α_0 argument can be higher than first reported, with good results up to α_0=4, or slightly higher. Fig. 3.9.1.6 and Fig. 3.9.1.7 illustrate plots of the RSSI threshold errors vs. discrete alpha values of Table 3.9.1.1 and Table 3.9.1.2, respectively.

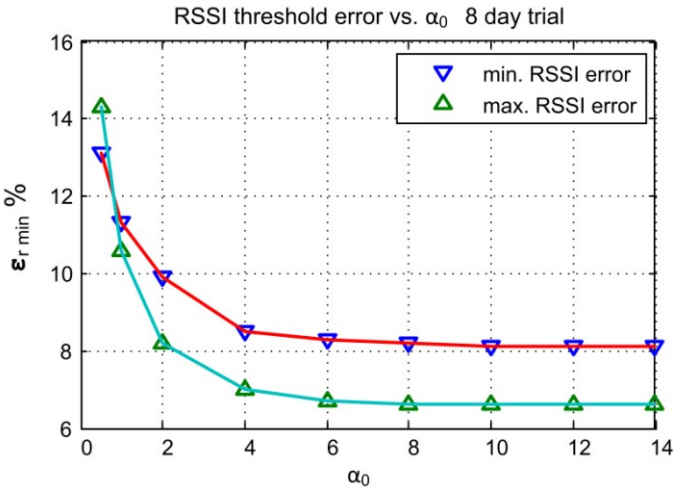

Fig. 3.9.1.6. Eight-day trial RSSI threshold error vs. α_0

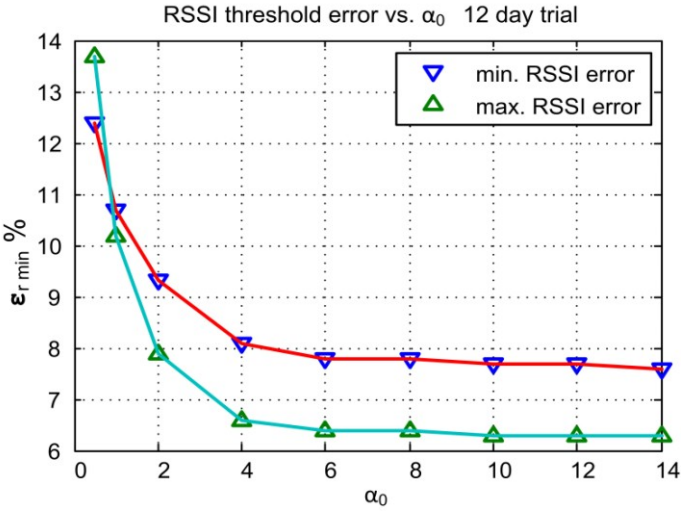

Fig. 3.9.1.7. Eight-day trial RSSI threshold error vs. α_0

Fig. 3.9.1.8 and Fig. 3.9.1.9 represent transmission power plots of eight and twelve-day trials vs. different alphas, respectively. In both plots, the average and minimum transmission power metrics are very similar for different α_0 values. After evaluating the TRH TPC performance with different α_0 values, it is apparent that α_0 can be much higher than previously assumed. The updated α_0 limit can be as high as 6 because the average transmitted power stays the same and error performance does not improve much afterward. Moreover, after α_0=6 the maximum transmission power increases unnecessarily.

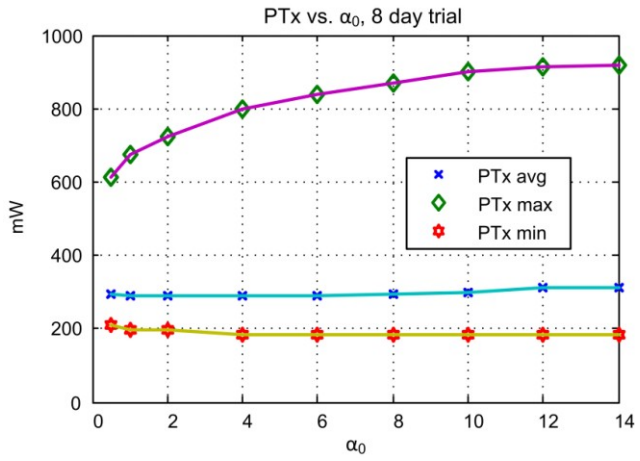

Fig. 3.9.1.8. Transmission power vs. α_0, eight-day trial.

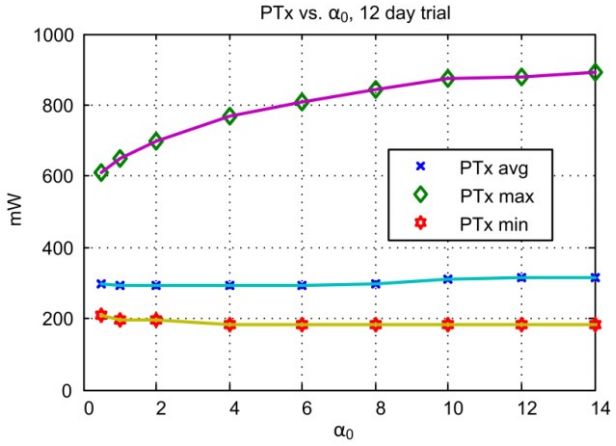

Fig. 3.9.1.9. Transmission power vs. α_0, twelve-day trial.

3.9.2 RSSI hysteresis selection.

Other relevant TRH TPC parameters are the minimum and maximum RSSI thresholds; the gap between them establishes a RSSI hysteresis zone, where the controllers power level output remains in a steady state response even when very small input variations occur [117]. Without this so called hysteresis zone the controller would continually compensate the Tx power level with any slight RSSI change, which might make the scheme unstable by over stressing the radios re-configuration process. Originally, the TRH controller set point was established to be exclusively the desired RSSI minimum value, r_{min}. Afterward, a maximum RSSI limit, r_{max}, was proposed and implemented in my deployments. Both set points determine the controllers RSSI hysteresis zone, or $RSSI_{Hys}$. Various simulation experiments were done changing the RSSI hysteresis width to determine the influence that

threshold selection has on the RSSI behavior. Fig. 3.9.2.1 and Fig. 3.9.2.2 show initial results with α_0=6 using eight days worth of data testing two different hysteresis zones. Fig. 3.9.2.1.(a) illustrates the RSSI result and Fig. 3.9.2.2.(a) shows the transmission power involved in the process of a trial run with r_{max}=-75dBm. In contrast, Fig. 3.9.2.1.(b) is the RSSI plot and Fig. 3.9.2.2.(b) is the P_{Tx} plot with a maximum RSSI threshold of -70dBm.

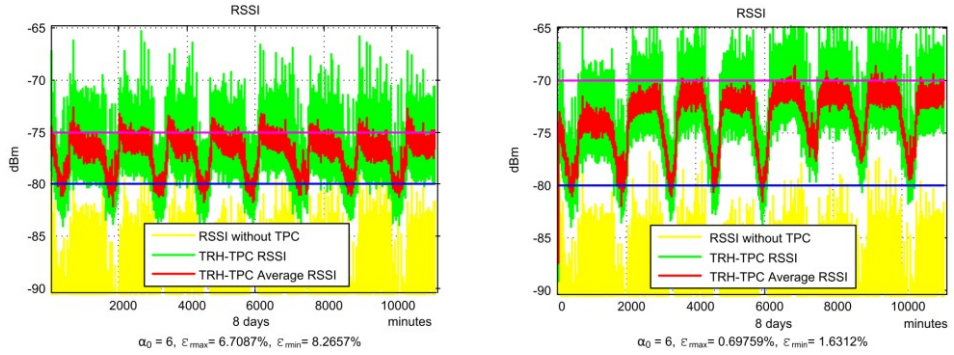

(a) (b)

Fig. 3.9.2.1. RSSI behavior with α_0 = 6, (a) r_{max} = -75dBm and (b) r_{max} = -70dBm.

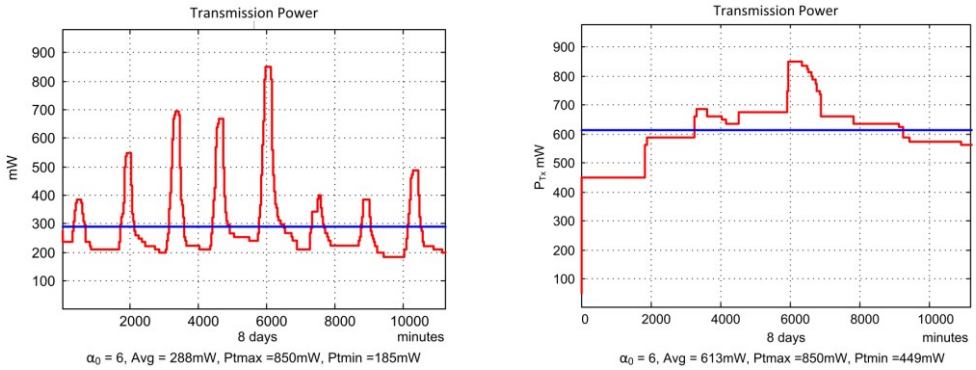

(a) (b)

Fig. 3.9.2.2. Transmission power behavior with α_0 = 6, (a) r_{max} = -75dBm, Pavg = 288mw; and (b) r_{max} = -70dBm, P_{avg} = 613mW.

After analyzing both Fig. 3.9.2.2.(a) and Fig. 3.9.2.2.(b), several issues are apparent, such as:

1. The average RSSI tends to stay near the maximum RSSI threshold.
2. The RSSI error metric is lower when the RSSI hysteresis is wider.
3. The transmission power behavior stops following the TRH gradient when the hysteresis gap is too wide.
4. As the hysteresis gap widens the average transmission power increases.

I did several experiments with different hysteresis gaps; all their results were very similar. We found that with a minimum RSSI of -80dBm the controller operates well up until a maximum threshold RSSI of -72dBm, which represents 3.28% of the entire RSSI span (this is considering a radio sensitivity of -100dBm). Another way of stating the main observation is: The transmission power behavior mostly follows the maximum TRH values if a wide hysteresis zone is used ($RSSI_{Hys} > 4\%$), which is an undesirable condition because the radio involved invests more transmission power than necessary to satisfy the minimum RSSI requirement.

3.9.3 Short average window size and compensation cycle issues.

For the purpose of maintaining stability against sudden climate changes and deep fading, we proposed that the TRH TPC algorithm operate with short averaged values to be able to react accordingly. These are simple mean averages, which add values of a particular variable (be it T, RH or RSSI) and divide them by the number of averaged samples. After every averaging operation, done every N_{avg} samples, the TRH controller determines if power compensation is needed, according to previous Algorithm IV. By default, in our initial deployments, we calculated the average every ten samples, $N_{avg} = 10$. We found that if we change the amount of averaged samples, widening the N_{avg} window, the transmission power behavior also changes. Fig. 3.9.3.1 shows two TRH controlled RSSI plots, with α_0=6. Fig. 3.9.3.1.(a) is the received signal strength using a N_{avg}=10 sample window, and Fig. 3.9.3.1.(b) is the RSSI behavior averaging $N_{avg} = 40$ samples.

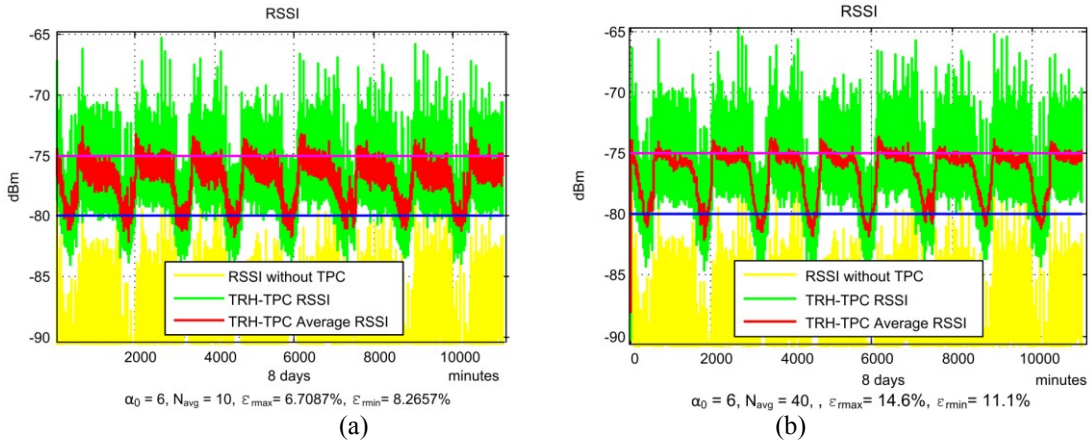

Fig. 3.9.3.1. RSSI behavior with $\alpha_0 = 6$, (a) $N_{avg} = 10$ and (b) $N_{avg} = 40$.

The RSSI curve of Fig. 3.9.3.1.(b) is much smoother than that of Fig. 3.9.3.1.(a). Nevertheless, in Fig. 3.9.3.1.(b) both RSSI threshold errors increased with more averaged samples. On the other hand, Fig. 3.9.3.2.(a) and Fig 3.9.3.2.(b) show the transmitted power plots in mW compensated every N_{avg} = 10 and N_{avg} = 40 samples, respectively. When we extended the averaging window from 10 samples to 40, the minimum transmitted power increased (from 185mW to 248mW), and the peak transmitted power decreased (from 850mW to 624mW). The overall effect of extending the averaging window caused an increase of the average power from 288mW to 316mW.

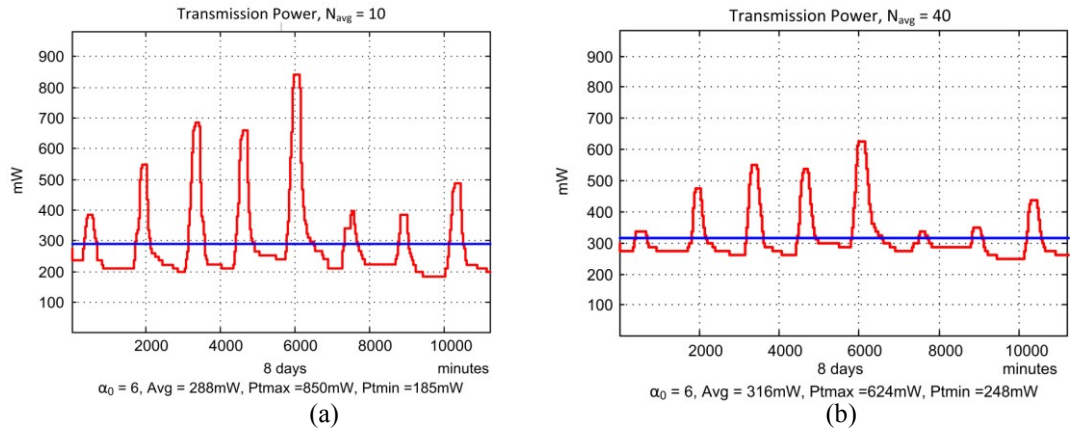

Fig. 3.9.3.2. P_{Tx} behavior with $\alpha_0 = 6$, (a) $N_{avg} = 10$ and (b) $N_{avg} = 40$.

Taking into account that these simulations use data samples acquired every Ts=10 seconds, with an averaging window of N_{avg}=10 samples, the time between power adjustments. T_{avg}, is 100 seconds (or 1.66 minutes). Likewise, with N_{avg}=40 samples power adjustments are made every 400 seconds (or 6.6 min.). The sensor sampling period depends on the application, but the time required to do TRH compensations depends on weather changes, which takes several minutes. Table 3.9.3.1 shows threshold error assessments and transmission power metrics obtained with different averaging windows. When widening the averaging window, two undesirable effects appear: (1) there is an unnecessary increase of the average transmitted power, representing useless power consumption, and (2) the amount of RSSI threshold errors increases notably.

Fig. 3.9.3.3 shows the plot corresponding to the RSSI errors listed in that Table 3.9.3.1 against the averaging time window T_{avg}. It is apparent that short averaging at less than 10 minutes yields better TPC results than otherwise. Also, it is notable that the most affected

performance metric when increasing the time window is the maximum RSSI error, after 10 minutes it climbs over 25%. In Fig. 3.9.3.4 illustrates the transmission power invested with different T_{avg} windows.

Table 3.9.3.1. RSSI minimum error and Tx power metrics of a twelve day simulation with different Navg sample window size, using α_0=6.

N_{avg}	T_{avg} min N_{avg}(Ts=10sec)/60	ε_{min} %	ε_{max} %	P_{Txavg} (mW)	P_{Txmin} (mW)	P_{Txmax} (mW)
5	0.83	5.4	3.7	268	135	872
10	1.66	8.3	6.7	288	185	850
20	3.33	10.2	12.1	307	223	699
30	5.00	11.1	14.8	312	236	649
40	6.66	11.3	18.8	316	248	624
50	8.33	11.5	22.3	316	261	611
60	10.00	11.6	24.8	318	261	586
70	11.66	11.8	26.0	319	261	573
80	13.33	12.2	27.3	320	261	561
90	15.00	12.4	30.9	320	261	548
100	16.66	12.8	33.1	320	261	536
150	25.00	12.9	39.9	319	261	499
200	33.33	13.1	40.3	319	273	474
300	50.00	13.8	44.3	318	273	436

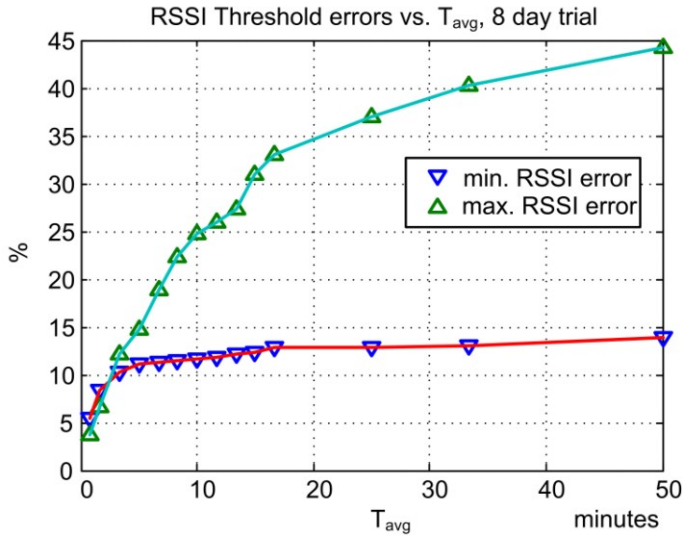

Fig. 3.9.3.3. Minimum and maximum RSSI error vs. T_{avg}, α_0=6.

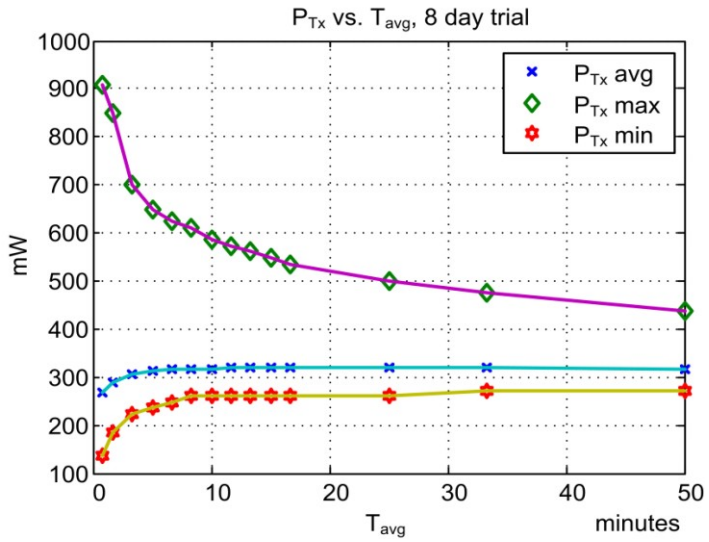

Fig. 3.9.3.4. Transmission power metrics vs. T_{avg}, α_0=6.

Although in Fig. 3.9.3.4 it might seem beneficial that with a wider T_{avg} window less transmission power is consumed, the RSSI errors of Fig. 3.9.3.3 discourages this idea.

3.9.4 Parameter optimization summary.

In this research effort most of the general properties of the TRH TPC proposal from previous work are corroborated, one such statement is that the range of the alpha coefficient is the key of this scheme. With the development and use of our TRH simulation environment, we have determined that the upper alpha bound can be higher, and the separation between maximum and minimum RSSI threshold impacts on the average power consumption. Furthermore, other issues for fine tuning the TRH TPC algorithm are now apparent, such as the need for an appropriate averaging window size, which in consequence sets the compensation cycle period for the TRH TPC operation.

Table 3.9.4.1 lists a brief summary of the updated criteria for the key TRH TPC parameters. Although some observations are tied to the particular test bed radio, the RSSI averaging period selection depends on how fast the wireless channel conditions change in real weather and not on the transceivers' characteristics.

Table 3.9.4.1. Updated TRH TPC parameter summary.

TRH TPC Parameter	Criteria	Description
α_0	$2 < \alpha_0 < 6$	TRH TPC gain coefficient for a good convergence considering $\varepsilon_{min} < 10\%$ and $\varepsilon_{max} < 10\%$.
$RSSI_{Hys}$	4% max.	Hysteresis percentage. $RSSI_{Hys} = 100*(r_{max}-r_{min})/(\text{Full range RSSI})$ For minimal Tx power waste.
$T_{avg} = Ts\ N_{avg}$	< 10 minutes	RSSI averaging period = TRH TPC cycle Cycle sensitive to wireless channel conditions, which depends on the weather. In this test bed we considered Ts = 10 sec. and $N_{avg} < 60$ samples.

By combining the criteria for all parameters, an optimum TRH TPC deployment can now be done. Let us consider a simulation with optimal parameters using the same wireless link conditions as before. A selection within the proposed bounds would be an alpha equal to α_0=4 (at the middle of the alpha range), an updated maximum RSSI threshold equal to r_{max}=-77dBm (that represents a relative hysteresis gap of $RSSI_{Hys}$=3% with r_{min} = -80dBm), and an RSSI averaging window equal to N_{avg}=6 samples every 10 seconds (T_{avg} = 60 seconds or T_{avg}=1 min < 10 min). Fig. 3.9.4.1 and Fig. 3.9.4.2 show the corresponding simulation results of the controlled RSSI and the transmission power invested in the process.

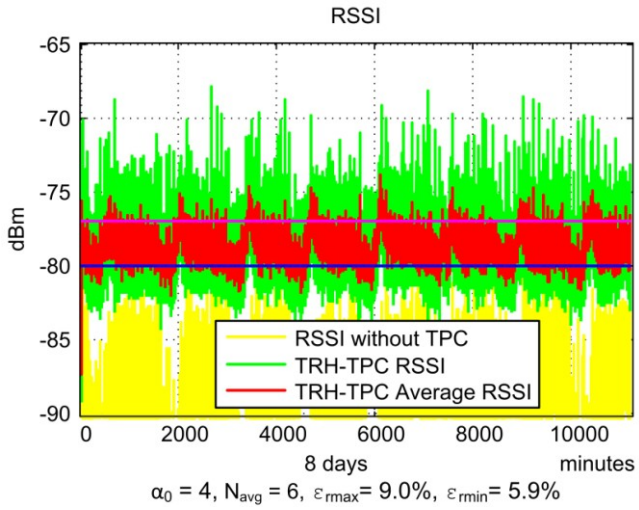

Fig. 3.9.4.1. RSSI result of an eight-day simulation using TRH parameters within the optimal range.

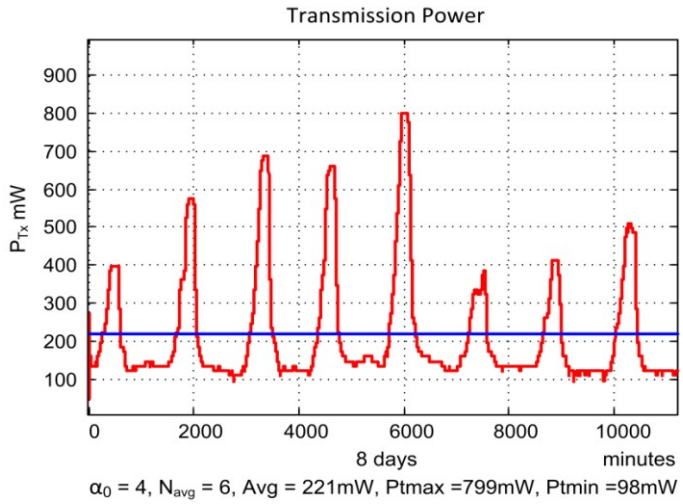

Fig. 3.9.4.2. Transmission power in mW of an eight-day simulation using optimal TRH parameters.

Notice in Fig. 3.9.4.1 that both average RSSI errors are less than 10% and in Fig. 3.9.4.2 the average Tx power is 221 mW, which is less than any of the recorded power averages in Table 3.9.1.1, Table 3.9.1.2 or Table 3.9.3.1.

For comparison purposes, let us consider another example with the same parameters, except that now the compensation period is longer using N_{avg} = 60 samples every 10 seconds (T_{avg}=600 seconds or T_{avg}=10 min). Fig. 3.9.4.3 shows the simulation result of the controlled RSSI and Fig. 3.9.4.4 the transmission power invested in the process.

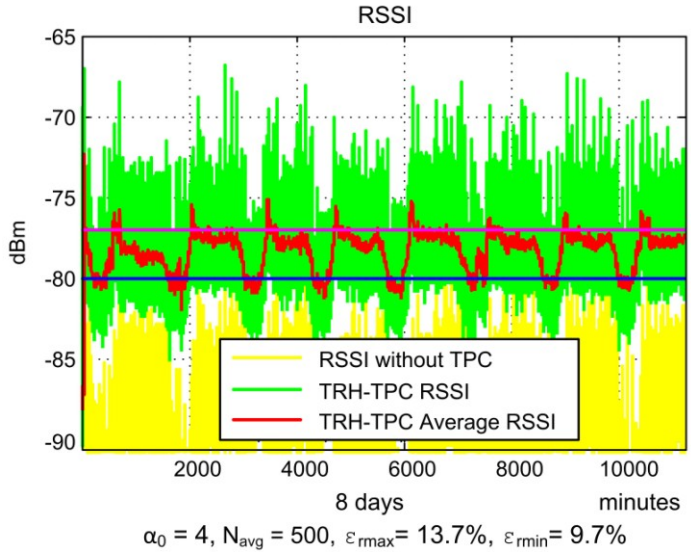

Fig. 3.9.4.3. RSSI result of an eight-day simulation using optimal TRH parameters with a higher T_{avg} period than the example of Fig. 3.9.4.1.

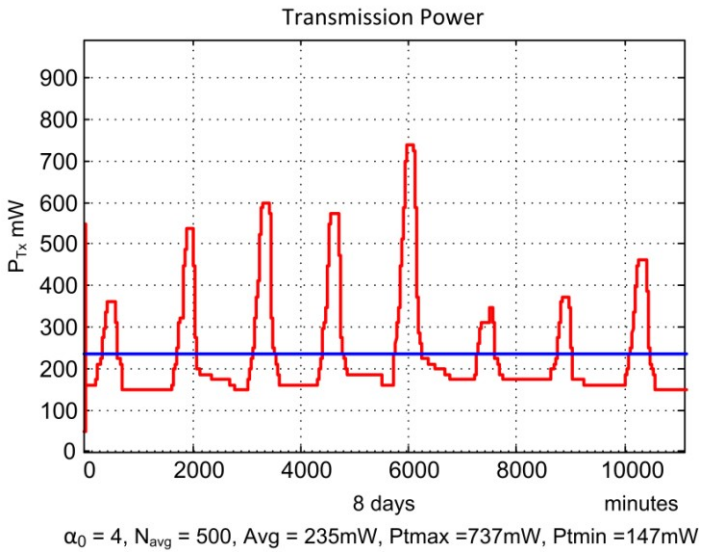

Fig. 3.9.4.4. Transmission power in mW of an eight-day TPC simulation using optimal TRH parameters with a higher T_{avg} period than the example of Fig. 3.9.4.2.

Fig. 3.9.4.3 shows that, this time, the only RSSI error that is within the <10% objective is ε_{min}. Moreover, in Fig. 3.9.4.4 the average Tx power is 235 mW, which is less than any of the recorded power averages in Table 3.9.1.1, Table 3.9.1.2 or Table 3.9.3.3. These findings corroborate that by combining the best parameter options for deployment, the current TRH algorithm will operate in an optimal manner.

3.10 Real CLH deployment and TRH experimental results.

Deployment of the updated TRH TPC algorithm was done once more on two CLH systems near the beach, and they were left working for several days transferring gathered environmental data and communications performance metrics. For comparison purposes, a third CLH with no TPC was also deployed. The experimental CLH system software queries the AC4490 radio for instantaneous RSSI readings at its receiver. It is useful to determine a short average RF noise floor and possible interfering sources occupying the wireless channel. These metrics reflect the quality of the communications channel and are intended to be compared to the actual TRH gradient and the algorithms transmission power gain adjustments.

3.10.1 Experimental platform for long-term CLH deployment.

A similar hardware deployment was done in a harsh environment as previously described in sub-section 2.3.4, this time more robust cases were used as the one shown in Fig. 3.10.1.1. Furthermore, and updated TRH TPC algorithm implementation was done with the optimal criteria in mind, similarly to the initial TRH TPC testing described in section 3.2.

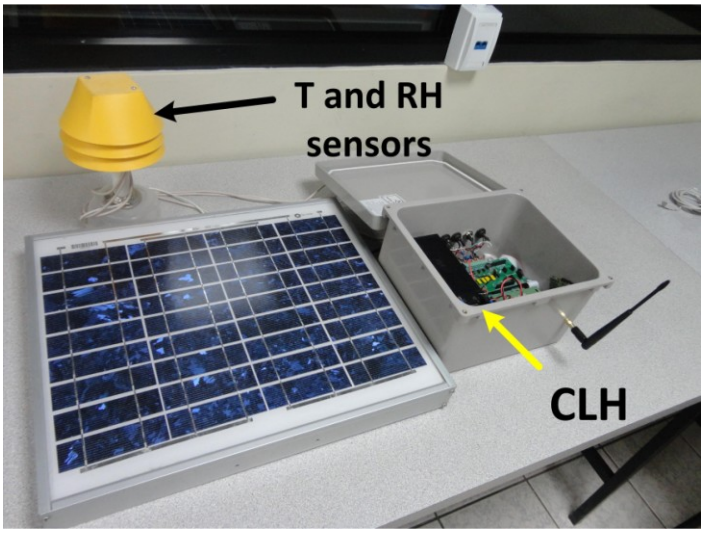

Fig. 3.10.1.1. Long range communications CLH system for remote harsh environment deployments.

The antennas of both CLH and BS systems were fitted with RF attenuators to emulate a longer distance between them as explained in sub-section 3.1.3. This time, a 2.5 Km distance emulation was setup, although the CLH systems were only 5m from the BS. The systems were deployed near the beach on a rooftop, with the aim of exposing the CLH to variable harsh temperature and humidity conditions for TRH TPC testing.

3.10.2 Updated TRH TPC deployment results.

Three ArduinoMega based CLH systems were left operating exposed to beach front weather conditions, as shown in the illustration of Fig. 3.10.2.1. One CLH was setup to transmit at a fixed power level, and the other two operating with the real time TRH TPC algorithm. Software was developed using the controllers native C++ for embedded systems. Messages sent by the CLH towards the BS were answered by an acknowledgement message, ACK, as explained in sub-section 2.2.3. During this feedback process, relevant metrics were communicated back to the CLH for its TRH TPC operations.

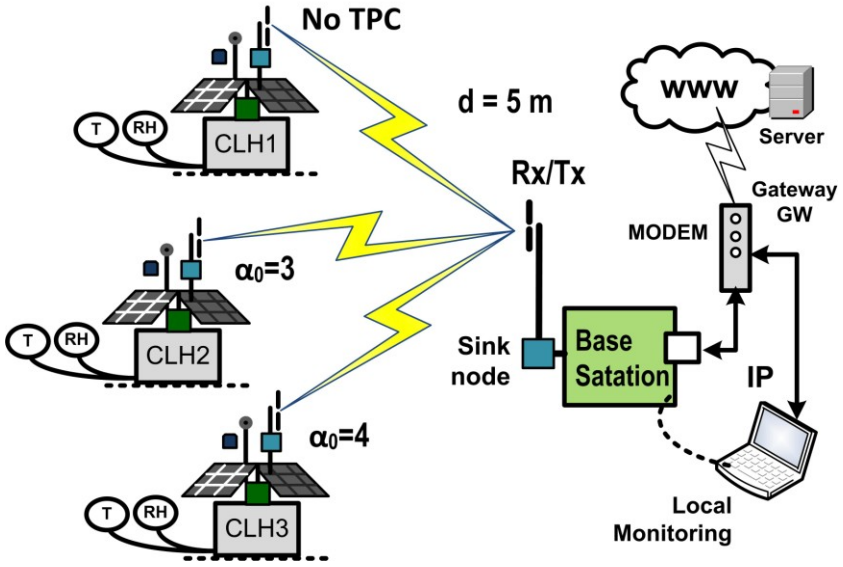

Fig. 3.10.2.1. Experimental CLH setup for final test of the TRH TPC scheme.

All CLH systems were programmed to gather T and RH data and to maintain a counter of the ACK messages received back from the BS against the total of messages sent after each transmission. Being that CLH-1 served as the reference system it was not programmed with TPC, its radio was configured to transmit at a fixed 200mW transmission power level according to the minimum power needed to reach a 2.5Km distance. Using the previous wireless power budget calculations, the estimated RSSI level should be -73dBm by excluding a fade margin. Meanwhile, CLH-2 and CLH-3 were programmed with the updated TRH TPC approach operating with α_0=4 and α_0=3, respectively. Their radios were also configured at the same 200mW starting Tx power level.

In the case of CLH-1, Fig. 3.10.2.2.(a) shows its resulting RSSI levels, Fig. 3.10.2.2.(b) is its temperature plot and Fig. 3.10.2.2.(c) is its RH measurements plot. Notice that the curves are reciprocal when comparing the RSSI with temperature, and the curves are proportional when comparing the RSSI with relative humidity. Also, Fig. 3.10.2.3 shows the simultaneously measured RF signals at CLH-1 receiver input, notice that again its shape is reciprocal to the RSSI curve of Fig. 3.10.2.2.(c). The resulting CLH-1 PRR during this time is presented in Fig. 3.10.2.4, PRR performance worsens during the day when the RSSI values are at their lowest near -95dBm.

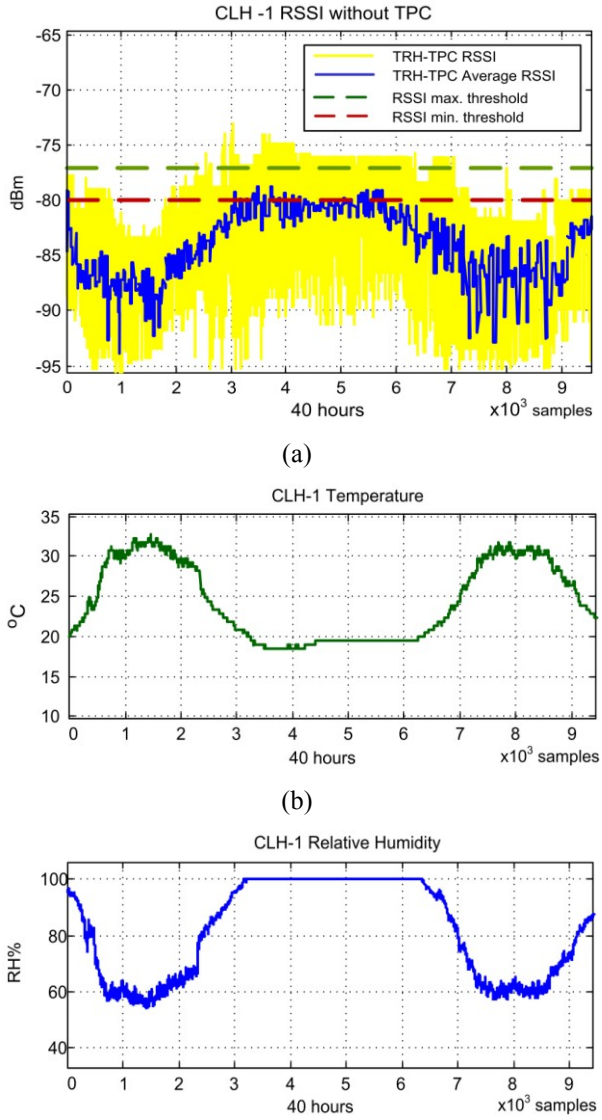

Fig. 3.10.2.2. Reference CLH-1 without TPC (a) RSSI values, (b) T and (c) RH readings.

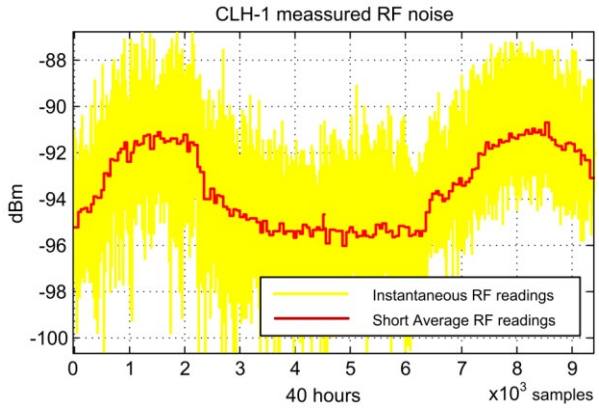

Fig. 3.10.2.3. CLH-1 measured RF noise and/or interference.

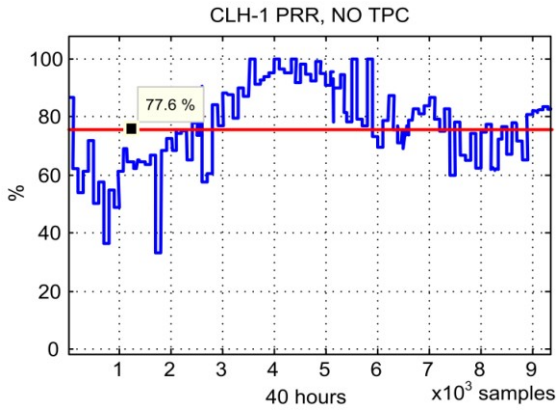

Fig. 3.10.2.4. CLH-1 Packet Received Rate, operating without TPC and no retries reached 77.6%.

Meanwhile, figures 3.10.2.5.(a) and 3.10.2.5.(b) show CLH-2 measured T and RH. Figures 3.10.2.6.(a) and 3.10.2.6.(b) illustrate CLH-2 calculated TRH gradient and measured RF noise floor at the time, notice that they have a similar shape. Moreover, Fig. 3.10.2.7 shows CLH-2 transmission power adjustments, which follow the TRH gradient and noise floor changes.

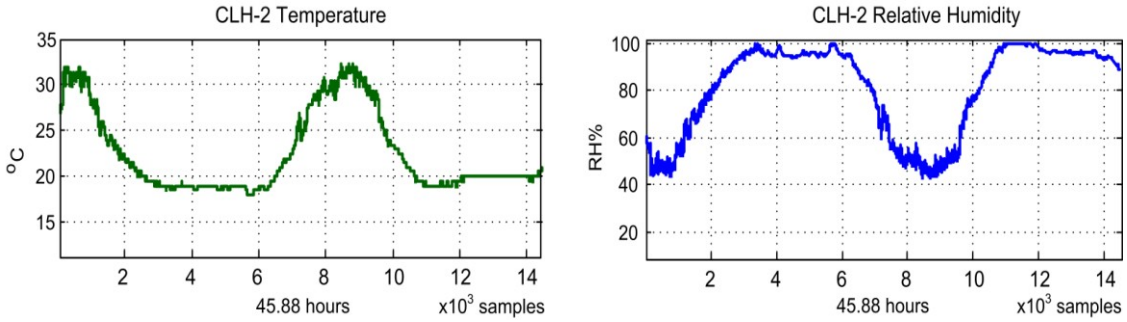

(a) (b)

Fig. 3.10.2.5. Two day CLH-2 (a) temperature and (b) relative humidity measurements.

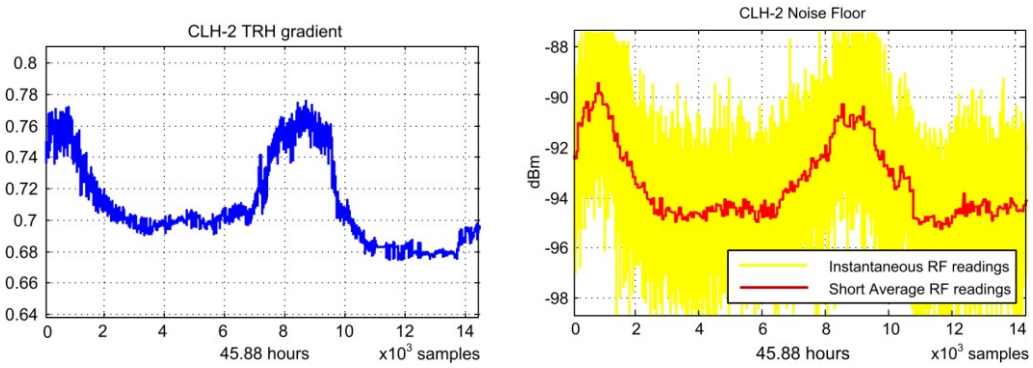

(a) (b)

Fig. 3.10.2.6. Two day CLH-2 (a) TRH gradient and (b) measured noise floor in dBm.

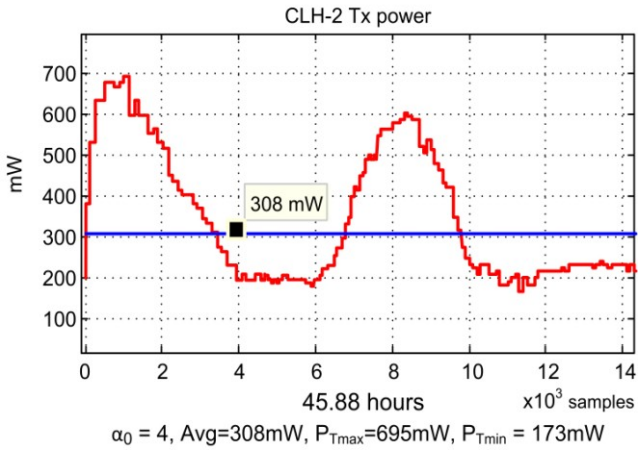

Fig. 3.10.2.7. Two day CLH-2 transmission power level adjustments.

The resulting two day CLH-2 RSSI readings, measured at the BS and fed back to cluster-head, are plotted in Fig. 3.10.2.8. The average CLH-2 RSSI (curve plotted in blue) was maintained within the maximum and minimum RSSI thresholds or hysteresis zone. And in Fig. 3.10.2.9 a two-day CLH-2 PRR performance is illustrated obtaining a 96.94% average, which is 19% better than CLH-1 performance operating with no TPC.

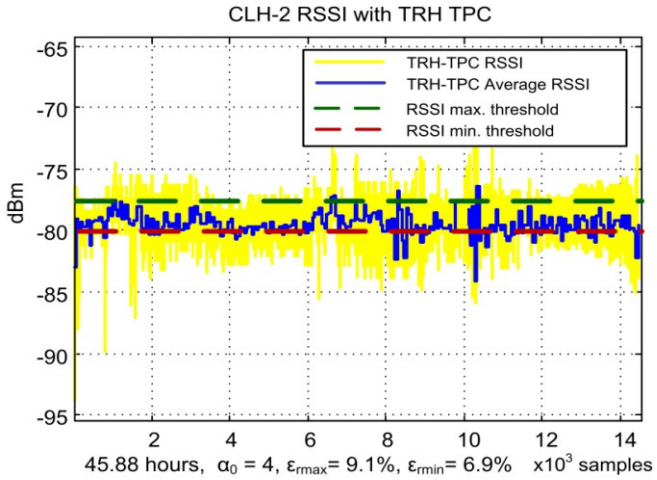

Fig. 3.10.2.8. Two day CLH-2 controlled RSSI.

Meanwhile, figures 3.10.2.10.(a) and 3.10.2.10.(b) show the temperature and relative humidity measured by the third CLH system. Also, figures 3.10.2.11.(a) and 3.10.2.11.(b) illustrate the temperature TRH gradient calculated by CLH-3 and the measure RF noise floor at the same time. And Fig. 3.10.2.12 represents CLH-3 plotted transmission power adjustments, notice that it follows the TRH gradient and RF noise floor changes.

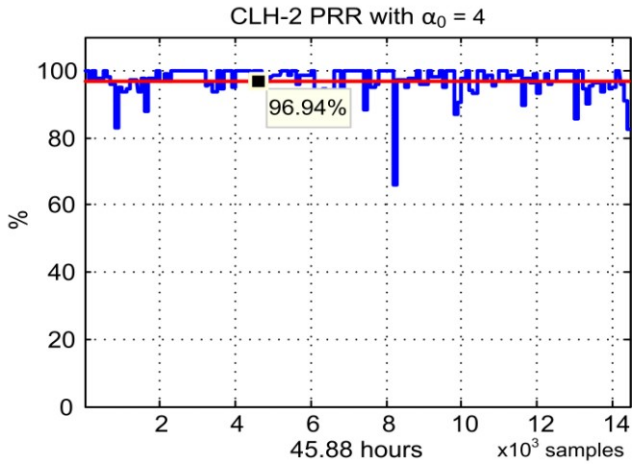

Fig. 3.10.2.9. Two day CLH-2 with TRH TPC packet received rate, with no Tx retries reached a 96% PRR average.

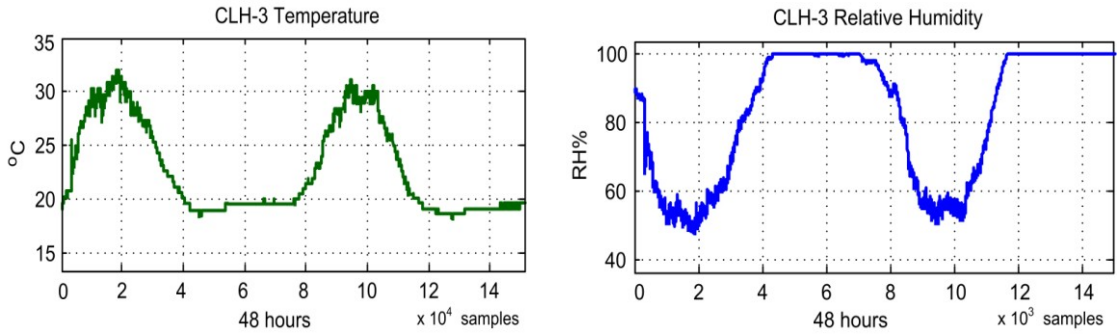

(a) (b)

Fig. 3.10.2.10. Two-day CLH-3 (a) temperature and (b) relative humidity measurements.

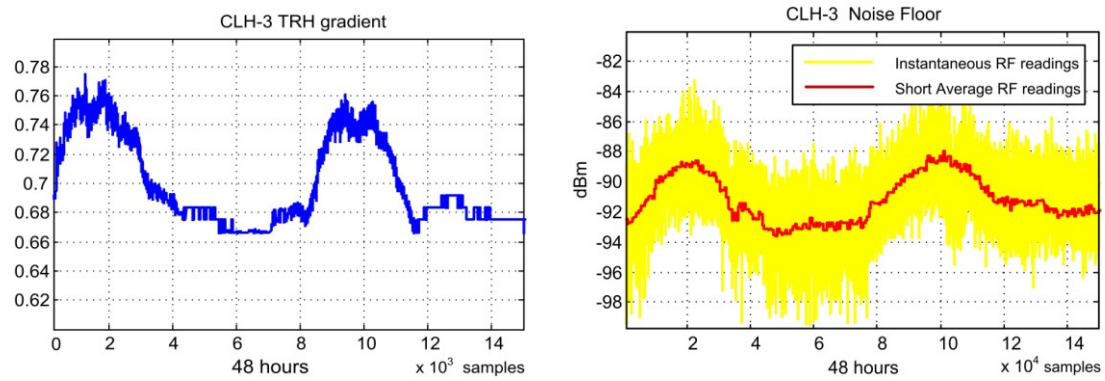

(a) (b)

Fig. 3.10.2.11. Two-day CLH-3 (a) TRH gradient and (b) measured noise floor in dBm.

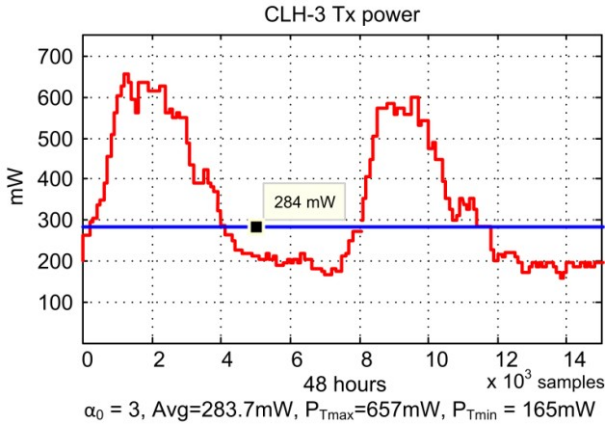

Fig. 3.10.2.12. Two-day CLH-3 transmission power level adjustments.

The overall RSSI performance of CLH-3 to BS communications is shown in Fig. 3.10.2.13, and its PRR performance is illustrated in Fig. 3.10.2.14, which achieved a 95% PRR.

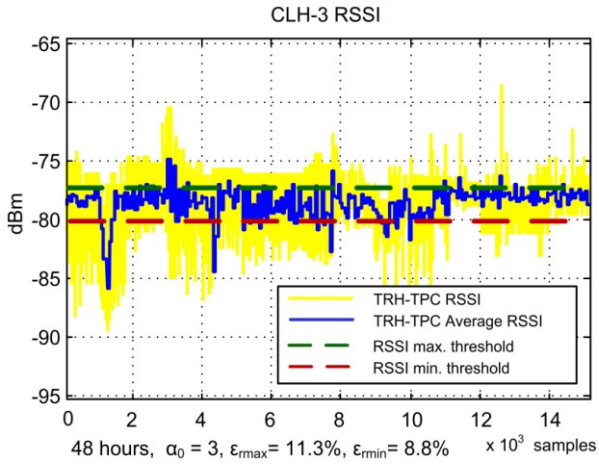

Fig. 3.10.2.13. Two-day CLH-3 controlled RSSI.

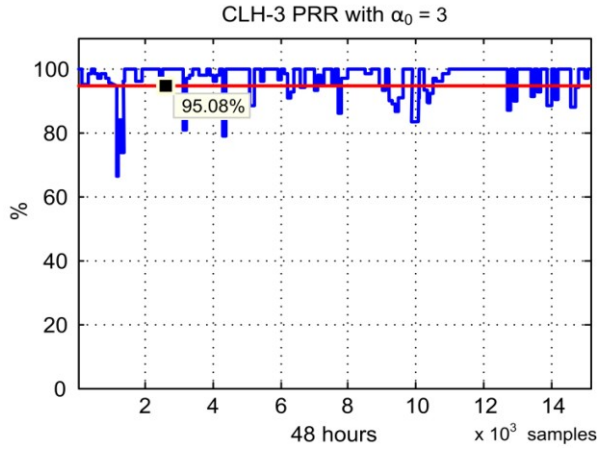

Fig. 3.10.2.14. Two-day CLH-3 with TRH TPC packet received rate, with no retries reached a 95% average.

Table 3.10.2.1 summarizes the performance comparison between CLH system operations. Although CLH-1 reached the RSSI target a few times, transmitting at a fixed 200mW level, only during the night it performed nearly as expected with an RSSI average 2dB under the minimum threshold. Nevertheless, CLH-1 achieved a poor -88dBm RSSI daytime average, which adversely affected its PRR reaching only a 77% packet delivery rate. In contrast, most of the time CLH-2 and CLH-3 maintained their RSSI averages within the minimum and maximum RSSI thresholds. This was reflected on their overall PRR performance, by delivering to BS over 95% of their transmitted packets.

Table 3.10.2.1. Two-day performance comparison of the updated TRH TPC.

CLH	**RSSI avg** Day / Night dBm	**PRR** %	**PL**	**P_{Tx}** mW Non-linear Max. / min.	**P_{Tx}** (dBm)	**P_{Tx}** mW average
1 (no TPC)	-88 / -82	**77**	36	208	20.1	208
2 ($\alpha_0 = 4$)	-79 / -77	**96**	67 max 38 min	695/ 230	28.4 / 23.6	308
3 ($\alpha_0 = 3$)	-79 / -77	**95**	65 max 32 min	657 / 165	28.2 / 22.2	284

For a medium term operational view, the following figures show a seven-day CLH-2 behavior measured at a different time frame than the previous experiments. Figures 3.10.2.14, 3.10.2.15, 3.10.2.16 illustrate the temperature, RH and TRH gradient determined by the CLH-2 system during the seven day experiment. Likewise, Fig. 3.10.2.17 show the CLH-2 measured RF noise floor, which has a similar shape than the TRH gradient of Fig. 3.10.2.16. Furthermore, Fig. 3.10.2.18 illustrates the Tx power adjustments done by the updated TRH TPC algorithm trying to compensate against changing RF channel conditions. CLH-2 achieved a 263mW average and during night it went down as low as 140mW, which is better than the calculated 200mW Tx power for a 2.5Km distance from the intended receiver.

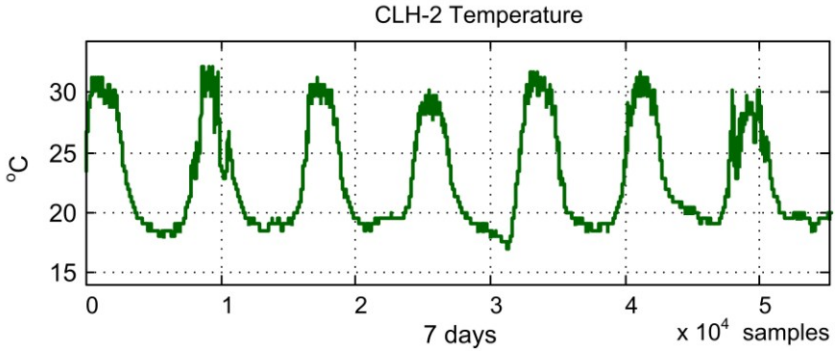

Fig. 3.10.2.14. CLH-2 seven-day temperature measurements.

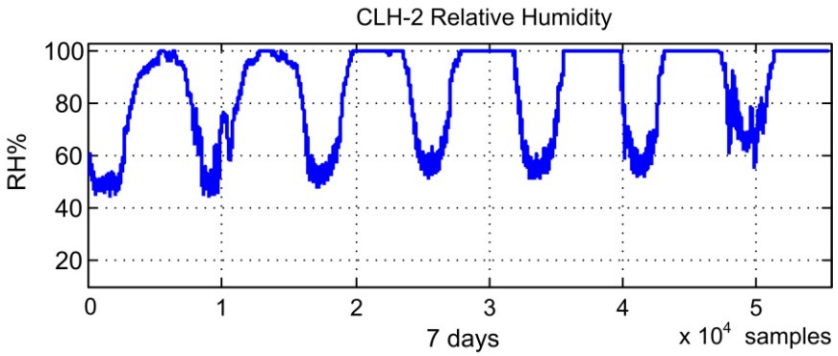

Fig. 3.10.2.15. CLH-2 seven-day relative humidity measurements.

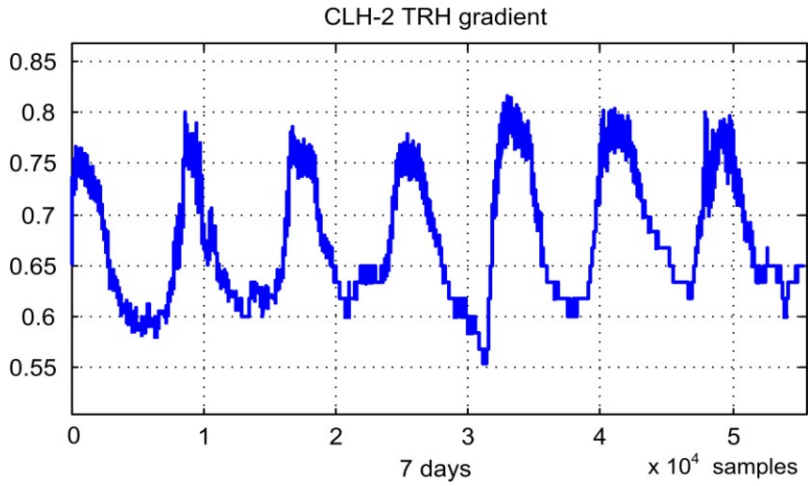

Fig. 3.10.2.16. CLH-2 seven-day TRH gradient behavior.

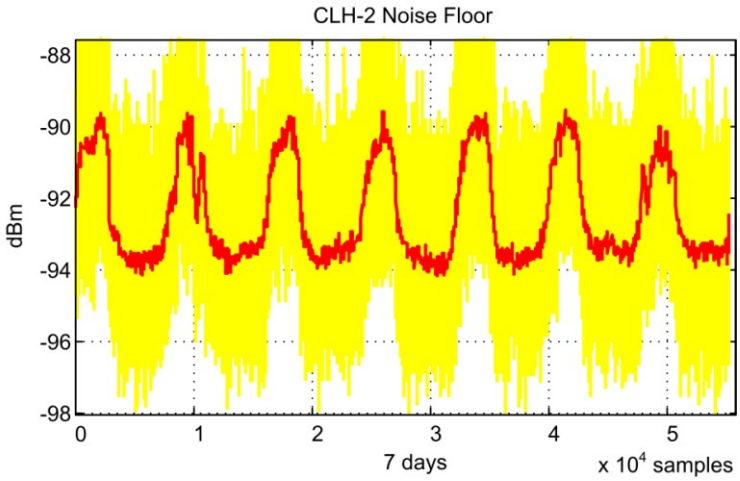

Fig. 3.10.2.17. CLH-2 seven-day RF noise floor measurements.

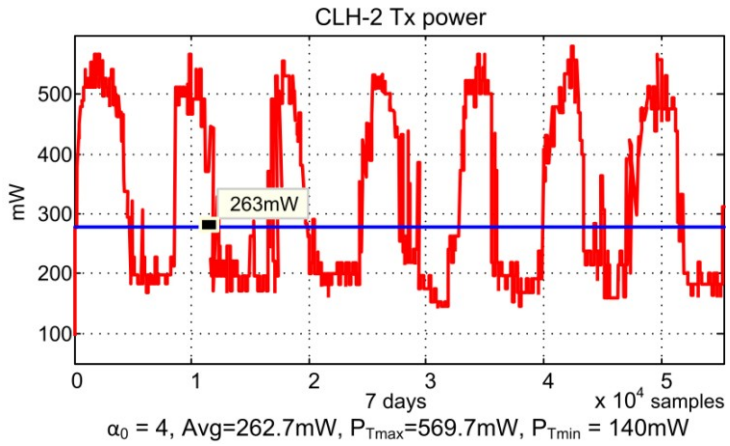

Fig. 3.10.2.18. CLH-2 seven-day transmission power levels adjustments.

The overall RSSI and PRR performances of the seven-day CLH-2 experiment are shown in figures 3.10.2.19 and 3.10.2.20, respectively. The measured RSSI levels were kept within the TRH TPC hysteresis zone, with a minimum RSSI error of 3.5% and the maximum RSSI error of 5.1%, which is better than expected performance obtained from the simulation results of section 3.9. Likewise, the PRR performance was over 95%, which is a very good result considering that the radios had their Tx retry feature disabled. These results corroborate the initial TRH TPC experimental results of section 3.5 and the optimal criteria results of sub-section 3.9.4.

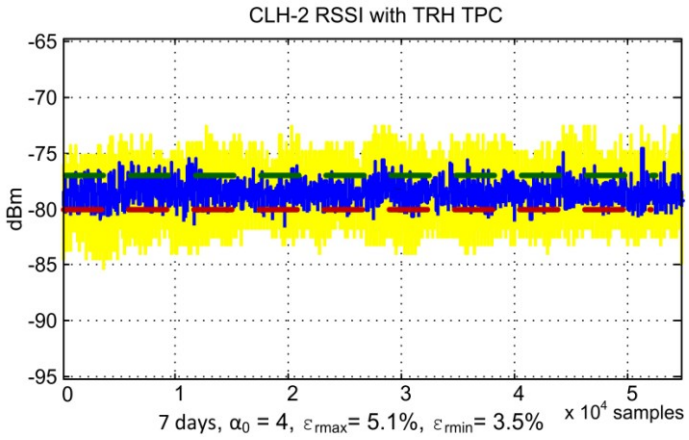

Fig. 3.10.2.19. CLH-2 seven day RSSI performance.

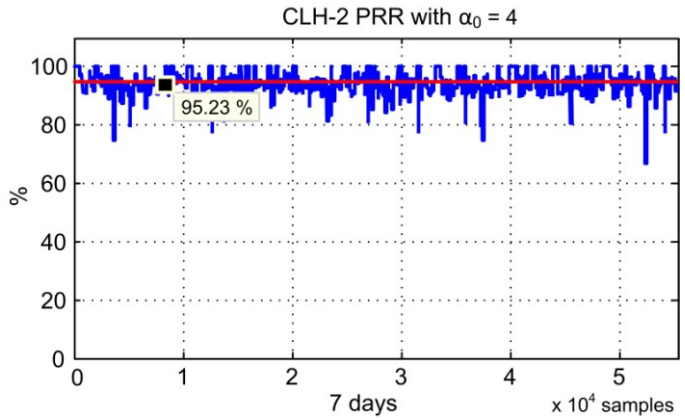

Fig. 3.10.2.20. CLH-2 seven-day PRR performance.

Although the simulation results reflect in part a real world TRH TPC behavior, because it uses real RF noise floor samples and actual T and RH measurements, it cannot account for spurious RF signals or faulty antennas and wave guide connections. Nevertheless, these final real deployment results corroborate the effectiveness of the simulation platform by obtaining similar RSSI averages using the optimal parameter values, with a very good overall PRR of over 90% without transmission retries.

Summarizing, in this Chapter, I presented my proposal for a TRH TPC scheme. I started by analyzing environmental data such as temperature and relative humidity, and compared their variations with simultaneous RSSI variations. Afterwards, I proposed an expression for the TRH gradient that depends on a so-called alpha gain coefficient as a means for transmission power compensation. The initial model was a closed loop controller with RSSI value feedback, using a single minimum RSSI threshold. After evaluating its performance, I determined that by adding a second maximum RSSI threshold the controller became more stable. To shorten the time needed to evaluate the TRH TPC performance, I developed a simulation platform using real T, RH and noise values measured previously by long range environmental wireless sensor systems. After many simulation runs, using a wide range of parameter values, and analyzing the results, I determined a set of optimum TRH TPC parameter ranges that affect the overall wireless power consumption. And finally, I deployed the updated TRH TPC operating on real wireless systems, and compared their operation against a system without TPC, which confirmed the expected RSSI and PRR performance.

Chapter IV. Conclusions

The idea behind the TRH gradient became apparent after developing a WSN experimental framework, validating sensor measurements, and observing how T and RH affect the RSSI with the selected technology. The TRH gradient follows the RF noise floor behavior and is proportional to the shape of the resulting RSSI signals. This thesis focused on developing a novel TPC scheme based on T and RH changes, along with very short RSSI feedback averages, to establish the amount of transmission power required for outdoor WSN communications. This approach deploys the TRH gradient as the argument of a logarithmic function that calculates the controller's gain, which is also adjusted by another parameter called α_0. This non-linear gain function avoids transmission power instability by dampening the overall RSSI gain when the RSSI errors increase drastically; or by augmenting the gains magnitude when the RSSI error is present but not significant enough to be mitigated entirely by a linear RSSI gain increase. I found an optimal range for this α_0 coefficient after long periods of experimentation, that produce effective gain variations against changing RSSI conditions. Initially, I worked with a TPC scheme with a single controller set-point, which I call the minimum RSSI threshold or r_{min}. Afterwards, I included a second set-point to the control model by adding a maximum RSSI threshold or r_{Max}. This updated approach is intended to maintain TPC stability within a RSSI *hysteresis* zone, which is limited by r_{min} and r_{Max}. Another issue under study was the impact that the RSSI average time window has on the total transmission power estimation. During this time window, short mean RSSI averages are done and used at the end of the cycle to do the actual Tx power compensation. Another interpretation is that the RSSI averaging time window sets the minimum time between discrete Tx power updates. In the next sections, the details of the contributions of this thesis are presented, as well as perspectives of deploying the proposed TRH TPC algorithm in harsh environment conditions and future related work that includes potential application spaces.

4.1 Accomplishments and Contributions.

The most important contribution of this work, not found in the literature, is that it proved that -not just temperature but- both T and RH can be used to determine a gain factor for an effective RSSI feedback TPC algorithm, applied to outdoor long range WSN. Meanwhile, the first accomplishment was reached when the initial TRH TPC single set-point prototype model was successfully deployed, with a 92% PRR performance result. This accomplishment was the stepping stone towards refining the proposed model by adding a RSSI hysteresis TPC for stability purposes. After many efforts and data gathering experiments, an important mile stone was reached when I developed an efficient and realistic TRH TPC simulation platform with the updated control model. This useful experimentation tool accelerated the process of correcting the previous optimal TRH TPC parameter ranges. And during the final experimentation stage, my last accomplishment was the actual deployment of the updated optimal TRH TPC model, which performed at a 95% PRR and more than 85% of the resulting RSSI values kept within the designated RSSI hysteresis zone. The latter confirms that the main contribution of this body of work was determining with certainty the optimal parameters and the behavior of an original proposal for a TPC based on T and RH.

4.2 Future work.

After finishing this thesis, there is still work left to be done:

- The most-pressing aspect is the issue of the type of mathematical expression used for TRH gain value calculations, besides using the proposed logarithmic function other simpler paradigms might be suitable or more efficient.
- The other important issues are the optimal TRH TPC parameter ranges, and determining if these are not technology dependent, through real world deployment and testing with different types of radios. Although the basic TRH algorithm principles and criterion are my contributions, other work can be done to determine how much is or is not dependent on the deployed radio technology.
- Considering that other types of digital radios also use the link quality indicator, as a wireless performance metric, further work might also involve using this LQI instead of the RSSI feedback approach, only if the technology allows it.

- Other pending work has to do with comparing the performance of this TRH TPC approach against conventional adaptive TPC approaches, running on systems using the same radio technology for fairness. Different TRH TPC proposals can surge from this line of research, which might include a modified adaptation approach using a hybrid mean-squared error estimate approach.
- Determining a precise wireless channel characterization from a telecommunications point of view, involving air temperature, moisture and pressure, might open the door to possibly developing deterministic approaches of TPC for WSN applications.
- And finally, another unexplored aspect has to do with the appropriate application spaces for this scheme, this is related with the need of harsh environment real deployment testing to determine the complete benefits or disadvantages of using this approach in real outdoor WSN applications.

Many ideas arise from a novel approach; here there is still much work to be done as the previous list shows. For example, the impact on power consumption is an issue not yet considered. Likewise, collaborative efforts between wireless systems can be included in the mix if local onboard sensors fail. In real deployments, fault tolerant issues have to be addressed, and surely several other application specific problems will come up when trying to deploy this TRH TPC paradigm.

References

[1] J.J. Evans. **Undergraduate research experiences with wireless sensor networks.** IEEE Frontiers in Education Conference: Knowledge Without Borders, Opportunities Without Passports, 2007, FIE '0y. 37th Anual. 10-13 Oct, 2007. Milwaukee, WI, USA. ISSN 0190-5848.

[2] A. Forster, M. Jazayeri. **Hands-on Approach to Teaching Wireless Sensor Networks at the Undegradute Level**. ACM ITiCSE 2010, Bilkent, Turkey.

[3] Pei Huang, Li Xiao, S. Soltani, M. W. Mutka. **The evolution of MAC protocols in Wireless Sensor Networks: A Survey**. IEEE Communications Society, Communications Surveys & Tutorials, IEEE. Vol. 15, Issue 1. First quarter 2013. p. 101 - 120.

[4] Akilandereswari, B. Santhi and B. Baranidharn. **A survey on energy conservation techniques in Wireless Sensor Networks.** ARP Journal of Engineering and Applied Sicences. Vol 8, No. 4, April 2013. ISSN 1819-6608.

[5] A. A. Alhameed Alkhatib, G. Singh Baicher. **An overview of Wireless Sensor Networks**. 2012 International Conference on Computer Networks and Communication Systems, CNCS 2012, IPCSIT col. 35, IACSIT Press, Singapore.

[6] D. Villa, et al. **Ubiquitous Virtual Private Network: A Solution for WSN Seamless Integration.** Sensor Journal. Jan. 2014; 14(1): 779-794.

[7] G. Anastasi, M. Conti, M. Di Francesco, A. Passarella. **Energy conservation in Wireless Sensor Networks: A survey.** Ad Hoc Networks. Volume 7, Issue 3, May 2009, 537-568.

[8] H. Cotuk, K. Bicakci, B. Tavli, E. Uzun. **The Impact of Transmission Power Control Strategies on Lifetime of Wireless Sensor Networks.** IEEE Transactions on Computers, Vol. PP, Issue: 99. 7/31/2013. ISSN: 0018-9340.

[9] Dongjin Son, Bhaskar Krishnamachari, John Hedemann. **Experimental study of the effects of transmission power control and blacklisting in wireless sensor networks.** First Anual IEEE Communications Society Conference on Sensor and Ad Hoc Communications and Networks, 2004. Page(s): 289 - 298.

[10] Luis M. L. Oliveira. **Wireless Sensor Networks: a Survey on Environmental Monitoring.** Journal of Communications, Vol. 6, No. 2, April 2011. Academy Publisher, doi: 10.4304/jcm.6.2.143-151.

[11] G. Barrenetxea, F. Ingelrest, G. Schaefer, M. Vatterli. **Wireless Sensor Networks for Environmental Monitoring: The SensorScope Experience.** IEEE International Zurich Seminar on Communications. 12/14 March 2008, pages 98 - 101. ISBN: 978-1-4244-1681-3.

[12] Peter Roberson. **Using Data Loggers.** Science Teachers' Workshop 2004. Sydney, Australia.

[13] Mark Rhodes. **Underwater Electromagnetic Propagation**. Hydro International electronic magazine. 2006. http://www.hydro-international.com/issues/articles/id697-Underwater_Electromagnetic_Propagation.html. Last visited on November 2010.

[14] Dolujanov, M. **Propagation of radio waves.** Moscou, YPCC. Translation by Boris Kuznetsov .1995. ISBN: 5884170823.

[15] Shlomi Arnon . **Underwater optical wireless communication network**. Optical Engineering Journal special issue. 2010. Presented at SPIE conference on Free-Space Laser Communications IX, August 2009.

[16] Heaher Brundage. **Acoustic Propagation Considerations for Underwater Communications**. M.S. in Mechanical Engineering thesis. Massacchusetts Institute of Technology. 2010.

[17] J. Preisig, **Acoustic propagation considerations for underwater acoustic communications network development.** in Proc. Underwater Networks, 2006, pp.1-5.

[18] Ian F. Akyildiz, Dario Pompili, Tommaso Melodia. **Challenges for efficient communication in underwater acoustic sensor networks**. ACM SIGBED Review - Special issue on embedded sensor networks and wireless computing. Volume 1 Issue 2, July 2004.

[19] Milica Stojanovic. **Underwater Acoustic Communication**. Northeastern University. Wiley Encyclopedia of Electrical and Electronics Engineering. 1999.

[20] P. Tyack, A. Fernández, L. Crim, A. Costidis, A. Wright and D. Cottingham. **Marine mammals and noise. A sound approach to research and management.** A Report to Congress of the U.S.A. from the Marine Mammal Commission. 2007.

[21] Whitlow W. L. Au & Kelly J. Benoit-Bird. **Automatic gain control in the echolocation system of dolphins.** Hawaii Institue of Marine Biology, University of Hawaii. Letter to nature, Vol. 423. Nature Publishing Group. 2003.

[22] Michael Lehning, Nicholas Dawes, Mathias Bavay, Marc Parlange, Suman Nath, and Feng Zhao. **Instrumenting the Earth: Next-Generation Sensor Networks and Environmental Science.** Microsoft Research. 2009.

[23] Philip W. Rundel, Eric A. Graham1, Michael F. Allen, Jason C. Fisher and Thomas C. Harmon. **Environmental sensor networks in ecological research**. New Phytologist Journal. 2009.

[24] Pedro Barbosa, Neil M. White, Nick R. Harris. **Design challenges in application-aware wireless sensor networks.** Conference on Information Systems and Technologies (CISTI), p. 16-19 June 2010, Santiago de Compostela. Spain.

[25] V.S. Hsu, J.M. Kahn, and K.S.J. Pister . **Wireless Communications for Smart Dust.** Technical Report. Department of Electrical Engineering and Computer Sciences . University of California at Berkeley. 1998.

[26] Joseph M. Kahn , Randy Howard Katz , Y Howard Katz , Kristofer S. J.. **Emerging Challenges: Mobile Networking for 'Smart Dust'**. Journal of Communications and Networks. 2000.

[27] Brett Warneke, Matt Last, Brian Liebowitz, Kristofer S.J. Pister. **Smart Dust: Communicating with a Cubic-Millimeter Computer**. Computer Journal. IEEE Computer Society. 2001.

[28] Yunbin Song. **Optical Communication Systems for Smart Dust**. M.S. thesis. Virginia Polytechnic Institute and State University. 2002.

[29] Yao-Jung Wen. **Smart Dust Sensor Mote Characterization.** Masters of Science at the University of California, Berkeley. 1999.

[30] Ian F. Akyildiz, Weilian Su, Yogesh Sankarasubramaniam, and Erdal Cayirci. **A Survey on Sensor Networks**. IEEE Communications Magazine. August 2002.

[31] Barjinder Singh Kaler, Er. Manpreet Kaur Kaler. **Challenges in Wireless Sensor Networks**. ACM SIGBED Review (2004). Volume: 1, Issue: 2, Publisher: ACM Press, Pages: 142-142.

[32] Chris Townsend, Steven Arms. **Wireless Sensor Networks: Principles and Applications**. Sensor technology handbook (2005) . Volume: 11, Issue: 6, Publisher: Newnes, Pages: 575-589.

[33] Ethan Culler-Mayeno. **A Technical Report: Wireless Sensor Networks and How They Work.** University of California Santa Barbara. 2006.

[34] Marcos Augusto M. Vieira, Claudionor N. Coelho, Jr. Diógenes Cecílio da Silva Junior José M. da Mata. **Survey on Wireless Sensor Network Devices**. Emerging Technologies and Factory Automation, 2003. Proceedings. ETFA '03. IEEE Conference.

[35] Azzedine Boukerche. **Algorithms and Protocols for Wireless Sensor Network**. Book Ed. John Wiley & Sons Inc. 2009.

[36] K.P. Ferentinos, and T.A. Tsiligiridis. **Energy-saving design adaptation of Wireless Sensor Networks with solar rechargeable batteries**. Computer Networks Journal. Volume 51, Issue 4, 14 March 2007, Pages 1031-1051.

[37] Carlos F. García-Hernández, Pablo H. Ibargüengoytia-González, Joaquín García-Hernández, and Jesús A. Pérez-Díaz. **Wireless Sensor Networks and Applications: a Survey**. IJCSNS Int 264 ernational Journal of Computer Science and Network Security, VOL.7 No.3, March 2007.

[38] Hemanta Kumar Kalita1 and Avijit Kar. **Wireless sensor network security analysis**. International Journal of Next-Generation Networks (IJNGN),Vol.1, No.1, December 2009.

[39] Dr. Geoff V Merret and Dr. Yen Kheng Tan. **Wireless Sensor Networks: Application-Centric Design**. Book published by InTech. 2010.

[40] Nelson Matthys, Rehan Afzal, Christophe Huygens, Sam Michiels, Wouter Joosen, Danny Hughes. **Towards Fine-Grained and Application-Centric Access**. Proceedings of the 2010 ACM Symposium on Applied Computing.

[41] Seung Jun Baek, Xiaohan Yu, Kyogu Lee and Hyunhak Kim. **Retrieval of the Extreme Values under Deadline Constraints in Wireless Sensor Networks**. Sensors Journal 2011, Vol. 11, p. 5229-5252.

[42] B. Raman and K. Chebrolu, **Censor networks: a critique of "sensor networks" from a systems perspective**, SIGCOMM Comput. Commun. Vol. 38, p. 75-78, 2008.

[43] Cinzia Cappiello, Fabio A. Schreiber. **Quality and Energy-Aware Data Compression by Aggregation in WSN Data Streams**. Seventh Annual IEEE International Conference on Pervasive Computing and Communications. PerSeNS 2009 Workshop. March 2009. pp. 634-639.

[44] Thomas M. Wendt, Leonhard M. Reindl. **Wake-Up Methods to Extend Battery Life Time of Wireless Sensor Nodes**. IEEE International Instrumentation and Measurement Technology Conference. Victoria, Vancouver Island, Canada, May 12–15, 2008.

[45] K. Padmanabhan, P. Kamalakkannan. **A Study on Energy Efficient Routing Protocols in Wireless Sensor Networks**. European Journal of Scientific Research, Vol.60 No.4 (2011), pp. 517-529. 2011.

[46] Winston Seah and Yen Kheng Tan. **Sustainable Wireless Sensor Networks**. Hard cover book, 574 pages. Publisher: InTech. December 2010.

[47] Sinchan Roychowdhury , Chiranjib Patra . **Geographic Adaptive Fidelity and Geographic Energy Aware Routing in Ad Hoc Routing**. Special Issue of IJCCT Vol.1 Issue 2, 3, 4; 2010 for International Conference [ACCTA-2010], 3-5 August 2010.

[48] Erzsebet Ravasz and Albert-Laszlo Barabasi. **Hierarchical organization in complex networks**. The American Physical Society Journal. 2003.

[49] Kazuo Iwama and Masaki Okita. **Compact Routing for Flat Networks**. 17th International Symposium on Distributed Computing. 2003.

[50] Maryam Soltan, Morteza Maleki, and Massoud Pedram. **Lifetime-Aware Hierarchical Wireless Sensor Network Architecture with Mobile Overlays**. IEEE Radio and Wireless Symposium, 2007.

[51] Anis Koubâa, Hassen Sallay, Mário Alves. **Real-Time Tracking and Reporting of Dynamic Events in Hierarchical Wireless Sensor Networks**. IPP-HURRAY! Research Group. Polytechnic Institute of Porto – School of Engineering. Rua Dr. António Bernardino de Almeida, 431, 4200-072 Porto, Portugal. 2007.

[52] Kavitha. C, K.V.Viswanatha. **A Hybrid Reliable Routing Technique (HRR) for Wireless Sensor Network**". International Journal of Computer Science and Network Security, VOL.9 No.3, March 2009.

[53] Shio Kumar Singh, M. P. Singh, and D K Singh. **Routing Protocols in Wireless Sensor Networks - A survey**. International Journal of Computer Science & Engineering Survey (IJCSES) Vol.1, No.2, November 2010.

[54] Jasmine Norman. **Connectivity and Coverage in Hybrid Wireless Sensor Networks using Dynamic Random Geometric Graph Model**. International journal on applications of graph theory in wireless ad hoc networks and sensor networks (GRAPH-HOC) Vol.3, No.3, September 2011.

[55] Jamal N. Al-Karaki, Ahmed E. Kamal. **Routing Techniques in Wireless Sensor Networks: A Survey**. IEEE Wireless Communications, Volume: 11, Issue:6, page(s): 6 – 28. 2004.

[56] Luis Javier García Villalba, Ana Lucila Sandoval Orozco, Alicia Triviño Cabrera and Claudia Jacy Barenco Abbas. **Routing Protocols in Wireless Sensor Networks**. Sensors Journal 2009.

[57] Thomas C. Henderson, Jong-Chun Park, Nate Smith and Richard Wright. **From Motes to Java Stamps: Smart Sensor Network Testbeds**. Proceedings of the International Conference on Intelligent Robots and Systems. 2003.

[58] Cheekiralla, S.; Engels, D.W.. **A Functional Taxonomy of Wireless Sensor Network Devices**. Broadband Networks, 2005. BroadNets 2005. 2nd International Conference on broadband sensors.

[59] Thomas Dellsperger, Thomas Burger, Linus Maurer, T. Christen, A. Mayer, S. Sital, D. Bateman, M. Muck. **RF transceiver architecture for cognitive radio user equipment**. End to End reconfigurability II. White paper. June 2007.

[60] Anil K. Maini. **Digital electronics. Principles, Devices and Applications**. John Wiley and Sons Press. 2007.

[61] MultiTech Systems. **AT Commands For GSM/GPRS Wireless Modems.** Reference guide. 2003.

[62] Conexant Systems, Inc. **AT Commands for SmartSCM, SmartACF, SmartACFL**, **and SC56D Modems.** Reference Manual. 2000 - 2001. All Rights Reserved.

[63] Matthew Loy, Raju Karingattil, Louis Williams. **ISM-Band and Short Range Device Regulatory Compliance Overview.** Texas Instruments Corp.. SWRA048 Application report, 2005.

[64] --. Digi Inc. **XBee™/XBee–PRO™ 2.4 GHz OEM RF Modules.** Product Manual v1.xCx – 802.15.4. Digi Inc. USA. 2008.

[65] Product specification sheet. AC4490 **900MHz Radio Module**. Laird Technologies, 2011.

[66] Laird Tech. **AC4490 900MHz Transceiver User's Manual.** Ver. 3.2.1, 2007.

[67] Libelium Comunicaciones Distribuidas S.L. ***Wasp mote technical guide.*** Document version 4.7 - 11/2013. http://www.libelium.com/es/development/waspmote/documentation/

[68] Arduino Open Hardware. **Arduino Mega 2560 Overview**. http://arduino.cc/en/Main/arduinoBoardMega2560. Last visited on 08/2013.

[69] Shio K. Singh, M.P. Singh, D.K. Singh. (2010). **A survey of energy efficient hierarchical cluster-based routing in wireless sensor networks**. J. of Advanced Networking and Applications. Vol. 2. Issue 2. P. 570-580.

[70] Erzsebet Ravasz, Albert-Laszlo Barabasi. (2003). **Hierarchical organization in complex networks**. The American Physical Society Journal.

[71] Joe Bardeweel. **Converting Signal Strength Percentage todBm Values**. WildPackets Inc. White Paper. November 2002.

[72] Chipcon. **C1020/1021 Received Signal Strength Indicator**. Application Note AN030. Texas Instruments. 2005.

[73] Maxstream. **Received Signal Strength Indicator**. Application Note XST-AN012a. Digi Inc.. 2004.

[74] Laird Tech. **AC4490 Developer Kit User's Manual.** Version 3.3. 2005

[75] Jerry Zhao, Ramesh Govindan. **Undersatnding Packet Delivery Performance In Dense Wireless Sensor Networks**. SenSys'03, November 5-7, 2003. Los Angeles, Ca, USA.

[76] E. Taira Procopio, et. al.. **Received Signal Strength Indication Modelling in Indoor Wireless Sensor Networks**. American Journal of Applied Sciences. 10 (9): 1043 - 1049, 2013. ISSN: 1546-9239.

[77] J. Vales-Alonso, et. al.. **Performaece evaluation of MAC transmission power control in wireless sensor networks**. ACM Computer Networks. Vol. 51, Issue 6, 25 april 2007, Pages 1483-1498.

[78] C. Albaladejo, P. Sánchez, A. Iborra, F. Soto, J.A. López and R. Torres. **Wireless Sensor Networks for Oceanographic Monitoring: A Systematic Review**. Sensors Journal, 10(7), p. 6948-6968, july 2010.

[79] Héctor Bustos-Serrano, Mariana Macías-Casrballo. **Reporte de datos del semestre 2008.2: Hidrología de Bahía Falsa, San Quintín, B.C.** Octubre 2008. Universidad Autónoma de Baja California. Facultad de Ciencias Marinas. REPORTE TÉCNICO No. FCM-2009-01.

[80] Newman, J.; Schall, G.; Schmalstieg, D.. **Modeling and Handling Seams in Wide-Area Sensor Networks.** 10th IEEE International Symposium on Wearable Computers. Issue Date: 11-14 Oct. 2006. On page(s): 51 – 54. ISSN: 1550-4816. Print ISBN: 1-4244-0597-1. INSPEC Accession Number: 10236844.

[81] O. Younis, M. Krunz, and S. Ramasubramanian. **Node Clustering in Wireless Sensor Networks: recent developments and deployments.** IEEE Network Transactions, Vol. 20, pp. 20-25, 2006.

[82] S. Bandyopadhyay and E. Coyle. **An Energy-Efficient Hierarchical Clustering for Wireless Sensor Networks.** Proceedings of IEEE INFOCOM, 2003.

[83] J.M. Castillo-Sencilla, P. C. Aranda, F.J.B. Outeirino, J. Olivares. **Experimental Procedure for the Characterization and Optimization of the Power Consumption and reliability in ZigBee Mesh Networks.** Third IEEE International Conference on Advances in Mesh Networks (MESH), pp. 13-16. 18-25 july 2010.

[84] A. H. Kioumars and L. Tang, **ATmega and XBee-based wireless sensing**. in Proceedings of the 5th International Conference on Automation, Robotics and Applications (ICARA'11), pp. 351–356, Wellington, New Zealand, December 2011.

[85] A. Rapp, **Arduino library for communicating with XBees in API mode**, 2012, http://code.google.com/p/xbee-arduino.

[86] **--**. **JavaScript Object Notation, 2014**, http://www.json.org/.

[87] **--**. **Laird, 2012**, http://www.lairdtech.com.

[88] Digi International, **Rabbit core RCM4300 c-programmable analog core module with microSD card storage and Ethernet.** User's Manual, 2010.

[89] C. Ortega-Corral, et al., **A "Lighter" JSON for message exchange in highly resource constrained wireless sensor** network applications, in Proceedings of the Congreso Internacional de Electronica (ELECTRO '12), Chihuahua, Mexico, October 2012.

[90] C. Ortega-Corral, et al., **End-to-End Message Exchange in a Deployable Marine Environment Hierarchical Wireless Sensor Network**, International Journal of Distributed Sensors, Vol. 2014, Article ID 950973, 18 pages. 2014. http://dx.doi.org/10.1155/2014/950973.

[91] I. Khemapech, A. Miller and I. Duncan. **A Survey of Transmission Power Control in Wireless Sensor Networks.** 8th Annual PostGraduate Symposium on the Convergence of Telecommunications, Networking and Broadcasting. PGNET 2007. ISBN: 1-9025-6016-7.

[92] Luiz H. A. Correia et. al.. **Transmission power control techniques for Wireless Sensor Networks**. Computer Networks Journal, Vol. 51. Elsevier. 2007. ISSN 4765-4779.

[93] W. Ye, J. Heidemann, and D. Estrin. **An energy-efficient MAC protocol for wireless sensor networks**, 2002.

[94] H. A. Correia Luiz, F. Macedo Daniel, A. C. Silva Daniel, L. dos Santos Aldri, A. F. Loureiro Antonio, Jose, and S. Nogueira Marcos. **Transmission power control in MAC protocols for wireless sensor networks**, 2005. 1089494 282-289.

[95] Joseph Polastre, Jason Hill, and David Culler. **Versatile low power media access for wireless sensor networks**. In Proceedings of the 2nd international conference on Embedded networked sensor systems, Baltimore, MD, USA. ACM Press..

[96] Dongjin Son, Bhaskar Krishnamachari, and John Heidemann. **Experimental study of the effects of transmission power control and blacklisting in wireless sensor networks**. In Proceedings of the First IEEE Conference on Sensor and Adhoc Communication and Networks, pages 289–298, Santa Clara, California, USA, 2004. IEEE. in proceedings.

[97] E. Jung and N. Vaidya. **A power control MAC protocol for ad-hoc networks**. In Proceedings of the Eighth Annual International Conference on Mobile Computing and Networking (MOBICOM), Atlanta,Georgia, 2002. ACM Press.

[98] J.P. Monks. **Transmission power control for multiple access wireless packet networks.** In Local Computer Networks, 2000. LCN 2000. Proceedings. 25th Annual IEEE Conference on, pages 12–21, 2000. in proceedings.

[99] J. Gomez and A. T. Campbell. **A case for variable-range transmission power control in wireless multihop networks**. In INFOCOM 2004. Twenty-third Annual Joint Conference of the IEEE Computer and Communications Societies, volume 2, pages 1425–1436 vol.2, 2004. in proceedings.

[100] S. Lin, J. Zhang, L. Gu, T. He, and J. Stankovic. **ATPC: Adaptive Transmission Power Control for Wireless Sensor Networks.** In Proceedings of SenSys'06, Nov. 2006.

[101] Junseok Kim, Sookhyeon Chang, Younggoo Kwon. **ODTPC: On-demand Transmission Power Control for Wireless Sensor Networks.** Information Networking, ICOIN 2008.

[102] Jaein Jeong, David Culler, Jae-Hyuk Oh. **Empirical Analysis of Transmission Power Control Algorithms for Wireless Sensor Networks.** 4th International Conference on Networked Sensing Systems, 2007. INSS '07. pp. 27 - 34.

[103] Yong Fu, Mo Sha, Gregory Hackmann, Chenyang Lu. **Practical Control of Transmission Power for Wireless Sensor Networks.** 20th IEEE International Conference on Network Protocols (ICNP), 2012.

[104] Kenneth Bannister, Gianni Giorgetti, Sandeep K.S. Gupta. **Wireless Sensor Networking for "Hot" Applications: Effects of Temperature on Signal Strength, Data Collection and Localization.** HotEmNets '08, June 2-3, 2008, Charlottesville, Virginia, USA. 2008 ACM 978-1-60558-209-2/08/0006.

[105] J. Thelen, D. Goense, K. Langendoen. **Radio wave propagation in potato fields.** 1st Workshop on Wireless Network Measurements, Riva del Garda, Italy. 2005

[106] C. A. Boano, et. al. **Hot Packets: A Systematic Evaluation of the Effect of Temperature on Low Power Wireless Transceivers.** 5th Extreme Conference on Communication, August 24-30, 2013, Thorsmork, Iceland.

[107] Jungwook Lee and Kwangsue Chung. **An Efficient Transmission Power Control Scheme for Temperature Variation in Wireless Sensor Networks**. Sensor, Vol. 11, 3078-3093 2011

[108] H. Wennerstrom et al. **A long-term study of correlations between meteorological conditions and 802.15.4 link performance**. In Proc. of the 10th SECON, 2013.

[109] Milda Tamošiūnaitė, Mindaugas Žilinskas, Milda Tamošiūnienė and Stasys Tamošiūnas. **Electromagnetic Waves. Chapter 8: Atmospheric Attenuation due to Humidity.** Book edited by Vitaliy Zhurbenko. ISBN 978-953-307-304-0. 2011. DOI: 10.5772/21430.

[110] A. Martínez-Sala, J.M. Molina-García-Pardo, E. Egea-Lopez, J. Vales-Alonso. **An accurate radio channel model for Wireless Sensor Networks simulation.** Journal of Communications and Networks. Vol. 7, issue: 4. Dec. 2005. ISSN: 1229-2370.

[111] Wayne Tomasi. **Electronic Communications Systems.** 5th edition. Book edited by Pearson Prentice-Hall. USA, 2003.

[112] Roy Blake. **Electronic Communications Systems.** 2nd. Edition. Delmar Thompson Publishing. 2001.

[113] John S. Seybold. **Introduction to RF propagation.** Wiley-Interscience, John Wiley & Sons, Inc. 2005.

[114] Henry L. Bertoni. **Radio Propagation for Modern Wireless Systems.** Pearson Education. 1999.

[115] Walter Debus. **RF Path Loss & Transmission Distance Calculations.** Axonn, LLC, Technical Memorandum. August 4, 2006.

[116] César Ortega-Corral. **Transmission Power Control based on Temperature and Relative Humidity.** 2014 IEEE Ninth International Conference on Intelligent Sensors, Sensor Networks and Information Processing (ISSNIP) Sympsoium on Sustainable and Adaptive Sensor Networks. Singapore, 21-24 April 2014.

[117] Faycal Ikhouane, Jose Rodellar. **Systems with Hysteresis: Analisis, Identification and Control using the Bouc-Wen Model.** Edition 1. Wiley Books, August 2007. ISBN: 0470032367.